CR 137669

NIELSEN ENGINEERING AND RESEARCH, INC.

OFFICES: 510 CLYDE AVENUE / MOUNTAIN VIEW, CALIFORNIA 94043 / TELEPHONE (415) 968-9457

COPY NO. 3

NASA CR-137669

ANALYSIS OF WAKE VORTEX FLIGHT TEST DATA BEHIND A T-33 AIRCRAFT

by

Gary D. Kuhn and Robert A. Jacobsen

NEAR TR 84

April 1975

Prepared under Contract No. NAS2-6973

by

NIELSEN ENGINEERING & RESEARCH, INC.
Mountain View, California

for

NATIONAL AERONAUTICS AND SPACE ADMINISTRATION
Ames Research Center

TABLE OF CONTENTS

ANALYSIS OF WAKE VORTEX FLIGHT TEST DATA BEHIND A T-33 AIRCRAFT

by Gary D. Kuhn and Robert A. Jacobsen*
Nielsen Engineering & Research, Inc.

SUMMARY

Measurements of the vortex system behind a T-33 aircraft were obtained by a Learjet equipped with a boom carrying a three-wire, hot-wire anemometry probe and other instrumentation. Analysis of the measurements using a computerized geometric method indicated the vortices had a core radius of approximately 0.11 meter with a maximum velocity of 25 meters per second. The hot-wire anemometer was found to be a practical and sensitive instrument for determining in-flight vortex velocities.

No longitudinal instabilities, buoyant effects or vortex breakdowns were evident in the data which included vortex wake cross sections from 0.24 to 5.22 kilometers behind the T-33.

INTRODUCTION

This report presents the results of a study of data obtained by the Ames Research Center staff in a flight test program designed to evaluate theories for trailing-vortex behavior and decay. Measurements were obtained of the vortex system behind a T-33 aircraft by a Learjet equipped with an instrumented boom. Measurements of velocity components were made using a three-wire, hot-wire anemometry probe mounted on the boom. Angle of attack and angle of yaw were determined from deflections of flow vanes mounted on the boom. In addition, roll angle, angular rates, linear accelerations, temperature and altitude were measured and recorded as a function of time.

Previous work in support of this flight test program aided in defining the parameters to be measured; the anticipated vortex characteristics, mutual interference between the probe aircraft and the wake, the response of certain instruments to be used in obtaining measurements, the effect of condensation on the wake vortices, and methods of data reduction. Also, recommendations were made to the effect that supporting data be obtained to define the environment in which the vortices persist and dissipate. A

---

*Aerospace Engineer, NASA/Ames Research Center, Moffett Field, California.

data reduction method was developed to reconstruct the velocity field and essential features of the vortex based on knowledge of the velocity components along some flight path through the vortex (ref. 1). In the study to be discussed herein, the data obtained from the flight test program were also used to evaluate a new method of reconstructing the vortex velocity field, employing the method of least squares.

SYMBOLS

d	distance behind T-33 aircraft, m or km
r	radius measured from vortex center, m
s_v	vortex wake span, m
u,v,w	velocity components in the x,y,z directions, respectively, m/sec
v_θ	tangential velocity, m/sec
v_r	radial velocity
V_L	velocity of Learjet, m/sec (true airspeed)
V_∞	velocity of T-33, m/sec (true airspeed)
V_E,W_E	components of errors in calculation of Learjet velocity
x,y,z	coordinates in inertial coordinate system (fig. 1); x is horizontal, positive pointing aft from the T-33, y is horizontal, positive to the right, and z is vertical, positive upward
α	angle of attack, degrees
β	yaw angle, degrees
Γ	circulation, m^2/sec
Γ_o	theoretical circulation of T-33
Δt	increment of time
δ	deviation of vortex span from mean value
λ_s	scale wavelength of atmospheric turbulence

ρ	density
σ'	rms turbulence velocity normalized by V_∞
ψ	heading angle of Learjet
ψ_o	heading angle of Learjet at beginning of a series of zig-zag traverses of vortex wake

Subscripts

HW	refers to hot-wire measurements

FLIGHT TEST DATA ACQUISITION

The vortex flow behind the T-33 airplane was probed in the manner described in figure 1. The T-33 flew at a constant air speed of 97.3 meters per second. The Learjet flew at speeds slightly greater than this beginning at a distance of approximately three-to-five kilometers behind the T-33 and traversing the vortex wake in a zig-zag fashion so that a series of several vortex measurements could be made. Smoke was injected into one of the vortices by a smoke generator mounted on one wing of the T-33. This made one of the vortices visible and thereby aided the Learjet pilot in aiming the measurement probe to intersect the core of the vortex. It was expected that this procedure would also result in the probe's passing close to the second vortex. Altitude was recorded constantly in the Learjet instrumentation. After each series of wake traverses, the Learjet was flown beside the T-33 in order to provide a recording of the T-33 altitude.

The data obtained in the flights consist of recorded output of the three wires of the hot-wire anemometry probe, accelerometer measurements, the altitude of the Learjet, the velocity of the Learjet, the outside air temperature, a heading angle, yaw angle of the Learjet, the pitch and yaw rates of the Learjet, and the angle of attack of the Learjet. Those data were continually recorded on magnetic tape during the flight tests. After the flight tests the data were digitized in time steps of one millisecond for two thousand steps spanning each wake traverse. The digitized data were then stored on magnetic tape for later processing by the IBM 360/65 computer. From the digitized velocity, acceleration, and angle data, the motion of the Learjet was calculated along with the motion of the probe

relative to the flight path of the Learjet. After processing, the hot-wire data were converted into three velocity components in a system having axes parallel to the principal axes of the probe aircraft. Subsequently, the motion of the probe aircraft was removed from the hot-wire velocity components to determine the vortex velocity field as follows:

$$u_V = u_{HW} - V_L \cos \beta_L \cos \alpha_L \tag{1}$$

$$v_V = v_{HW} - V_L \sin \beta_L \tag{2}$$

$$w_V = w_{HW} - V_L \cos \beta_L \sin \alpha_L \tag{3}$$

where the Learjet velocity, V_L, angle of attack, α_L, and yaw angle, β_L, were calculated as the average of the first one hundred values for each wake traverse data set. Each of the three quantities was assumed to be constant for the remainder of each wake traverse. The validity of that assumption will be examined subsequently. The remaining velocity components, u_V, v_V, w_V, are those due to the vortices. Those components were subsequently resolved into vertical and horizontal components in a coordinate system oriented in cross sections of the vortex wake with the y axis horizontal and perpendicular to the wake axis positive to the right, facing the T-33, the z axis vertical, positive downward and the x axis horizontal and parallel to the wake axis, positive forward. The origin of the y and z axes was defined for each wake traverse at the first position of the data set for a left-to-right traverse, or the last position for a right-to-left traverse. In subsequent analyses the data were converted to a system with y positive to the right and z positive upward with the horizontal velocity components positive in the direction of positive y and the vertical component positive upward.

METHODS FOR RECONSTRUCTION OF THE VORTEX CHARACTERISTICS

Geometric Method

In reference 1, a computer program was described which calculates the equations of lines normal to the resultant velocity vectors and locates the center of a vortex by averaging the points of intersections of the normal lines. Assuming an ideal vortex with circular, concentric streamlines

and negligible radial velocity and assuming small influences from the opposite wing-tip vortex, the normals to the resultant velocity vectors will all intersect at the same point. In practice, the resultant velocity vectors are not entirely concentric and the normal lines intersect in a small region. The apparent location of the center of the vortex is calculated by computing the average of the coordinates of the intersections of the normal lines. If the vortex centers are actually very close to the probe path, this method should accurately locate the vortex center. However, the accuracy of the method can be significantly limited by measurement errors, the influence of the opposite wing-tip vortex and other systematic deviations from the circular vortex model.

Least-Squares Method

It may be possible to achieve improved accuracy in the analysis of data containing random fluctuations by using a statistically based method such as the method of least squares. Such a method was demonstrated recently in reference 2 where aircraft trailing vortices were analyzed using a modified Newton-Raphson method to fit a theoretical vortex model to measured velocity data in such a way as to minimize the mean-square error. A slightly different approach has been developed recently by the senior author for analyzing wake velocity measurements behind aircraft with multiple wake vortices. The details of that method are presented in Appendix A. As a first approximation, the vortices are represented by inviscid vortices. The nonlinear mathematical expressions so produced are linearized with respect to an estimate of the positions and strengths of the vortices. The resultant expressions are solved for the unknown perturbations from the estimate by the method of least squares. The first estimate is updated and the process repeated iteratively until the solution converges. The availability of the flight test data provided an excellent opportunity to evaluate the usefulness and limitations of this method.

The first step in constructing the vortex characteristics using the least-squares program is to obtain an initial estimate of the locations and strengths of all the vortices expected to be present. This was accomplished using a program provided by Ames Research Center allowing the vectors and/or the normals to the velocity vectors to be displayed on a CRT computer terminal. In this way, the estimated initial values required for the least-squares program were obtained quickly and

conveniently. Plots of the normals to the velocity vectors along the flight path of the Learjet were obtained in the coordinate system established during the data reduction. The required vortex locations were then estimated by observing the intersections of the normals.

Two vortices were expected to be present in all wake cross sections, one from each wing tip. The initial vortex strengths to be used in the least-squares program were estimated to be of magnitude 74.3 meters squared per second. This is an approximate value based on the calculated vortex strength obtained from the known mass of the T-33 aircraft as a function of time, the velocity of the T-33, 97.3 meters per second, and the span, 8.99 meters, of the vortices assuming an elliptic span-load distribution on the T-33 wing (fig. 2).

DISCUSSION OF RESULTS

Characteristics of Wake

In Table I are listed some of the characteristics of the vortex wake. Three series of wake traverses are listed in the table. Included in the table are the distance of each wake cross section behind the T-33, the age of each cross section, the altitude of each wake cross section, and the total circulation to be expected according to the T-33 weight, velocity, altitude, and vortex span, assuming an elliptical span-load distribution on the T-33 wing. Also listed in the table is the lift coefficient of the T-33, calculated from the known mass, velocity and wing area of the T-33 and assuming the density of a standard atmosphere at 3.05 kilometers (10,000 feet) altitude.

Comparison of Methods of Analyses

In figure 3 are shown the normals to some of the velocity vectors along the path of the measuring probe through the wake for cross section 40 listed in Table I. The coordinates of the figure are the y and z coordinates measured from the beginning of the digitized data set as described previously, except that the y origin has been adjusted to be at the beginning of the set of points displayed. Data from every fourth point of 500 points spanning the wake are shown stretching from $y = 0$ meters to $y = 18.7$ meters. The path of the probe is nearly horizontal.

The lines representing the normals to the velocity vectors are drawn from the location of the measurement on the probe path in a direction 90° counterclockwise from the direction of the velocity vector at the point with a length proportional to the length of the velocity vector (see sketch below).

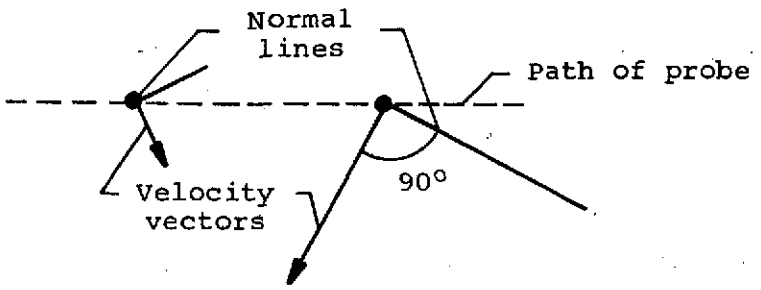

Thus, when the probe passes close to a vortex, the velocities are large, so the length of the normal lines is long. By this criterion, there appear to be two vortices in figure 3, one at approximately y = 6.0 meters, z = 0.0 meter, the other at approximately y = 12.5 meters, z = 0.0 meter. Since the long normal lines near y = 6.0 meters diverge beneath the probe path, it is concluded that that vortex is above the probe path and, using the orientation of the normal lines and the velocity vectors described previously, it is rotating clockwise. The long normal lines near y = 12.5 meters converge above the path, indicating a vortex, and again using the orientation of the normal lines as a guide, it is concluded that that vortex is rotating counterclockwise.

In this section, the geometrical and least-squares method of analysis will be compared by using both methods to obtain estimates of the location of the two vortices in the cross section discussed with reference to figure 3. In applying the geometrical program to the data, each vortex is treated separately. The effect of the other vortex is subtracted out by determining the measured downwash velocity halfway between the estimated positions of the two vortices, apportioning half to each vortex and subtracting an amount from the downwash velocity at other points proportional to the inverse of the distance from the midpoint. The estimated center locations were determined as the location of the reversal of the vertical velocity component from the tabulated data. In the case that this procedure results in an isolated symmetrical vortex, the lines drawn normal to the velocity vectors should pass through the center of the vortex. Errors in

the flow measurements, the data reduction, and errors in accounting for the presence of the second vortex limit the accuracy with which the vortex centers can be determined. In the case shown in the example, the vortices were both fairly close to the path of the probe. Therefore, the geometrical method should result in an accurate determination of the vortex centers.

The data used to calculate each vortex center were the 150 points approximately centered on the point of reversal of the vertical velocity component of each vortex. This corresponds to y coordinate values from 3.15 meters to 8.72 meters, and from 9.9 meters to 15.52 meters in figure 3. The vortex on the left will subsequently be referred to as vortex number 1. The calculated (x,y) coordinates of the two vortex centers are (6.03, 0.05) and (12.71, 0.207). In figure 4 are shown the nondimensional distributions of the resultant velocity, V_R, the axial velocity, u, and the circulation, Γ, with radial distance from the vortex center for each vortex. The velocities are the actual measured velocities while the radial distance is the distance from the point of measurement on the probe path to the calculated vortex center as determined by the geometrical program. The resultant velocity is normalized with respect to the T-33 speed, V_∞, and the circulation is normalized with respect to Γ_o, the theoretical circulation of the T-33. The resultant velocity, represented by the symbol 0 in figure 4 is the resultant of the two components, vertical and horizontal, of the velocity in the vortex cross section. It is plotted so as to indicate the direction of rotation of the vortices. Thus, in figure 4(a), the data for vortex 1 indicate a clockwise rotation so the velocities to the left of the vortex center are plotted as positive velocities while those to the right are negative. The opposite is true of vortex 2 in figure 4(b) indicating a counterclockwise rotation. The axial velocity distribution, represented by the symbol x, indicates that there was apparently negligible axial flow relative to the T-33. The periodic variation noted in the axial component and also present but more difficult to see in the resultant velocity is believed to be due to bending of the instrumentation boom which was not accounted for in the data processing. The circulation distribution, represented by the symbol + is the quantity

$$\frac{\Gamma}{\Gamma_o} = \frac{2\pi V_R r}{\Gamma_o}$$

The variation of the resultant velocity indicates that both vortices were very close to the path of the probe. The shortest distance from the probe path to the calculated center location for vortex 1 (fig. 4(a)) is 0.104 meter while that for vortex 2 (fig. 4(b)) is 0.296 meter. The vortex core radius was expected to be approximately 0.262 meter on the basis of a preliminary analysis described in reference 1 wherein vortex core radius measurements from wind-tunnel experiments on rectangular wings were scaled up to the T-33 span and doubled to account for the influence of span-load distribution. That suggests that the traverse of vortex 1 may have penetrated the core of the vortex. However, no such conclusion can be drawn from the data shown in figure 4(a), since there is no clear indication of a peak in the resultant velocity distribution. The circulation distribution is seen to increase from small values close to the vortex center but becomes highly scattered at distances greater than approximately 1.2 meter due to the high relative error of the velocities.

In order to compare the two methods of calculation of vortex characteristics, the results of applying the least-squares program to the same data as for figure 3 are shown in figure 5. In figure 5(a) is shown the distribution of lines drawn normal to the residual vectors remaining when the theoretically calculated vortex distributions are subtracted from the data. This figure is to be compared directly with figure 3. While some fairly large velocities remain, the vortex velocity field appears to have been accounted for since the normals to the residual vectors indicate no clear centers as they did in figure 3. In figures 5(b) and (c) are shown the distributions of tangential velocity, v_θ, and radial velocity, v_r, with distance from the calculated vortex center for each vortex. It will be recalled that in the least-squares calculation, both vortices are treated simultaneously. The solution in this case indicates that the vortices are slightly further from the probe path than was indicated by the geometrical method. The minimum radii are 0.246 meter and 0.44 meter compared to 0.104 meter and 0.296 meter calculated by the geometrical program. In figures 5(b) and (c) each vortex has been isolated in turn by subtracting the theoretical distribution of velocity for the other vortex from the data. Also the presentation of tangential and radial velocity components in this case instead of the resultant velocity as in the previous case allows a somewhat better assessment of the accuracy of the calculations.

The tangential velocity is represented by the symbol 0 in the figures while the symbol x is used for the radial component. The same sign convention is used for the tangential velocity as in figure 4, while the radial velocity is assumed positive if directed away from the vortex center. It is noted that for both vortex 1 (fig. 5(b)) and vortex 2 (fig. 5(c)), the radial component is small for most of each vortex, except near the calculated center. The reason for this is believed to be attributable to several sources of error. First, due to the uncertainty of locating the center, the relative error in calculation of distance between points on the probe path and the calculated vortex center is larger for points close to the center than for points far from the center. Another source of error in the least-squares analysis is the extent of the region from which the data were taken. The data used for the calculations illustrated in figure 5 were within a radius of approximately 3 meters for each vortex. Referring to figures 4(a) and (b), such a span includes a large amount of data with very poorly defined circulation in addition to a region where the circulation is significantly lower than the asymptotic value. In addition, the asymptotic value, though poorly defined, is clearly not equal to the theoretical value. The probable reason for this is bias in the velocity data, which will be discussed subsequently. The circulation predicted for the two vortices by the least-squares method was 49.98 square meters per second and 62.15 square meters per second, respectively. This is approximately 25 percent lower than the theoretical value of 73.86 square meters per second, calculated from the T-33 weight and velocity. This lack of agreement between the calculated and theoretical values is not surprising in view of the distribution of circulation noted previously in figure 4.

Another aspect of the data which can strongly effect the results of both the geometric and the least-squares methods is the presence of significant bias in the measurements. Such bias is present in much of the data discussed herein due to the fact that the motion of the Learjet was not uniform. It will be recalled that the Learjet velocity, angle of attack, and yaw angle were assumed to be constant at the value calculated as the average of the first one hundred of a total of two thousand values obtained during a wake traverse. A typical case in which that is not true is shown in figure 6 where a sketch of the recorded output of the Learjet instrumentation is presented. Clearly, none of the three quantities was constant throughout the wake traverse. In addition to large perturbations induced

on the angle of attack and yaw vanes by the wake, the long-term trend of the data indicates that the velocity increased, the angle of attack decreased, and the yaw angle increased as the Learjet passed through the wake. Thus, the Learjet motion was not the same at the end of the traverse, nor at the actual position of the vortex wake, as it was when the reference quantities were calculated. The magnitude of the error in the vortex velocities is, for the horizontal velocity component, referring to equation (2),

$$V_E = V_L(\sin \beta_c - \sin \beta_L)$$

where β_c is the local yaw angle relative to the undisturbed flow and β_L is the initial yaw angle from the average of the first one hundred points. Similarly, for the vertical component, equation (3)

$$W_E = V_L(\cos \beta_c \sin \alpha_c - \cos \beta_L \sin \alpha_L)$$

where α_c is the local angle of attack relative to the undisturbed flow. Thus, for $V_L \sim 91$ meters per second, and $\beta_c = 3^\circ$, $\beta_L = 1^\circ$, $\alpha_c = 5.0^\circ$, and $\alpha_L = 5.5^\circ$, $V_E = 3.2$ meters per second, $W_E = 0.5$ meter per second. The effect of these errors is clearly demonstrated in figure 7 where the vertical and horizontal vortex velocity components produced by subtracting the calculated Learjet velocity components from the hot-wire data are shown. Both components show a slight shift from the asymptotic value of zero, but the effect is most pronounced in the horizontal component, showing a maximum error of approximately 5 meters per second.

Compared to the peak velocities encountered in the vortices shown in figure 7, the bias errors are not large. However, the application of the least-squares program to such data must account for the bias since only a few of the total number of points considered have very high velocities. Thus, the data are weighted heavily by the bias velocities.

The error in locating the vortices is believed to be smaller for the geometrical program than for the least-squares program, due to the fact that that program relies on data within a small neighborhood of the vortex center. Thus, that program is not as strongly influenced by bias errors in the data at long distances from the vortices. Also, since the velocities near the vortices are large, the geometric program is not so strongly influenced by a small bias in one of the velocity components.

It is concluded that for the present investigation, the geometrical program can provide adequate information for analysis of the trailing vortices from the flight test data. The least-squares program is more sensitive to the asymptotic behavior of the measured data and requires that the data undergo additional processing in order to account more fully for the unsteady motion of the Learjet. The geometrical program was used exclusively for the remainder of this investigation.

Analysis of Vortex Cross Sections

The results of analysis of the vortex wake data with the geometrical method are summarized in Table II. Sections 41 and 43 showed insufficient information and so were not analyzed. The data for Section 57 were lost due to an instrumentation malfunction.

In figures 8 through 25 are shown the distribution of the normals drawn to the velocity vectors of every fourth point for the data from five hundred points spanning the cross sections listed in Table II. The scales of each figure are the same as described previously for figures 3 and 5(a). These plots indicate that in each cross section in most cases there was at least one well-defined vortex with a second being clearly present but not usually as close to the path of the probe and consequently not so well defined as the first. In several cases the normals to the velocity vectors indicate the presence of some other effect besides the vortices. For Section 43, for example, shown in figure 11, the hot-wire velocity data were somewhat obscured by the presence of a large amount of "noise" (extraneous random fluctuations), which is attributed to the presence of interference from the pilot's radio transmitter. It is difficult to see even a single vortex in that data. Section 44, figure 12 also indicates a confusing pattern of normals. It is not clear in these cases whether the vortices were far from the probe path or if the interference simply obscures the data. Another possibility is that vortex breakdown occurred somewhere between Sections 44 and 45 (between 3 and 4 kilometers behind the T-33), causing a rapid dispersion of the vorticity and consequent reduction of the velocities in the vortex.

In figures 26 through 41 are shown the variation of the normalized resultant velocity, axial velocity and circulation, with distance from the vortex center for the vortices from the remainder of the flight test

data as determined using the geometrical program. These figures employ the same scales and symbols as in figure 4. The symmetry of the velocity distributions indicates that the geometrical program had located the center of the vortices with reasonable accuracy. It was mentioned previously that the radius of the vortex core was expected to be approximately 0.262 meter based on an analysis discussed in reference 1. Only a few of the probe traverses passed within that distance from the vortex center, according to the geometrical analysis. The minimum distances from the probe path to the vortex centers are listed in Table III, along with the normalized velocity measured at that radius. According to Table III, the probe passed within the expected core radius for Sections 40, 42, 46, 48, 49, 54, 56, and 58. However, examination of the velocity distributions, (figs. 4, 28, 30, 32, 33, 38, 40, and 41) indicates that distinct peaks in the velocity are discernable only in the right-hand vortices (vortex 2) of Sections 46 and 58. Even in those cases, the actual core radius is not clearly defined since only one or two measurements occur in the core. The two cases indicate core radii of approximately 0.12 meter, and 0.14 meter, respectively. It is interesting to note that the normalized velocities and minimum radii from Table III appear to be distributed in such a way as to define a vortex with core radius of approximately 0.11 meter with a maximum normalized velocity of approximately 0.42 as shown in figure 42. For the T-33 velocity of 97 meters per second and a lift coefficient of 0.61, the maximum velocity is thus approximately 25 meters per second. The points represented by filled symbols in the figure correspond to Sections 42, 44, 47, 49, and 51 (see Table III). The deviation of those points from the rest of the data in figure 42 is believed to be due to the bias errors which were found to be present in the data of those sections as discussed previously.

It can be concluded from figures 26 through 42 that the probe probably penetrated the vortex core on several occasions. Since the data for the region $r < 0.2$ meter in figure 42 correspond to sections from 1.2 to 2.8 kilometers behind the T-33 (Sections 40, 46, 49, 54, 56, and 58, see Tables I and III), it appears that the vortex core had a constant radius for that distance. In order to verify that conclusion it would be necessary to obtain more detailed velocity distributions at more cross sections.

Atmospheric Characteristics

The outside air temperature was recorded for the entire flight of the Learjet. From that data, an approximate profile of the atmospheric temperature on the date of the tests can be constructed. The results are shown in figure 43. It can be shown that a state of neutral equilibrium exists in the atmosphere when an adiabatic arrangement of the air is present. Such an arrangement corresponds to a lapse rate of 9.84°C per kilometer. Further, an atmosphere with lapse rate less than 9.84°C per kilometer is found to be in stable equilibrium. At the altitude of the tests, 3,093 meters, the atmospheric lapse rate data on the day of the tests appears to correlate fairly well with a line representing neutral stability. It is concluded, therefore, that the atmosphere at the altitude of the tests was neutrally stable on the day of the tests. This conclusion is supported by the statements of the observers in the Learjet that the vortex wake appeared to be stable and that the atmosphere was very smooth; that is, had very little turbulence on the day of the tests.

Shape of the Vortex Wake

From the recorded altitude of the Learjet and the velocity and heading angles, it is possible to determine the location of each vortex cross section in terms of its altitude and its location behind the T-33. The distance of the Learjet behind the T-33 at any time is determined from the following expression.

$$d = \Delta t(V_L - V_\infty)\cos(\psi - \psi_o) \tag{4}$$

Calculating this expression in equal time increments from a time at which the Learjet was beside the T-33 back in time through a series of vortex traverses, the location of each vortex traverse, and its altitude at that time were determined. The results are shown in figure 44. It is noted that the altitude of the vortex wake varied only a few meters for two of the series of traverses, while for the third series the wake seemed to be approximately 36 meters higher at distances far from the T-33 than at closer distances. The altitude of the T-33 during the entire series of vortex traverses was held constant at approximately 3,093 meters, approximately 36 meters above the average altitude of the vortex wake

indicated by the measurements. The theoretical position of the vortex wake based on an inviscid vortex model with an estimated circulation of 74 square meters per second, a span of 8.98 meters and no vertical wind is also shown in figure 44. The uncertainty in determining the altitude of the vortex wake from the recorded data is estimated to be $\pm$ 4.5 meters. Therefore, it appears from the wake altitude measurements that some vertical motion may have been present in the atmosphere or was produced by a vortex instability or buoyant effect. No further conclusions can be drawn without further evidence such as photographs of the vortex wake or measurements at many more cross sections simultaneously.

Analysis of Vortex Wake in Crossflow Plane

The calculated spans of the vortices in the crossflow planes as determined by the geometrical analysis, are shown in figure 45 as a function of distance behind the T-33. Some dispersion is noted, but no clear regularity in the variation is evident. The mean vortex span is 7.95 meters, approximately 11 percent less than the 8.98 meters expected for elliptic span loading.

Also shown in figures 45 are the curves

$$s_v = 7.95 \pm 0.0192\sqrt{d} \qquad (5)$$

These curves approximate the variation to be expected by the theory of reference 1 for the variation of the vortex span far behind the generating aircraft. The specific values of the constants in equation (5) will be discussed subsequently.

In reference 1, a theory was discussed for the vortex motion at a distance d behind the generating aircraft, based on the premises that the vortex is a filament which has the transverse velocity locally of the turbulence at that point and the vortex does not respond to high frequency turbulence. That theory indicates that the root-mean-square deviation of the vortex varies with d as

$$\frac{\sqrt{\overline{\delta^2}}}{\sigma'} = d\sqrt{\frac{2}{\pi}\tan^{-1}\left(\frac{\lambda_s}{d}\right)} \qquad (6)$$

where λ_s is a scale wave length of the turbulence. For cases where λ_s/d is large (small d or large λ_s), the relation becomes

$$\frac{\sqrt{\overline{\delta^2}}}{\sigma'} = d \tag{7}$$

where σ' is the rms turbulence velocity, normalized by V_∞ and at the other extreme, where λ_s/d is small (large d or small λ_s)

$$\frac{\sqrt{\overline{\delta^2}}}{\sigma'} = \left(\sqrt{\frac{2}{\pi}\lambda_s}\right)\sqrt{d} \tag{8}$$

Thus, for a given condition of atmospheric turbulence the vortex deviation is proportional to d at short distances behind the generating aircraft and proportional to $\sqrt{d}$ at greater distances. For the data shown in figure 45, the rms deviation of the vortices from the mean span, is

$$\sqrt{\overline{\delta^2}} = 0.957 \text{ meter} \tag{9}$$

The mean distance of all the measured vortices behind the T-33 is

$$d = 2{,}480 \text{ meters} \tag{10}$$

Using equation (8) a family of curves can be drawn representing the variation of the rms deviation with distance, d, using λ_s and σ' as parameters. The curve representing one standard deviation, $\sqrt{\overline{\delta^2}}$, should enclose 68.26 percent of the data if the data are distributed in a random fashion. According to reference 1, the value

$$\sigma' = 0.004$$

corresponds to negligible turbulence. Using this value and the measured rms deviation, equation (8) yields

$$\lambda_s = 36.24 \text{ meters}$$

at the mean distance, 2,480 meters behind the T-33. This is a reasonable value for low altitudes, based on the results of reference 3. Substituting into equation (8)

$$\sqrt{\overline{\delta^2}} = 0.0192\sqrt{d}, \text{ meters}$$

The curves representing this result are the curves given by equation (5) shown in figure 45. It is noted that 61 percent of the data are enclosed by these curves.

Within the parametric curves shown in figure 45, the data for the third series of measurements seems to oscillate about the mean span. However, whether this oscillation has any significance cannot be determined from the available data alone. As mentioned previously, more data such as photographs or simultaneous measurements at many locations are needed to verify the existence of any systematic deviation from a straight, parallel vortex configuration. Taken as a whole, the data of all three series appear to be distributed in a random fashion with dispersion with distance behind the T-33 describable by concepts based on the response of the vortices to turbulence alone.

The orientation of the vortex wake is indicated in figure 46 where the angle between the horizontal and the line of centers of the vortices as determined from the geometrical analysis is plotted with distance from the T-33. The wake is observed to be nearly horizontal, with a maximum inclination of 7°.

CONCLUDING REMARKS

Measurements of the vortex system behind a T-33 aircraft were obtained by a Learjet equipped with a boom carrying a three-wire, hot-wire probe and other instrumentation. Analysis of the measurements indicated that the vortices had a core radius of approximately 0.11 meter with a maximum velocity of 25 meters per second. The core radius appeared to be constant for up to 3 kilometers behind the T-33.

Atmospheric temperature measurements made during the flight indicated that at the altitude of the vortex wake measurements (3.093 kilometers) the atmosphere during the tests was in a condition of neutral stability. Also, the atmospheric turbulence was small. The vertical motion of the vortex wake was found to deviate somewhat from the theoretical motion to be expected for a pair of constant strength, constant span, vortices indicating the presence of a vertical atmospheric motion, or a longitudinal instability of the vortex wake itself. The deviation is believed to be most probably due to atmospheric motion since the distribution of the vortex span with distance behind the T-33 was found to correspond to that

which could be expected if the vortices were subject to perturbations by atmospheric turbulence, rather than the systematic deviation which would be expected from motion induced by longitudinal instability.

The results of this investigation indicate that the hot-wire probe is a practical and sensitive instrument for determining in-flight vortex velocities. The symmetry observed in the calculated vortex velocity distributions indicated that the geometrical analysis developed in reference 1 provided reasonable estimates of the location of the vortex centers, even for cases in which the probe passed some distance from the vortex core.

NIELSEN ENGINEERING & RESEARCH, INC.
Mountain View, California
February 1975

REFERENCES

1. Spangler, S. B., Dillenius, M. F. E., Schwind, R. G., and Nielsen, J. N.: Assessment of a Wake Vortex Flight Test Program. NEAR TR 48, Nielsen Engineering & Research, Inc., July 1974.

2. Taylor, L. W. and McLaughlin, M. D.: A Modified Newton-Raphson Analysis of Flight Measurements of the Trailing Vortices of a Heavy Jet Transport. NASA TN D-7404, August 1974.

3. MacCready, P. B., Jr.: Turbulence Measurements by Sailplane. J. Geophys. Res., vol. 67, no. 3, March 1962, pp. 1041-1050.

TABLE I.- BASIC WAKE CROSS-SECTION STATISTICS.

Series	Section	Time (mm:sec)	Range (km)	Vortex Age (sec)	Altitude (km)	T-33 Circulation (m^2/sec)	T-33 Lift Coefficient	Symbols Used In Figs. 44, 45 & 46
1	38	42:00	2.88	30	3.069	74.14	0.6270	○
1	39	42:29	2.11	22	3.069	73.95	0.6260	○
1	40	42:50	1.42	15	3.069	73.86	0.6260	○
1	41	43:10	0.70	7	3.075	73.77	0.6257	○
1	42	43:30	0.24	2	3.069	73.77	0.6253	○
2	43	46:00	5.22	54	3.005	73.49	0.6226	□
2	44	46:24	4.02	41	3.045	73.39	0.6221	□
2	45	46:44	3.13	32	3.045	73.39	0.6218	□
2	46	47:10	2.22	23	3.045	73.30	0.6213	□
2	47	47:26	1.81	19	3.045	73.21	0.6210	□
2	48	47:44	1.48	15	3.045	73.21	0.6207	□
2	49	48:00	1.18	12	3.045	73.11	0.6200	□
2	50	48:12	0.91	9	3.045	73.11	0.6200	□
3	51	54:00	4.04	42	3.078	72.46	0.6138	△
3	52	54:19	3.63	37	3.078	72.46	0.6135	△
3	53	54:40	3.15	32	3.057	72.37	0.6131	△
3	54	54:57	2.78	29	3.057	72.37	0.6128	△
3	55	55:21	2.35	24	3.042	72.19	0.6123	△
3	56	55:41	2.05	21	3.042	72.19	0.6119	△
3	57	56:13	1.43	15	3.042	72.09	0.6114	△
3	58	56:32	1.17	12	3.042	72.09	0.6110	△

TABLE II.- SUMMARY OF RESULTS OF VORTEX WAKE ANALYSIS.

Vortex	Section No.	Vortex Coordinates		Vortex Span (m)	Vortex Wake Inclination (degs.)	Symbols Used In Figs. 44, 45 & 46
		y (m)	z (m)			
1	38	2.76	0.87	6.57	4.5	○
2		9.31	1.39			
1	39	5.77	0.96	9.77	-0.11	○
2		15.54	0.94			
1	40	6.03	0.05	6.68	1.23	○
2		12.71	0.20			
1	41	---	--	--	--	
2		---	--	--	--	
1	42	10.31	0.94	7.02	0.80	○
2		17.33	1.03			
1	43	---	--	--	--	
2		---	--	--	--	
1	44	6.45	0.39	9.17	3.75	□
2		15.62	0.99			
1	45	7.72	1.19	9.53	1.58	□
2		17.24	1.45			
1	46	5.59	0.08	8.10	0.80	□
2		13.69	0.19			
1	47	5.31	1.37	7.54	0.16	□
2		12.85	1.39			
1	48	2.73	0.14	7.89	7.32	□
2		10.64	1.14			
1	49	4.47	0.33	6.89	-6.19	□
2		11.32	-0.41			
1	50	5.58	-2.14	9.28	2.66	□
2		14.85	-1.71			
1	51	2.04	0.99	8.59	6.74	△
2		10.57	2.00			
1	52	4.74	1.61	7.55	-1.06	△
2		12.29	1.47			
1	53	3.03	1.20	8.59	-0.69	△
2		11.62	1.09			
1	54	5.00	1.16	7.55	-5.17	△
2		12.52	0.48			
1	55	4.70	0.27	7.27	-1.37	△
2		11.96	0.09			
1	56	7.62	-0.25	7.85	2.27	△
2		15.46	0.06			
1	57	---	--	--	--	
2		---	--	--	--	
1	58	6.35	-0.16	7.61	1.70	△
2		13.96	-0.07			

TABLE III.- MINIMUM PROBE-TO-VORTEX CENTER DISTANCES AND CORRESPONDING NORMALIZED VELOCITIES.

Vortex	Cross Section	r_{min} (m)	$\frac{V_R}{V_\infty C_L}$ at r_{min}
1	38	0.335	0.222
2		0.991	0.113
1	39	1.200	0.083
2		1.393	0.163
1	40	0.104	0.424
2		0.296	0.259
1	42	0.018	0.500
2		0.252	0.280
1	44	0.317	0.060
2		0.512	0.059
1	45	0.789	0.080
2		0.948	0.115
1	46	0.503	0.232
2		0.064	0.292
1	47	0.863	0.116
2		0.637	0.282
1	48	0.256	0.264
2		0.732	0.166
1	49	0.393	0.382
2		0.177	0.357
1	50	0.999	0.131
2		1.061	0.113
1	51	0.515	0.051
2		1.228	0.171
1	52	0.613	0.155
2		0.780	0.085
1	53	1.005	0.088
2		0.887	0.150
1	54	0.418	0.233
2		0.073	0.315
1	55	0.905	0.153
2		0.841	0.153
1	56	0.098	0.416
2		0.140	0.360
1	58	0.119	0.427
2		0.064	0.291

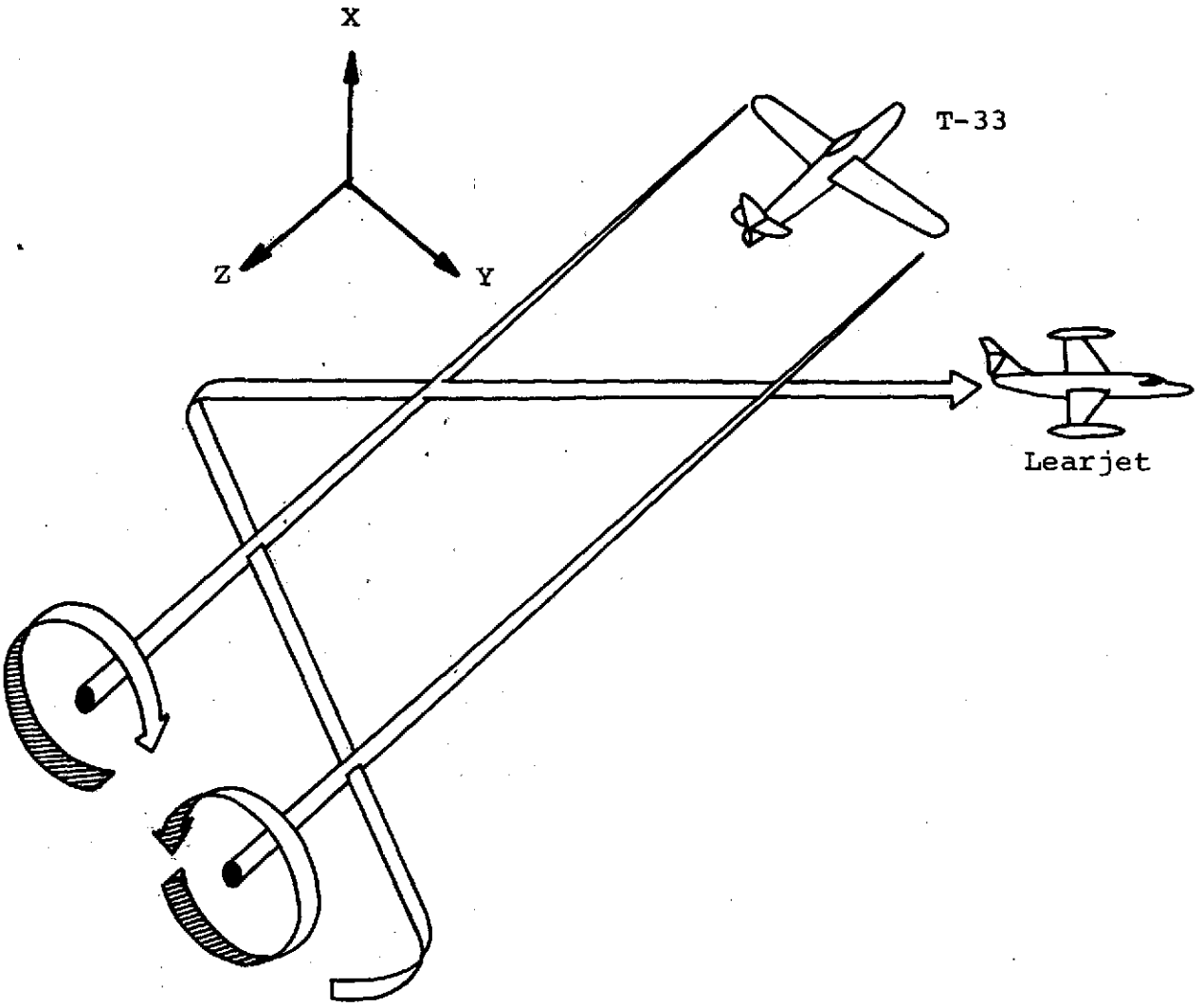

Figure 1.- Method of Probing the Vortex Wake.

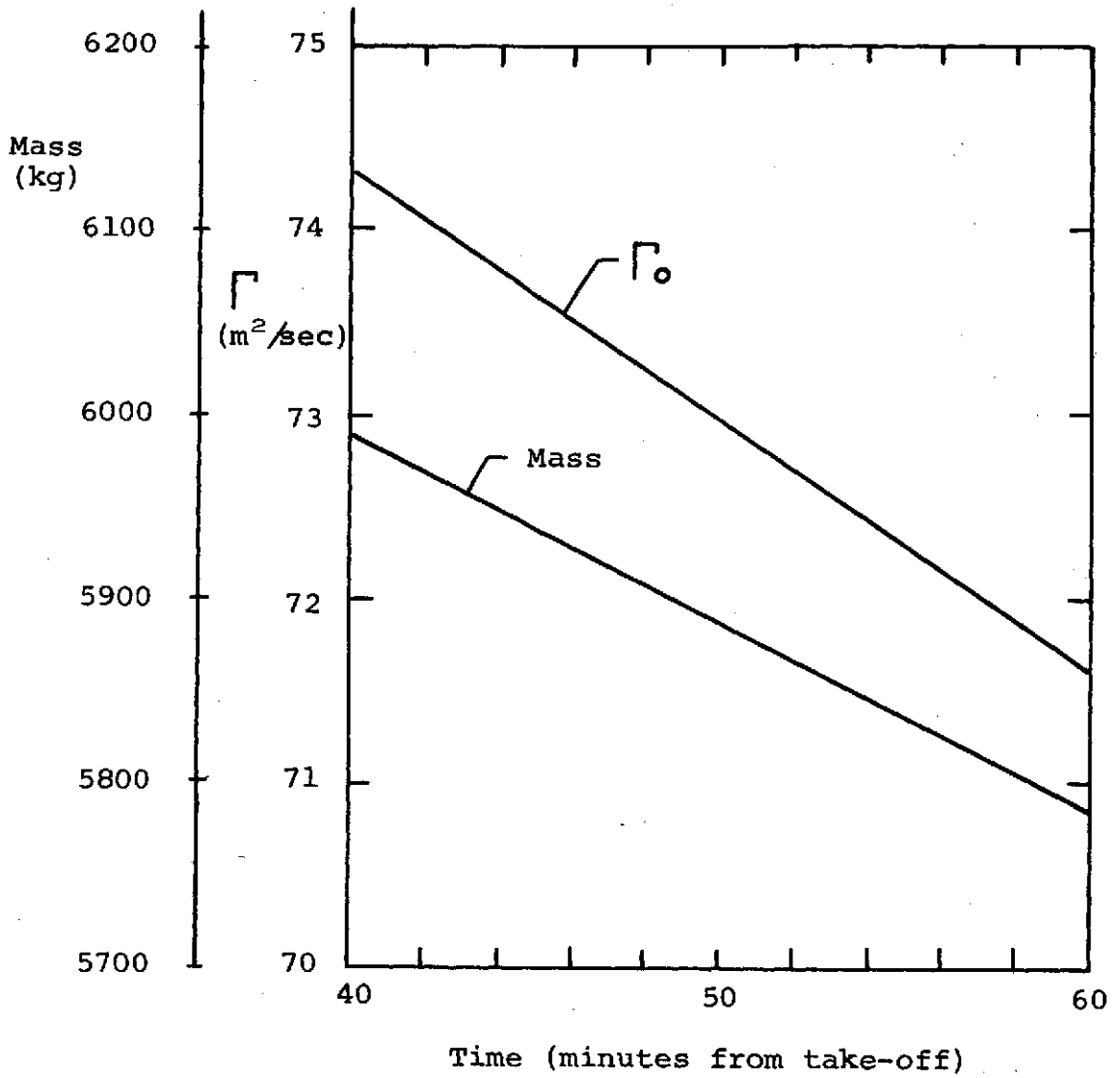

Figure 2.- Mass and theoretical circulation of T-33.

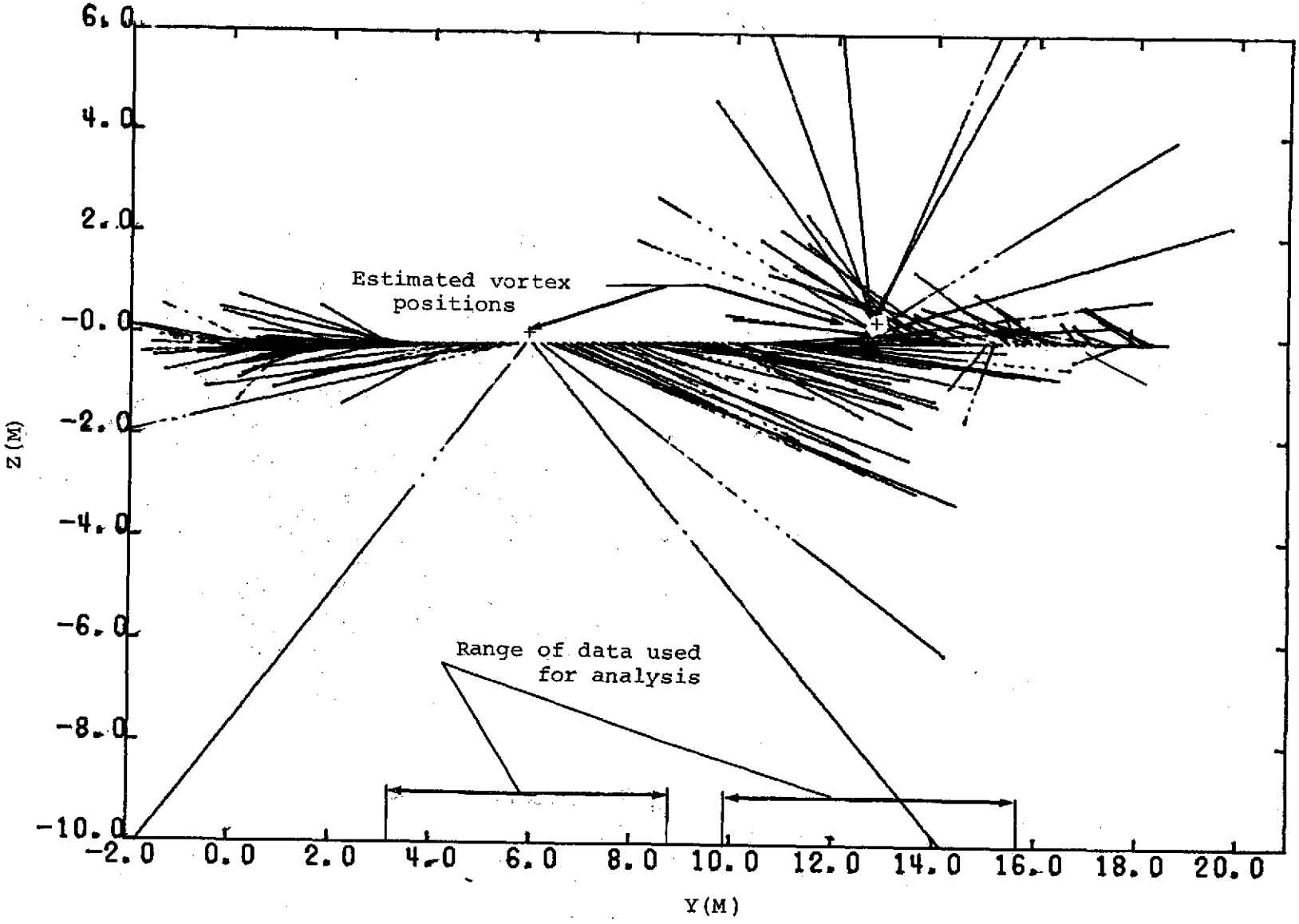

Figure 3.- Plot of normals to velocity vectors for Section 40.

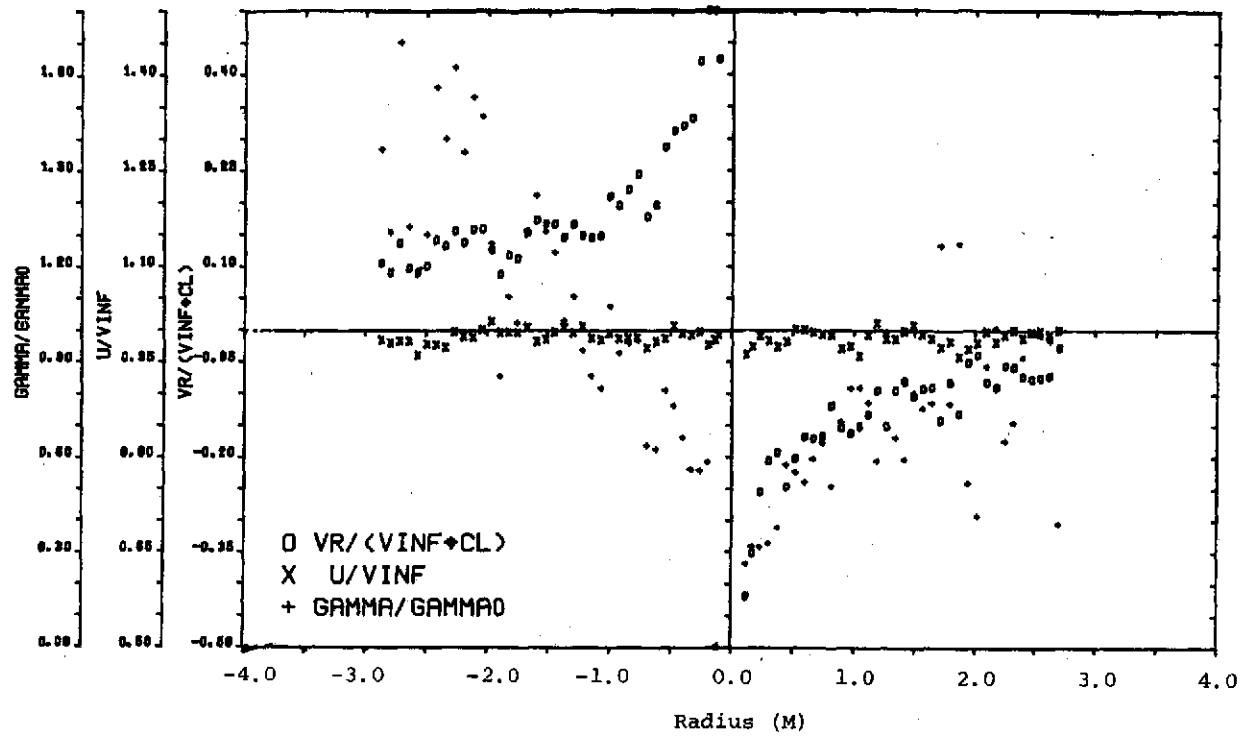

(a) Vortex 1.

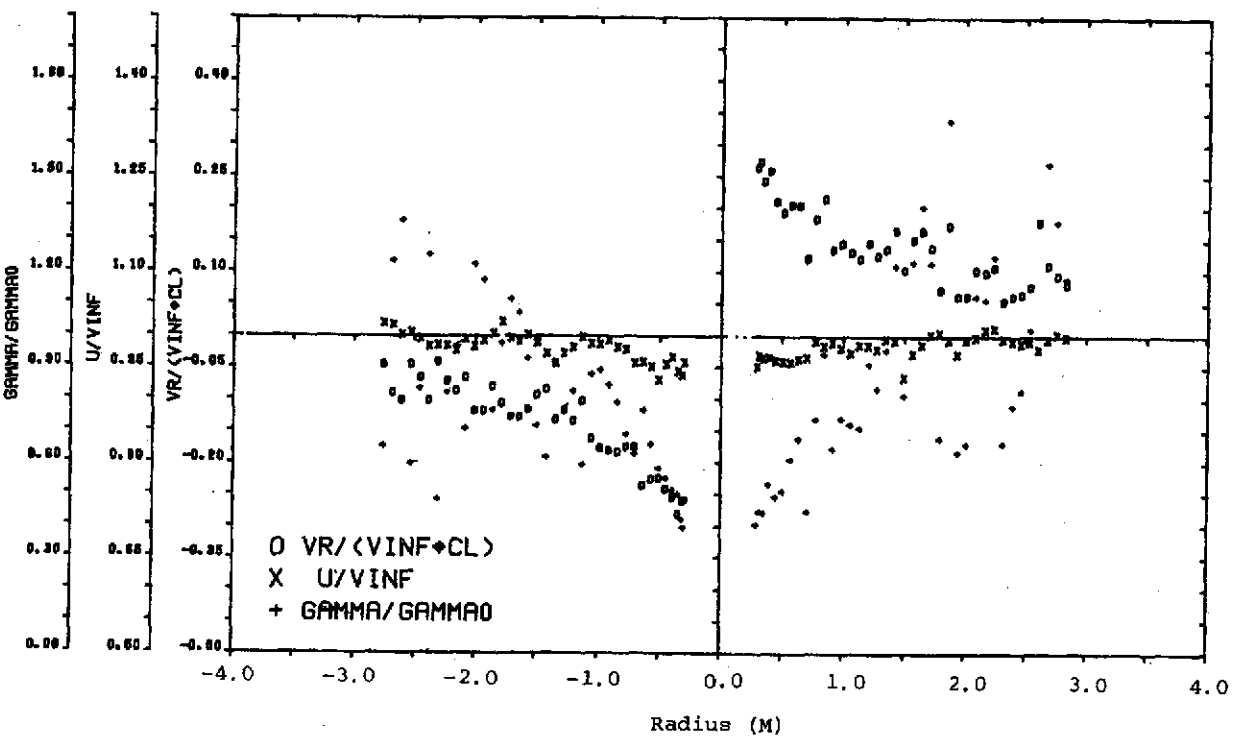

(b) Vortex 2.

Figure 4.- Velocity and circulation distributions from geometrical analysis for Section 40.

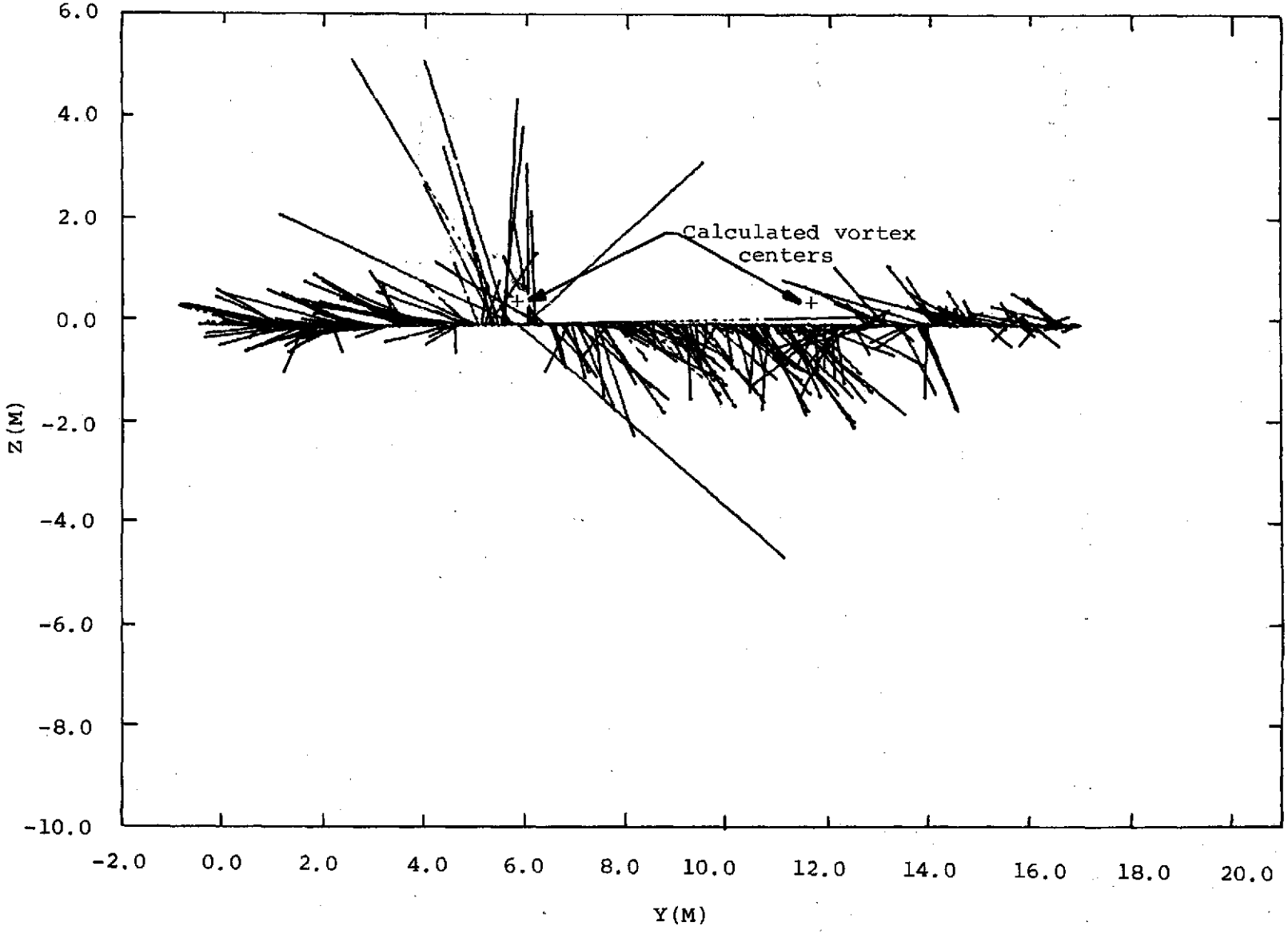

(a) Plot of normals to residual velocity.

Figure 5.- Results of least-squares analysis of vortices for Section 40.

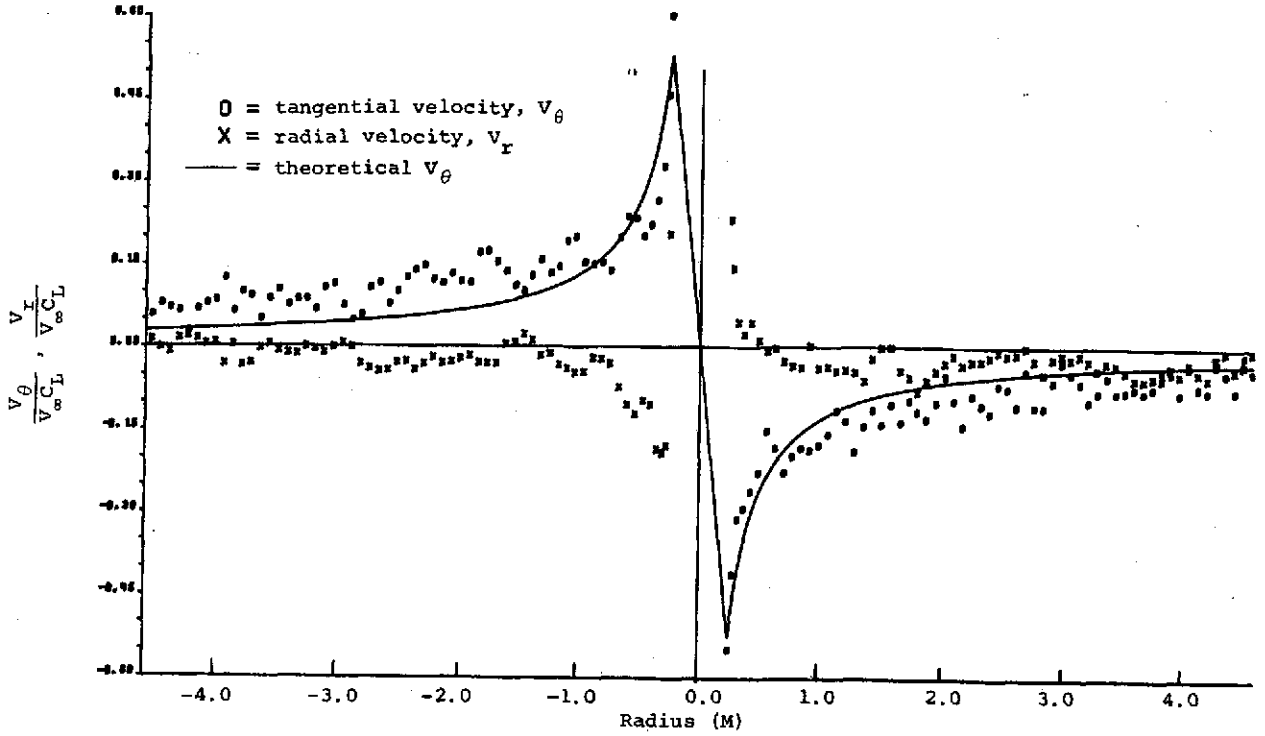

(b) Tangential and radial velocity components for vortex 1.

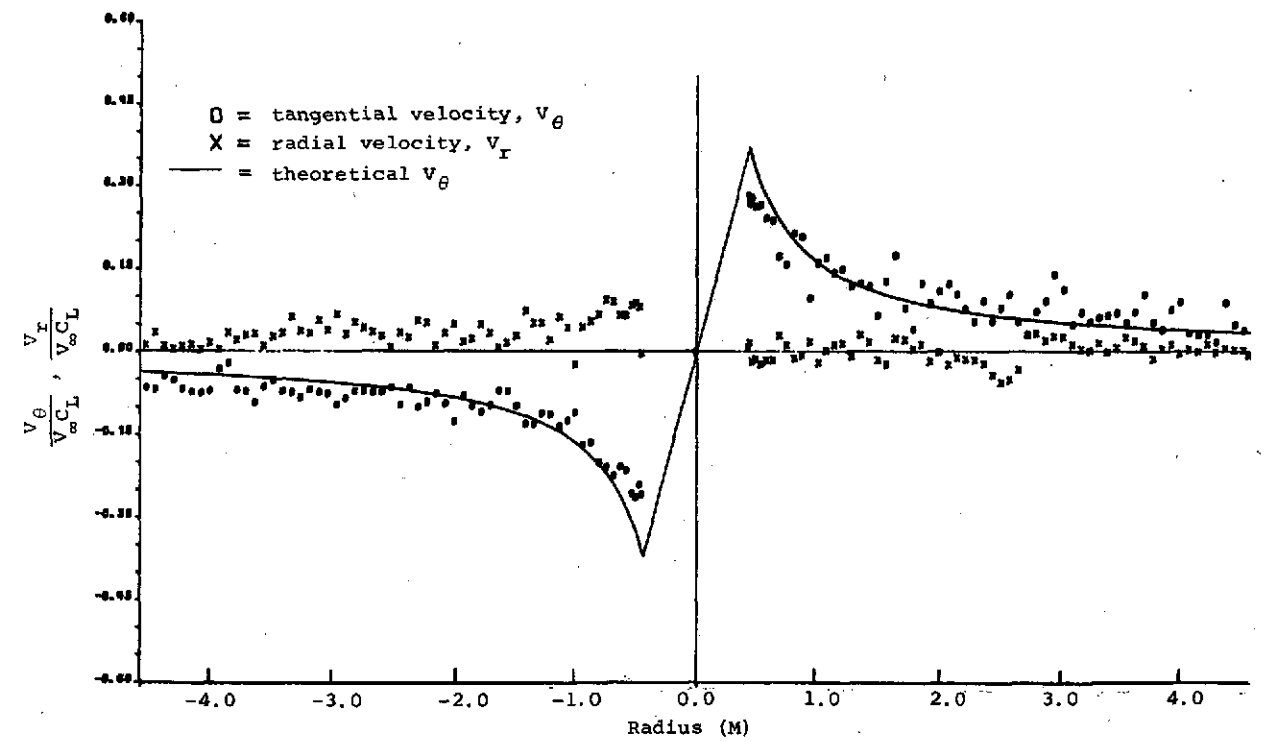

(c) Tangential and radial velocity components for vortex 2.

Figure 5.- Concluded.

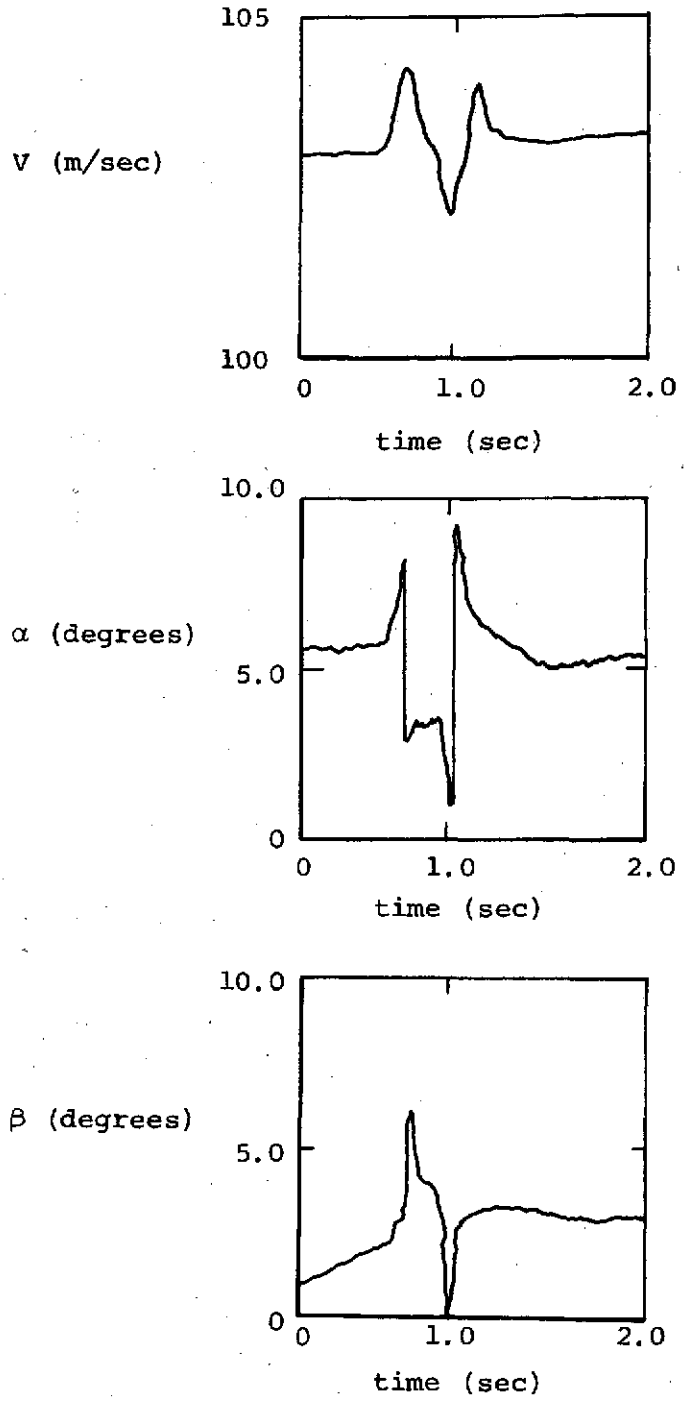

Figure 6.- Sketch of recorded variation of Learjet parameters through one wake.

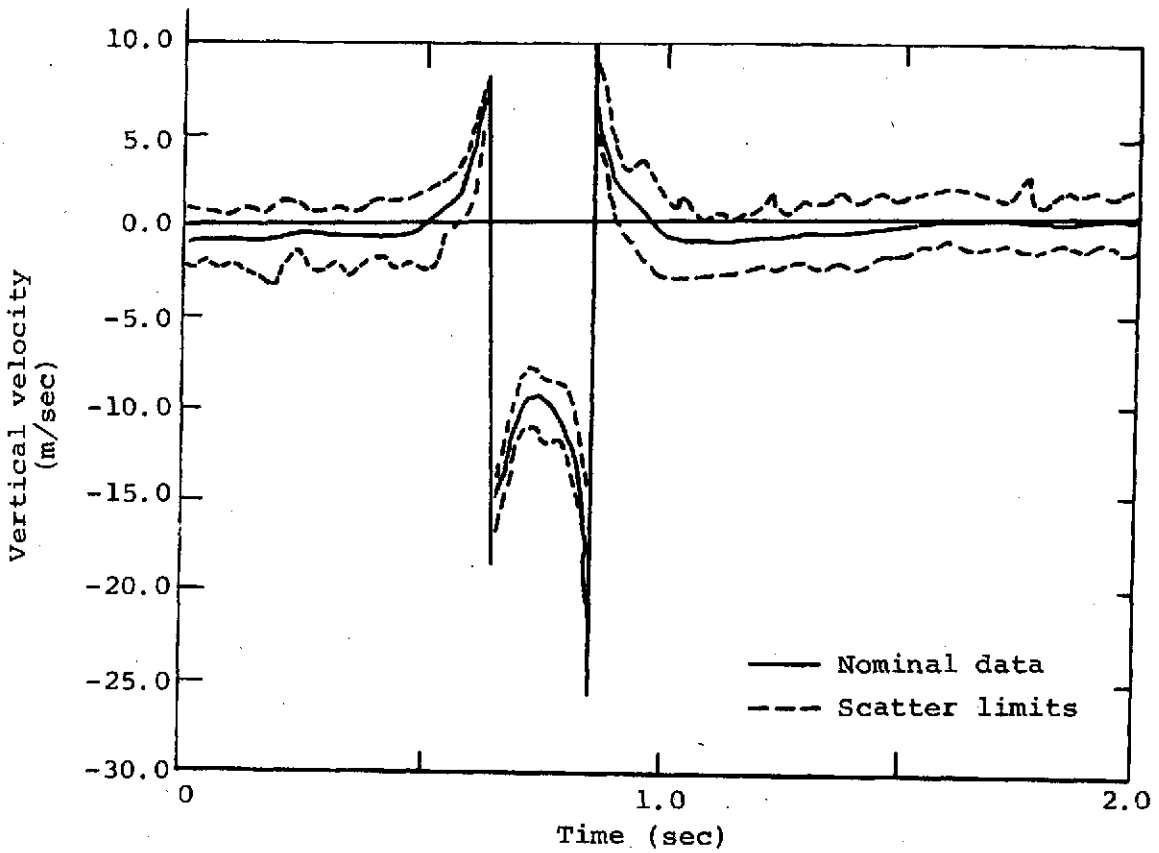

(a) Vertical velocity.

Figure 7.- Vortex velocity components.

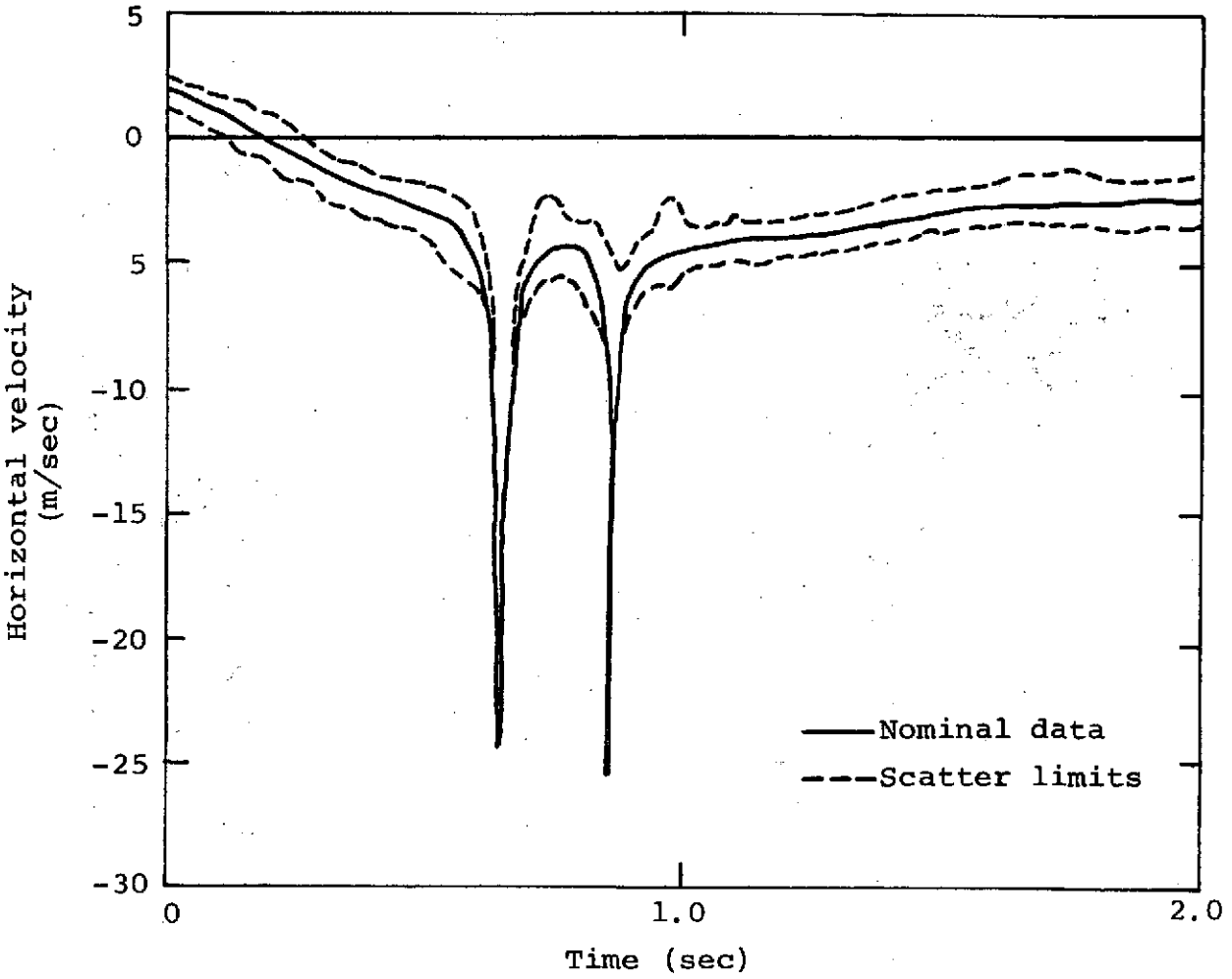

(b) Horizontal velocity.

Figure 7.- Concluded.

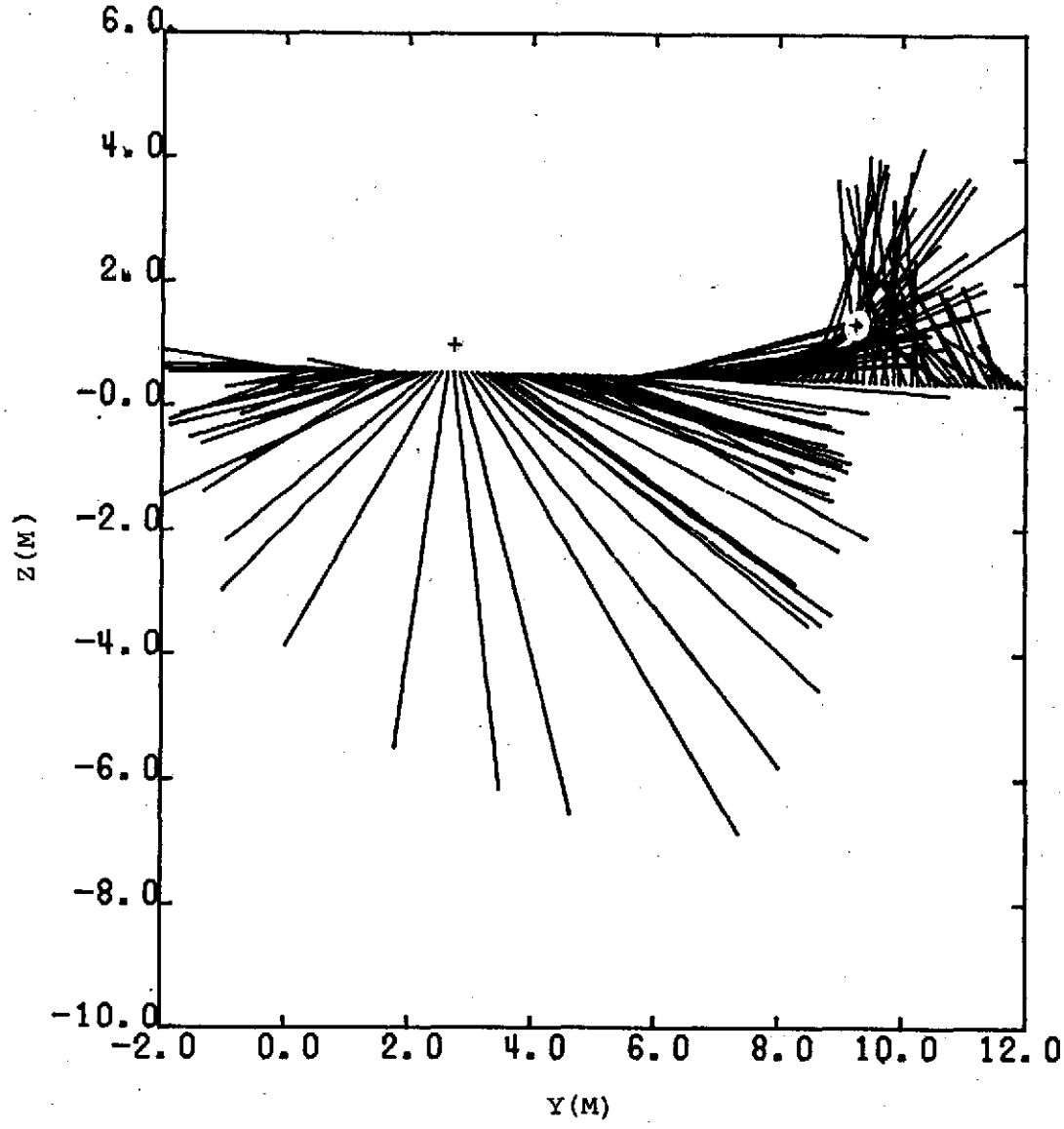

Figure 8.- Plot of normals to velocity vectors for Section 38.

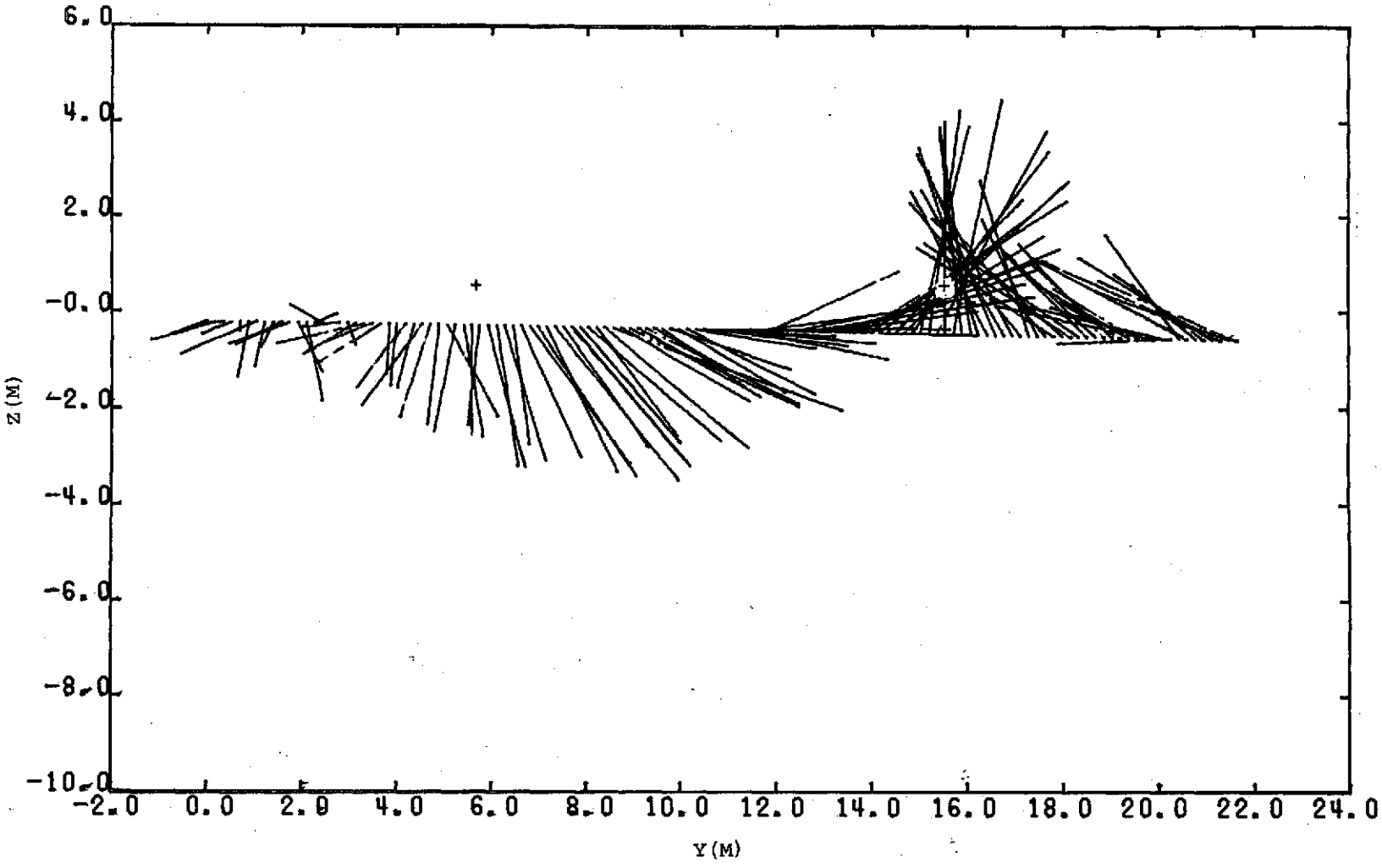

Figure 9.- Plot of normals to velocity vectors for Section 39.

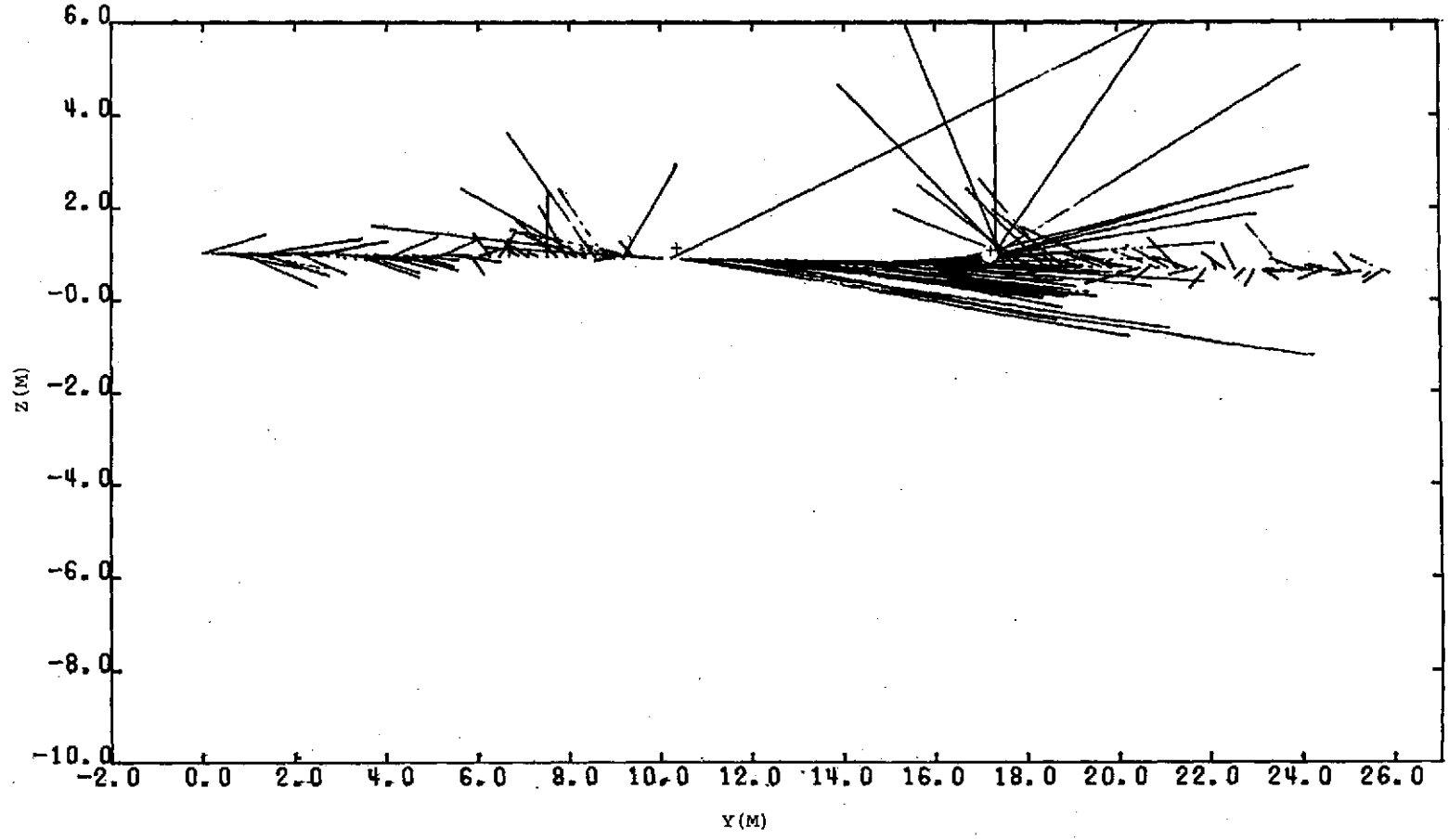

Figure 10.- Plot of normals to velocity vectors for Section 42.

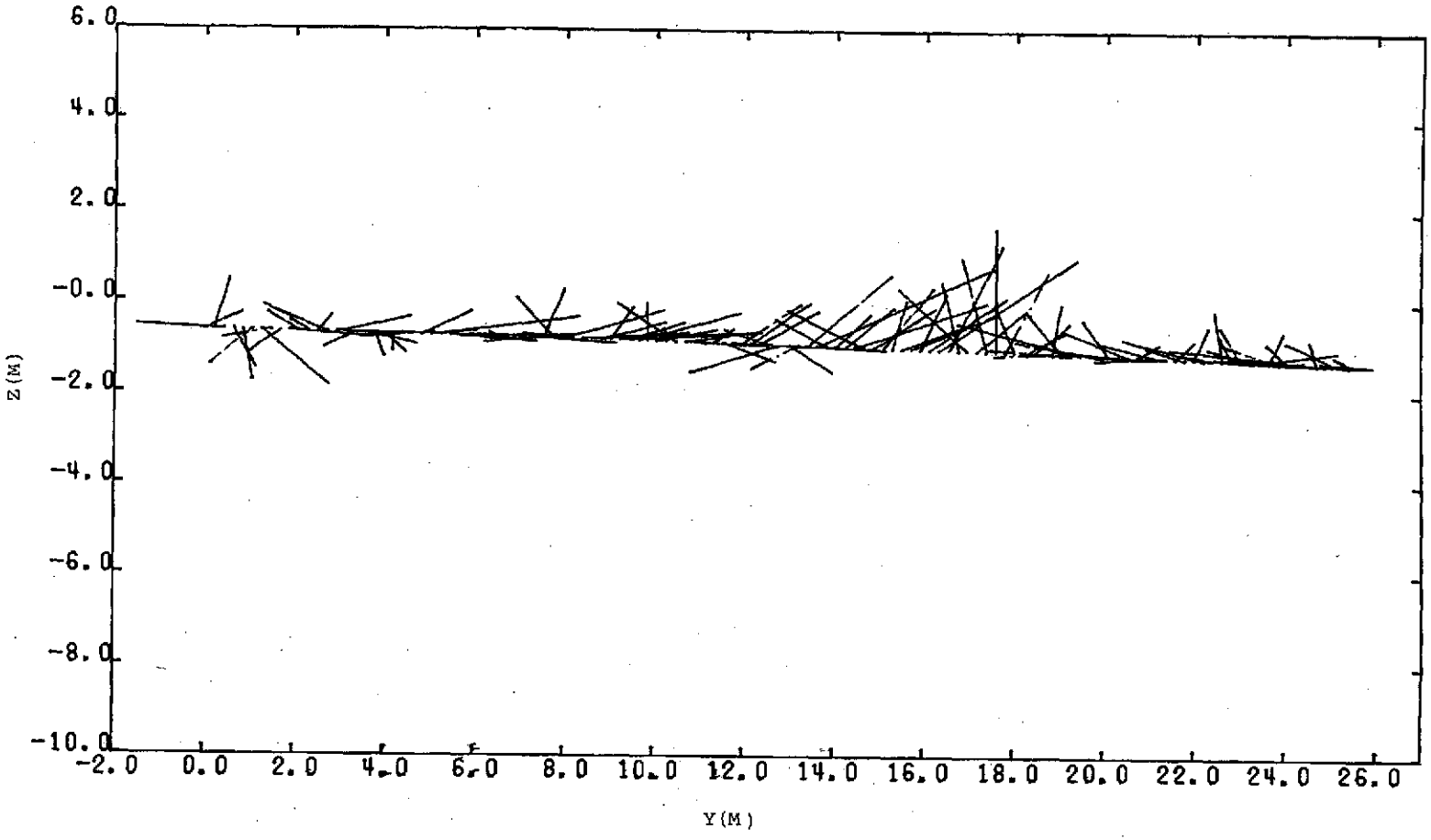

Figure 11.- Plot of normals to velocity vectors for Section 43.

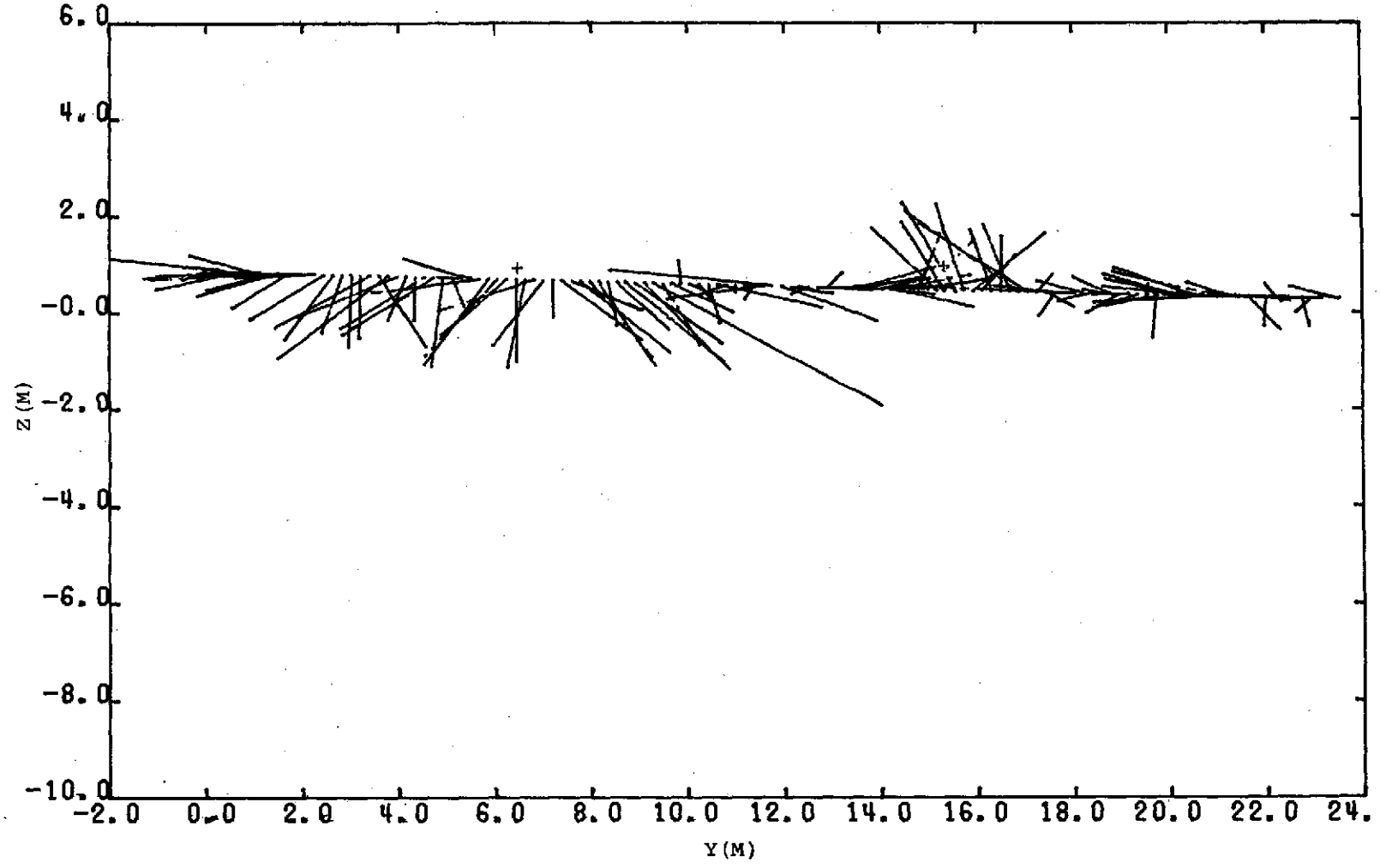

Figure 12.- Plot of normals to velocity vectors for Section 44.

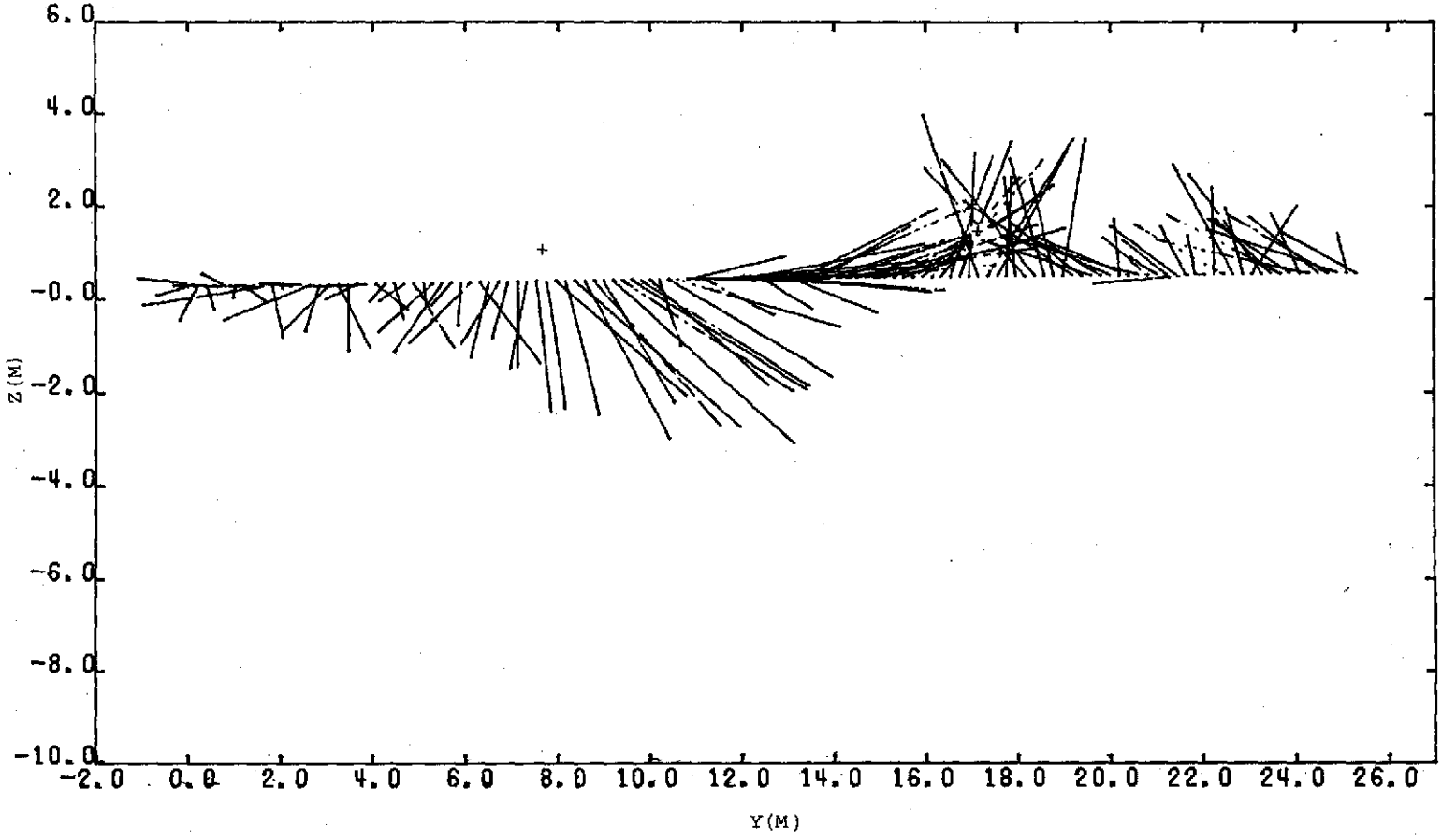

Figure 13.- Plot of normals to velocity vectors for Section 45.

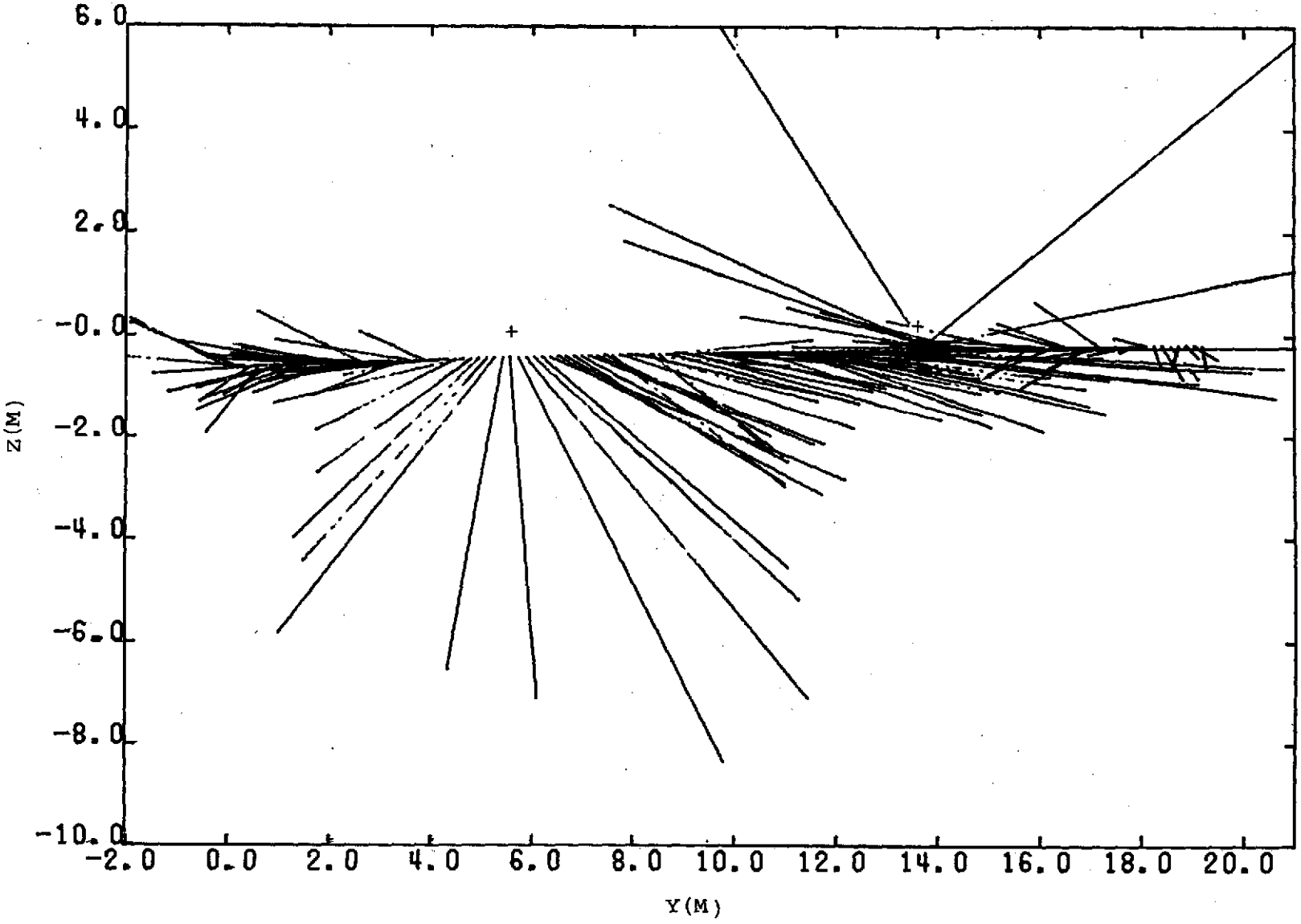

Figure 14.- Plot of normals to velocity vectors for Section 46.

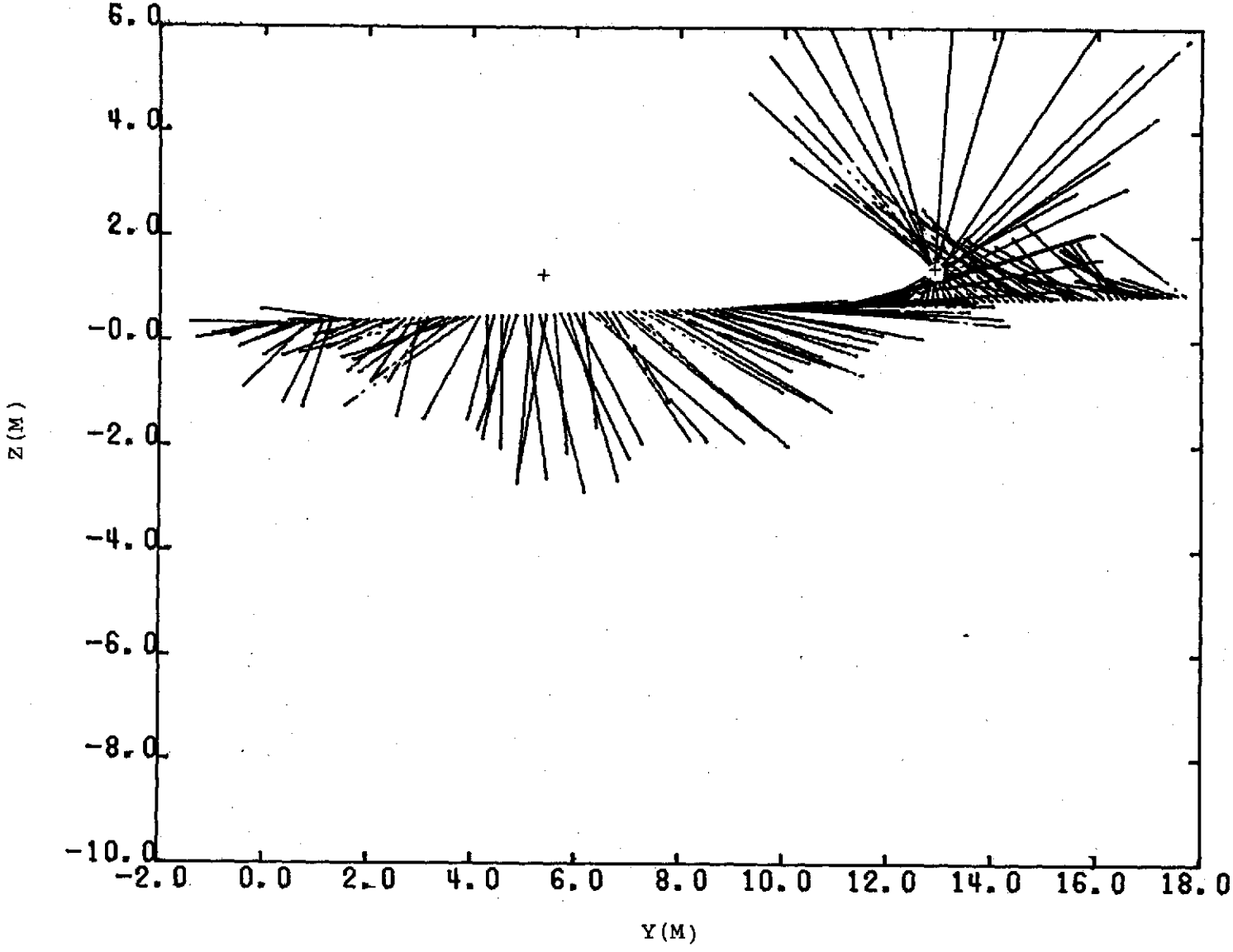

Figure 15.- Plot of normals to velocity vectors for Section 47.

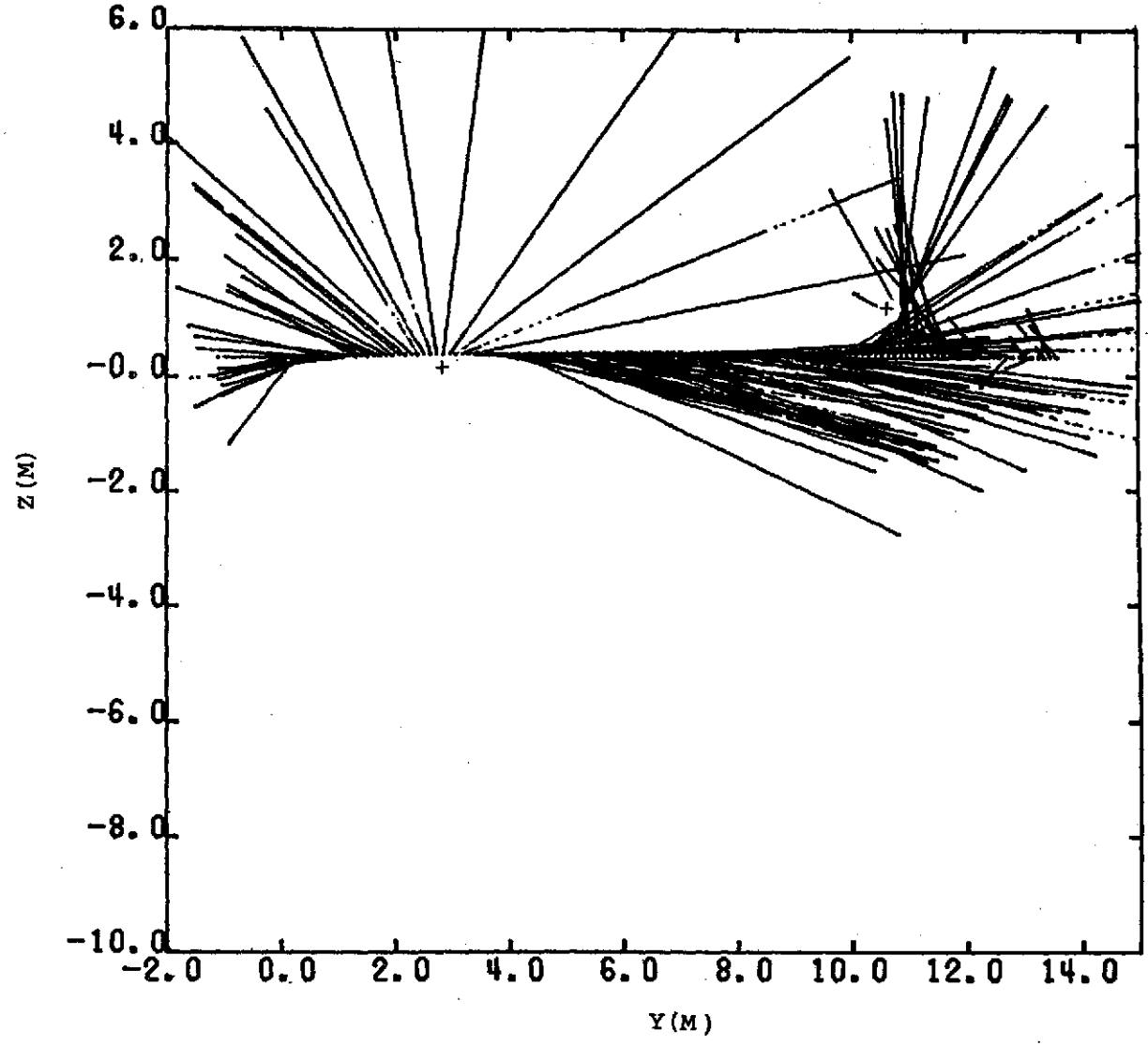

Figure 16.- Plot of normals to velocity vectors for Section 48.

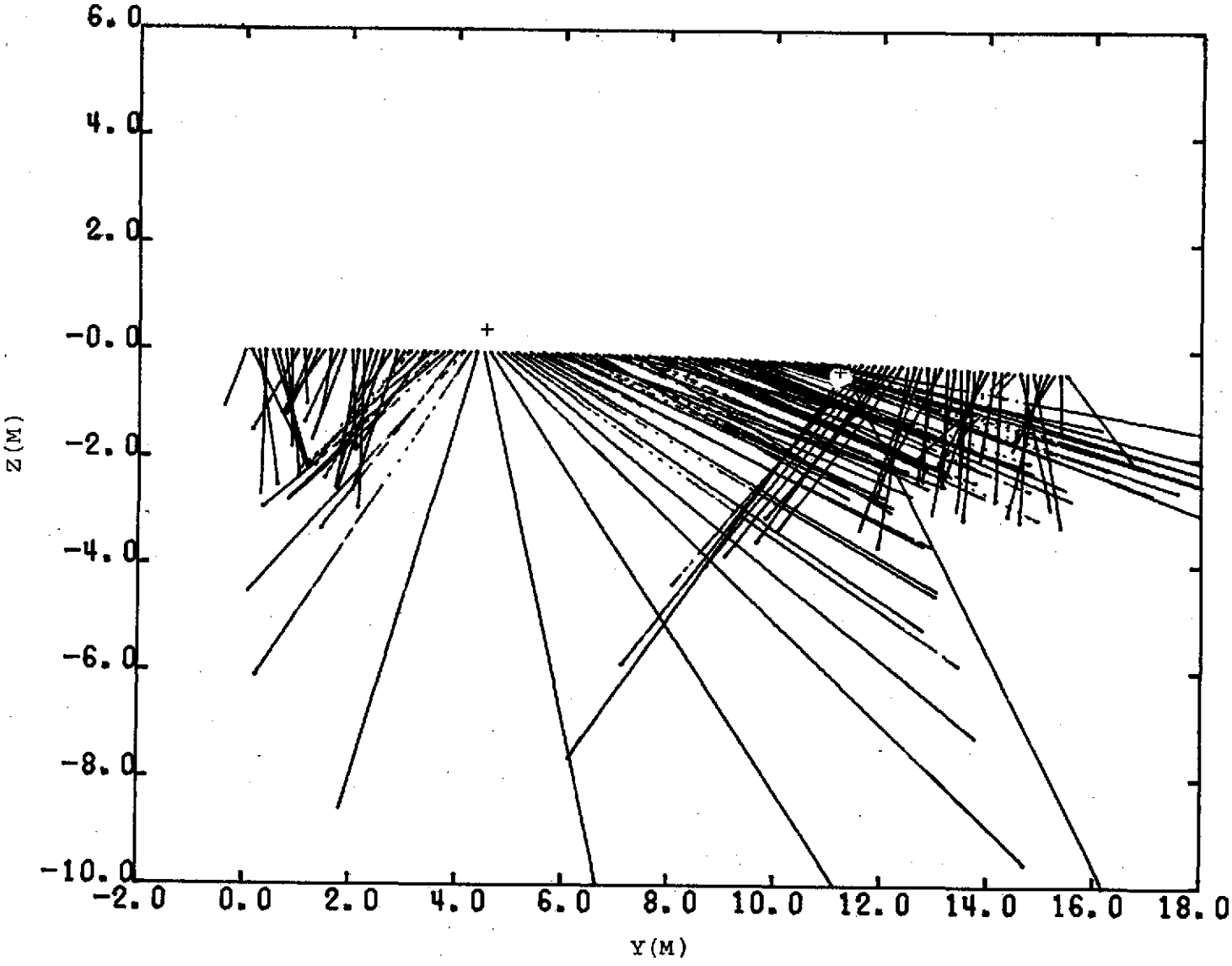

Figure 17.- Plot of normals to velocity vectors for Section 49.

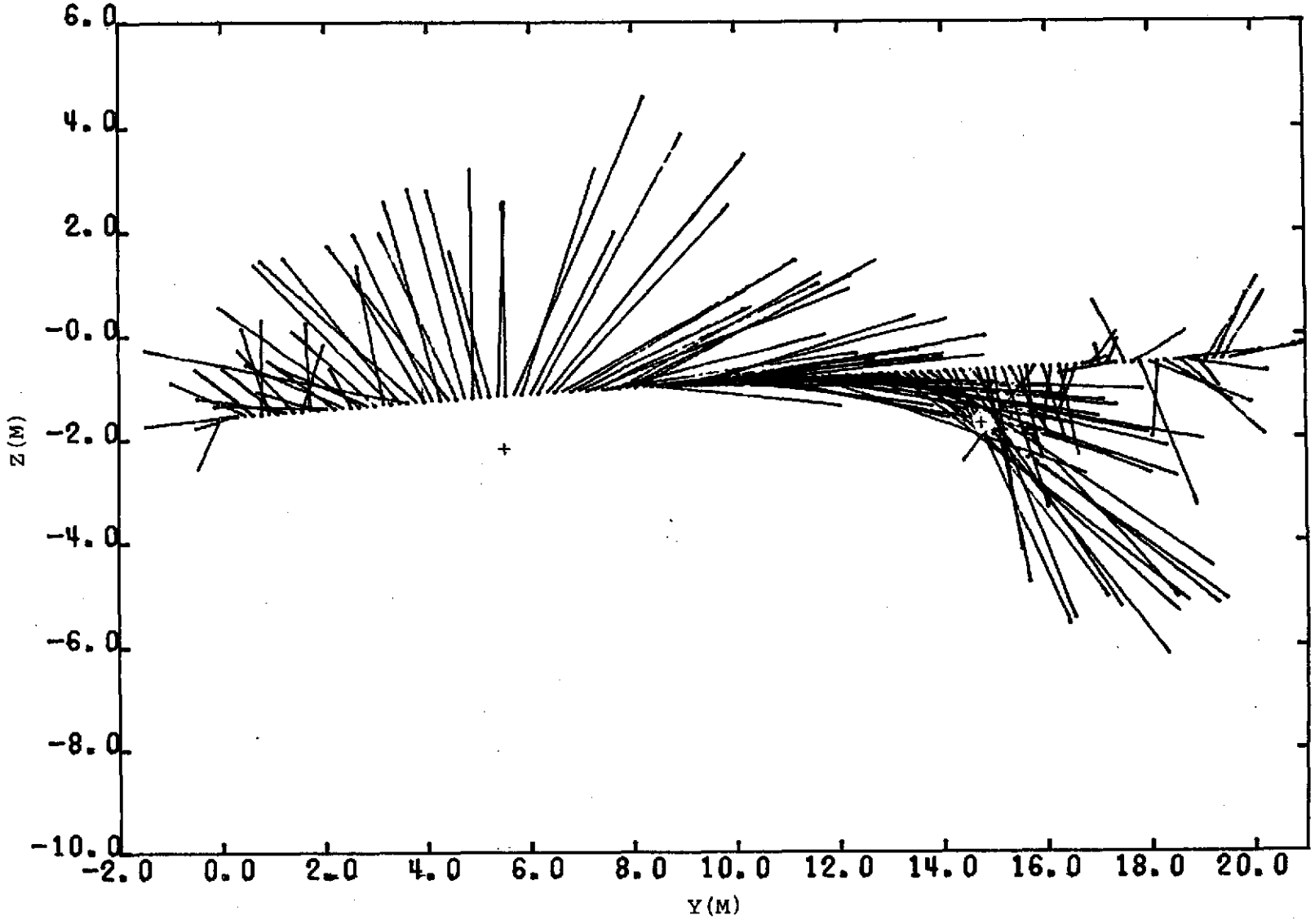

Figure 18.- Plot of normals to velocity vectors for Section 50.

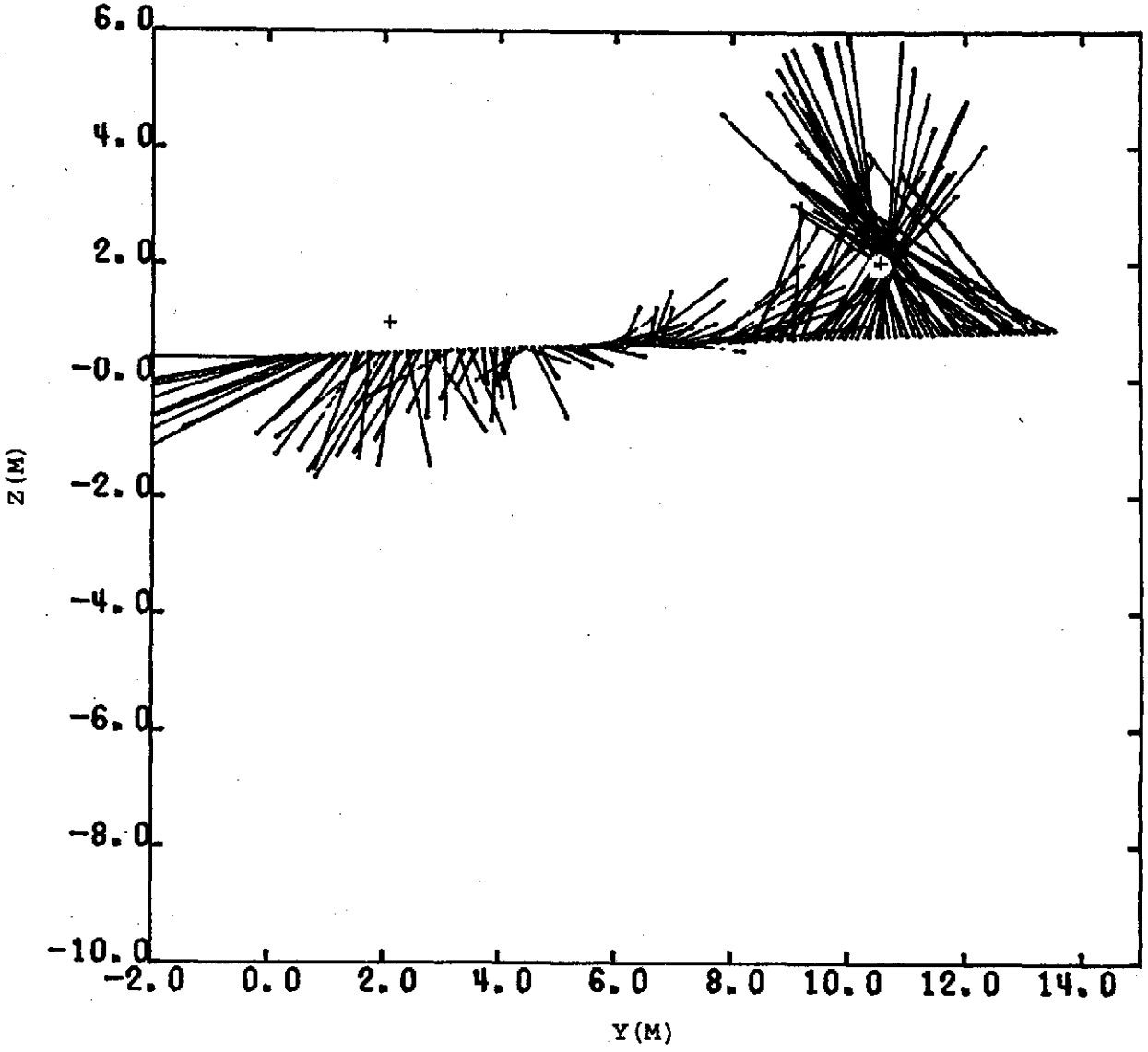

Figure 19.- Plot of normals to velocity vectors for Section 51.

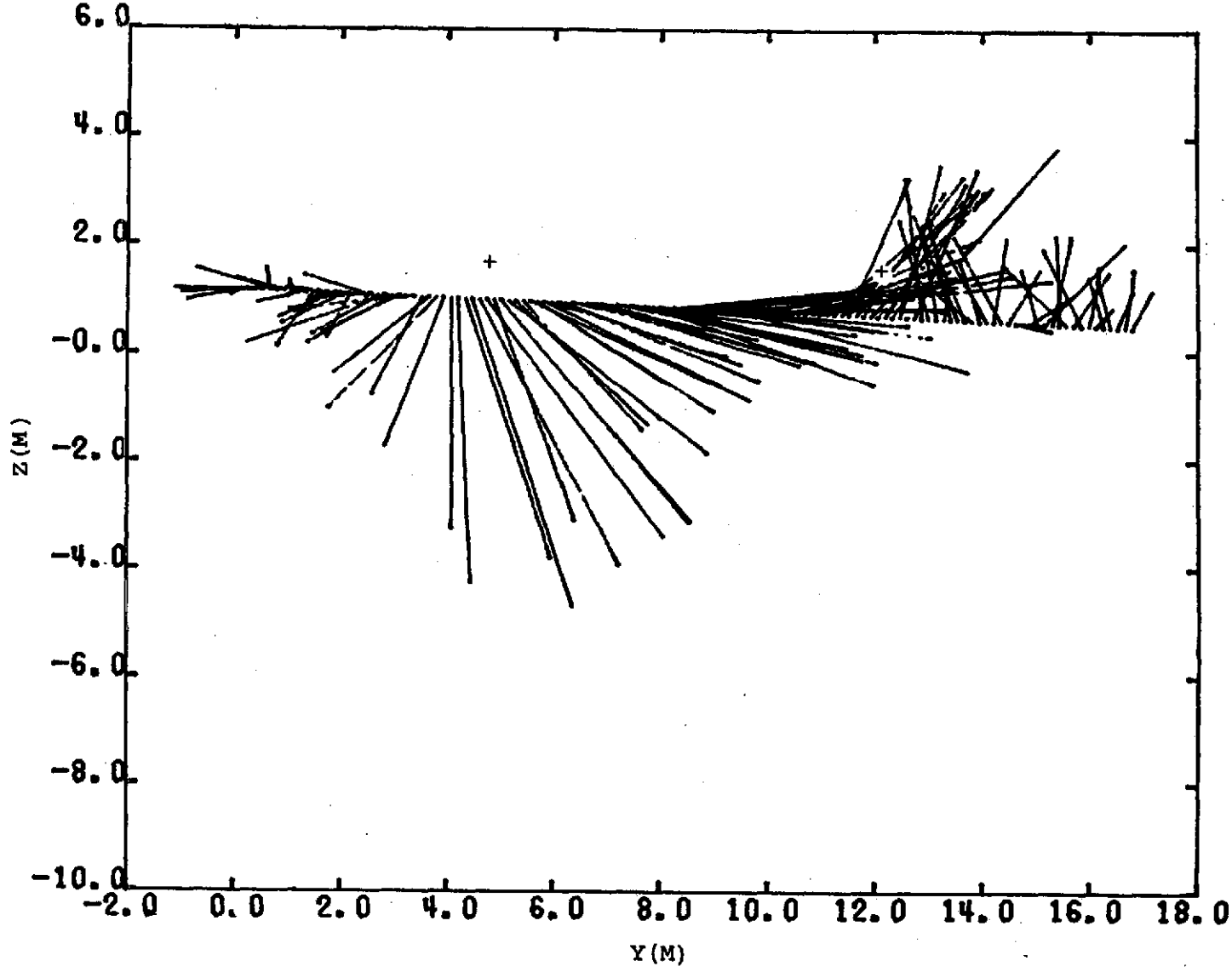

Figure 20.- Plot of normals to velocity vectors for Section 52.

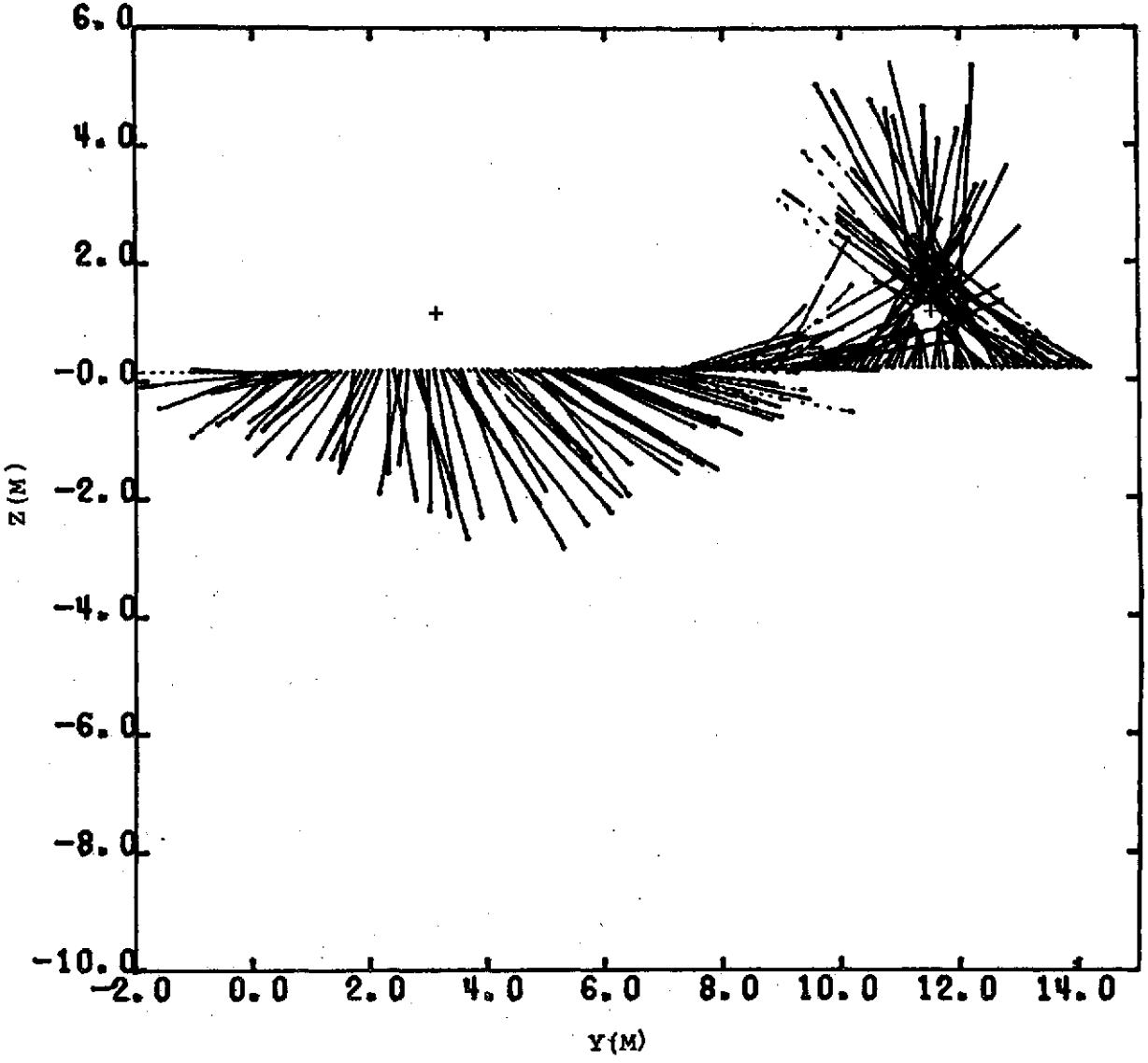

Figure 21.- Plot of normals to velocity vectors for Section 53.

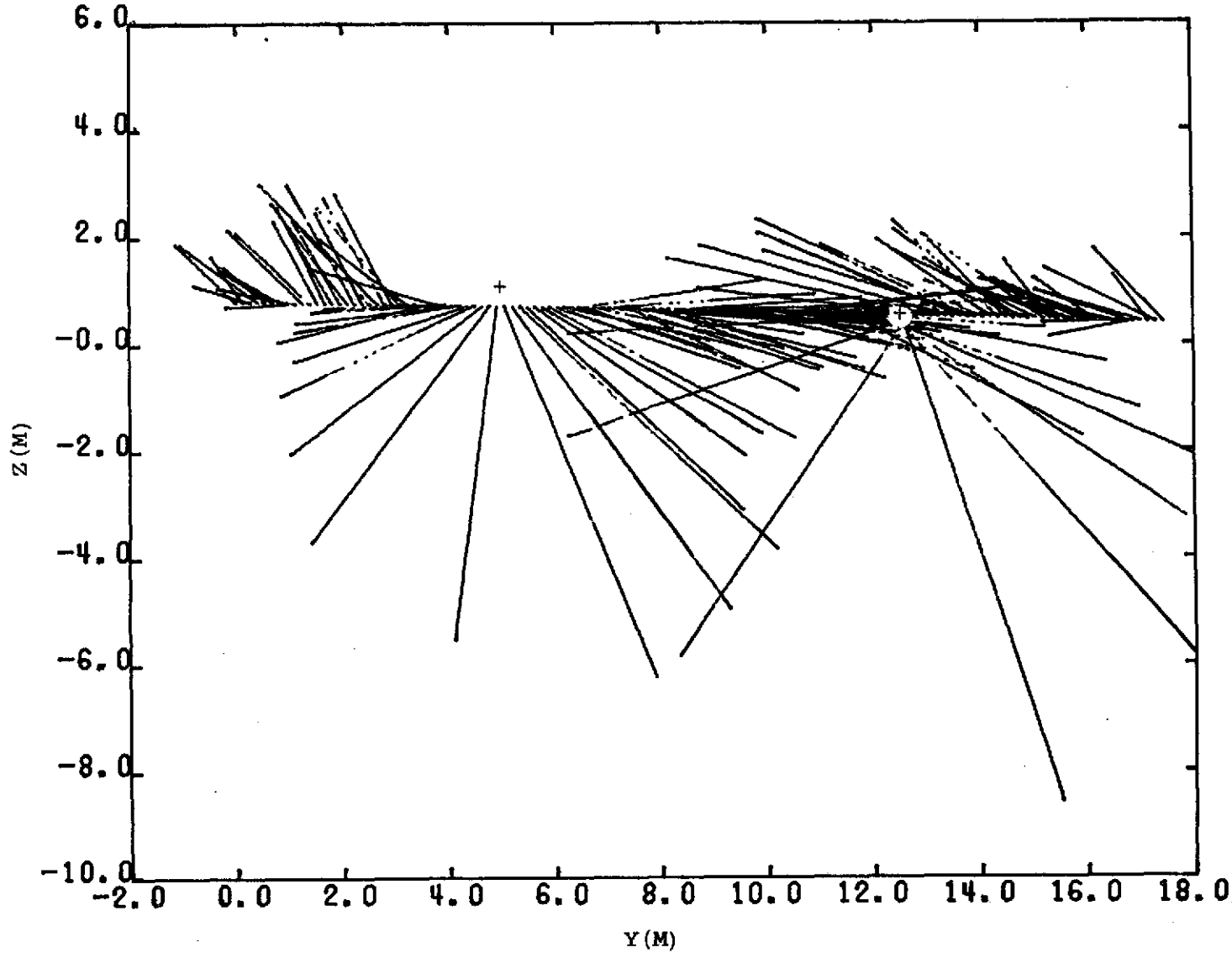

Figure 22.- Plot of normals to velocity vectors for Section 54.

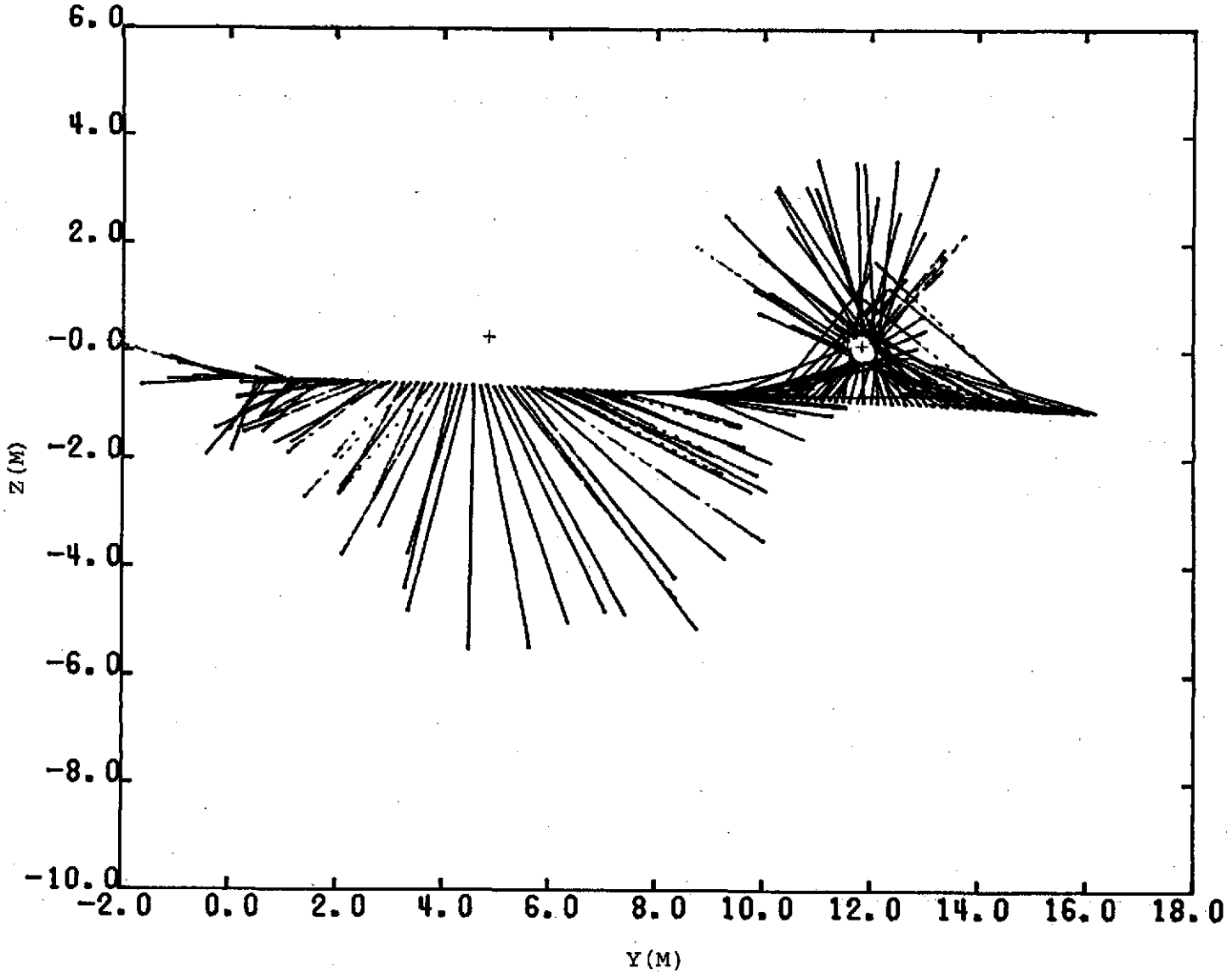

Figure 23.- Plot of normals to velocity vectors for Section 55.

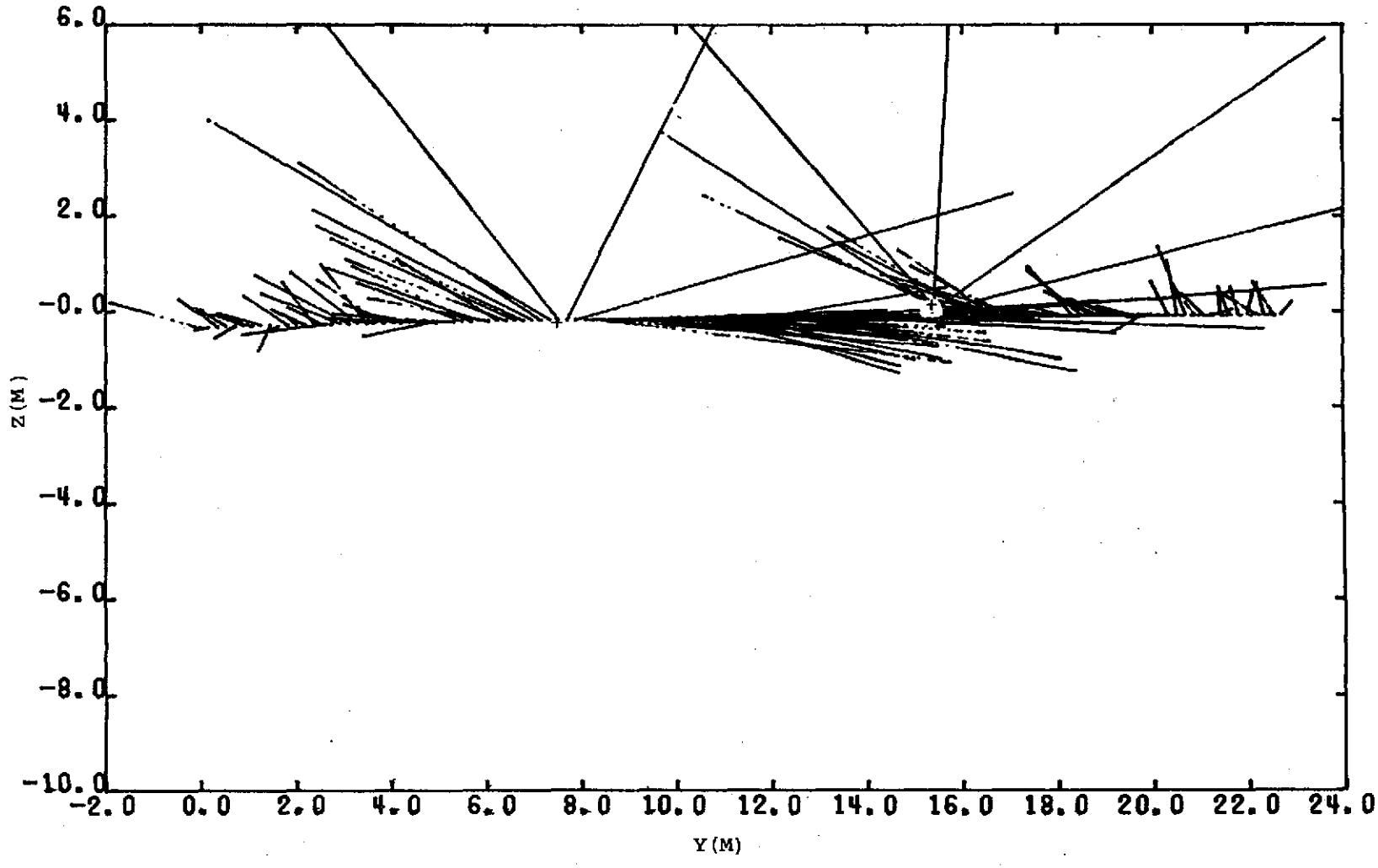

Figure 24.- Plot of normals to velocity vectors for Section 56.

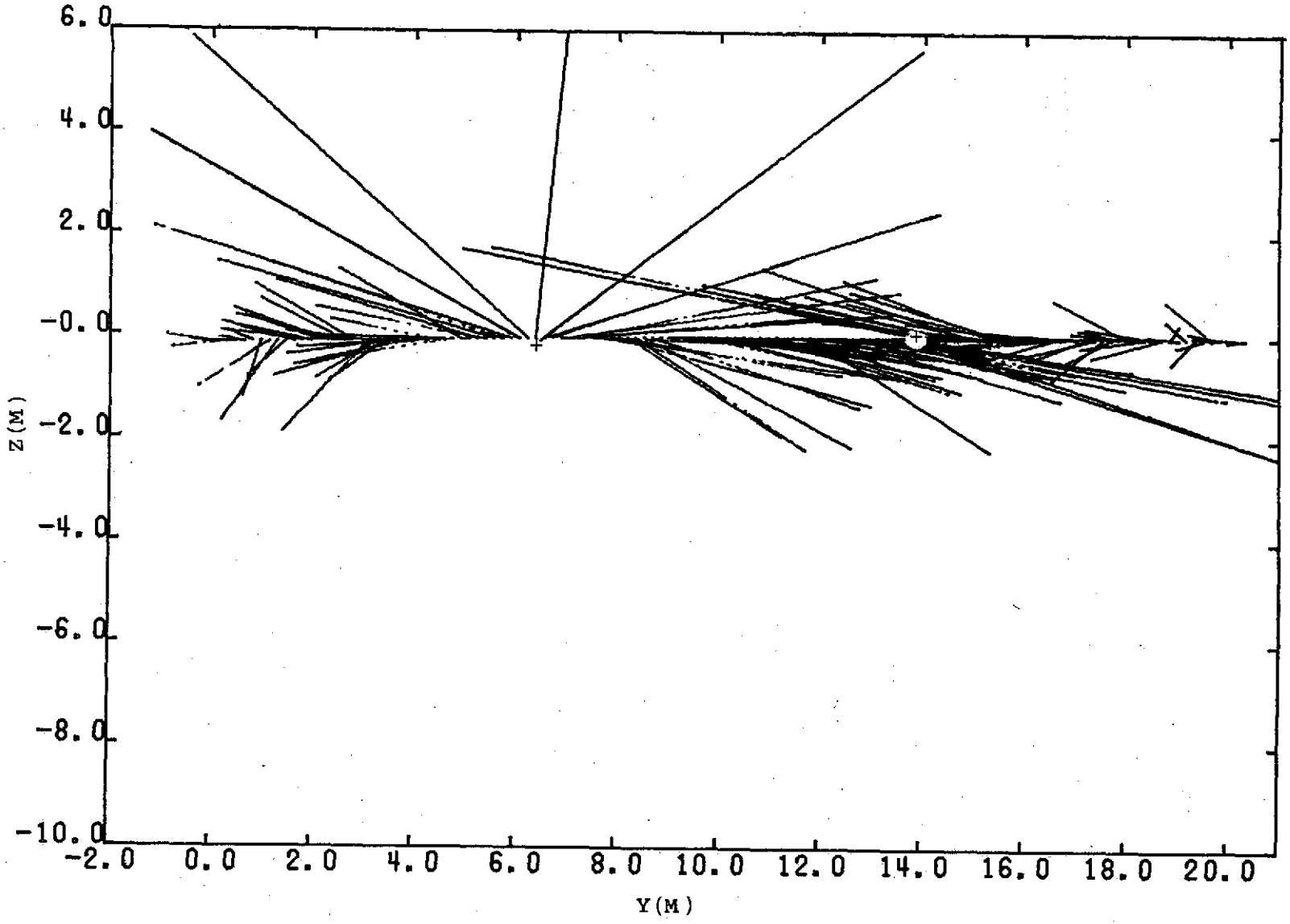

Figure 25.- Plot of normals to velocity vectors for Section 58.

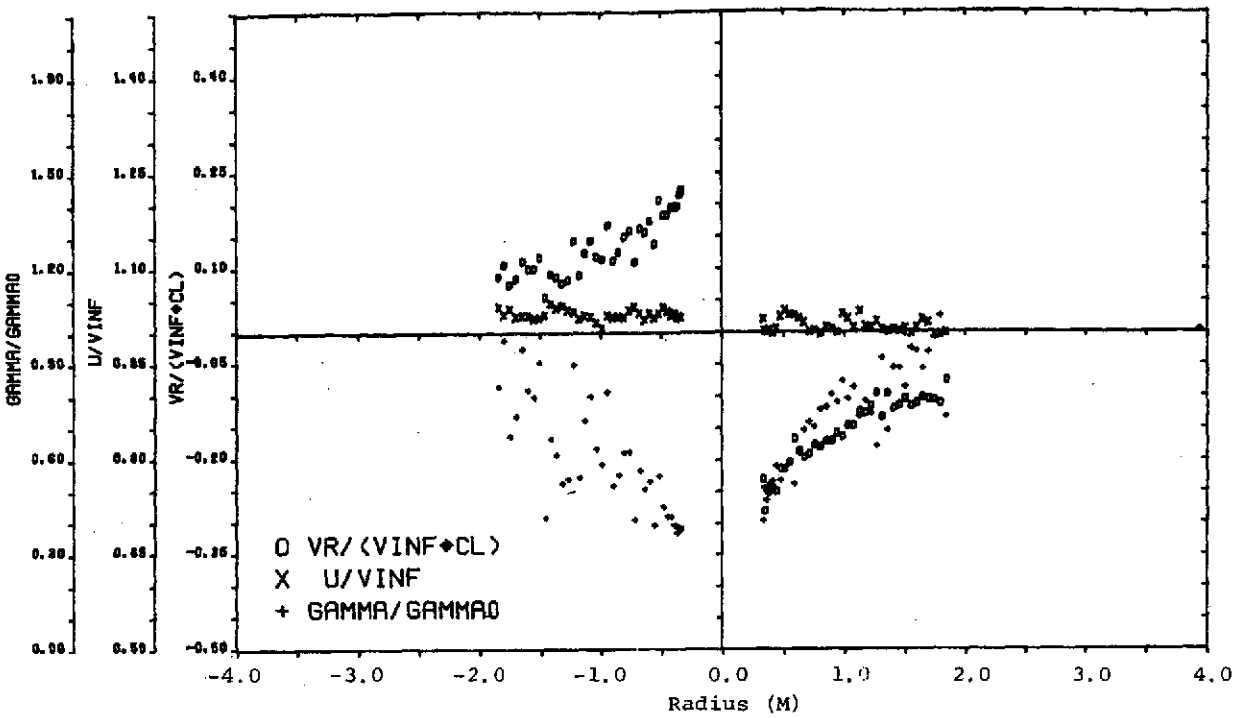

(a) Vortex 1.

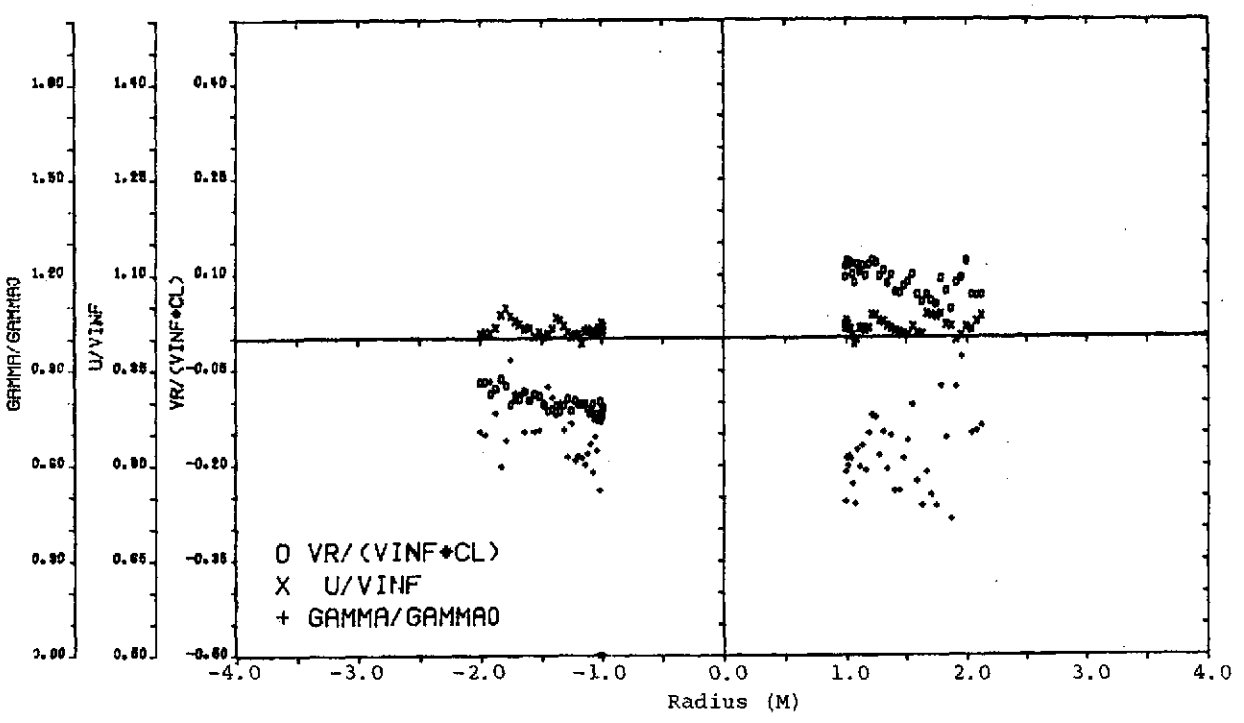

(b) Vortex 2.

Figure 26.- Velocity and circulation distributions for Section 38.

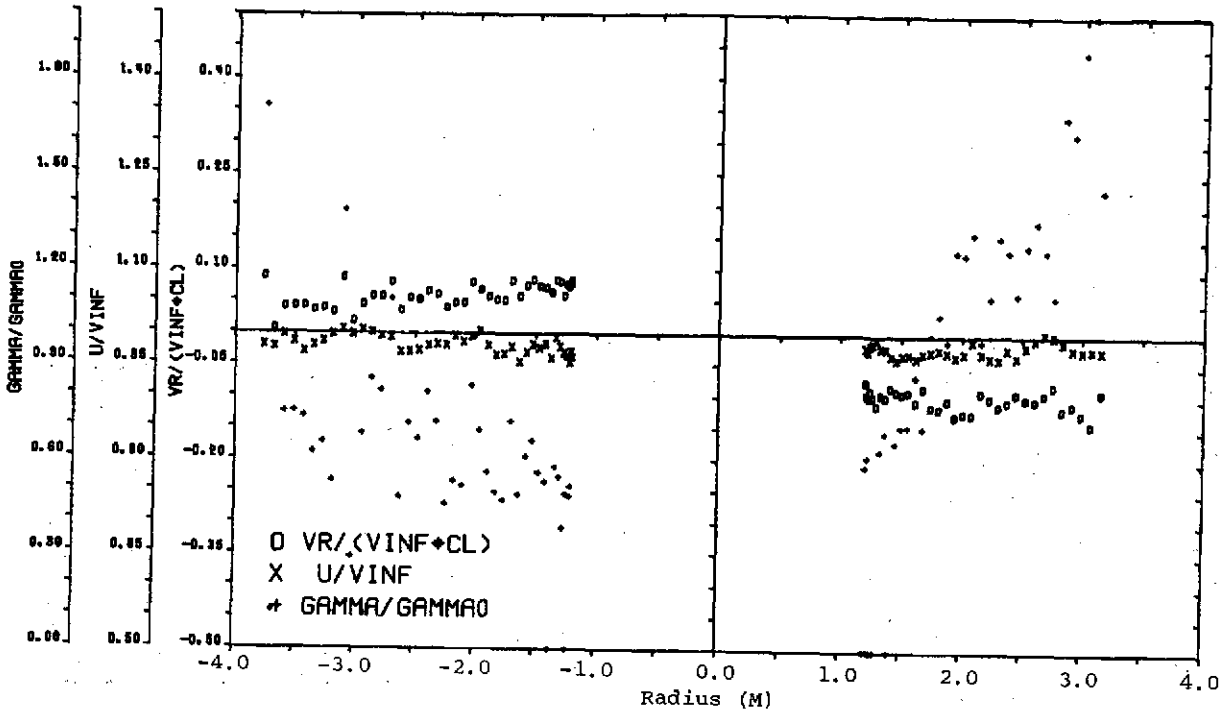

(a) Vortex 1.

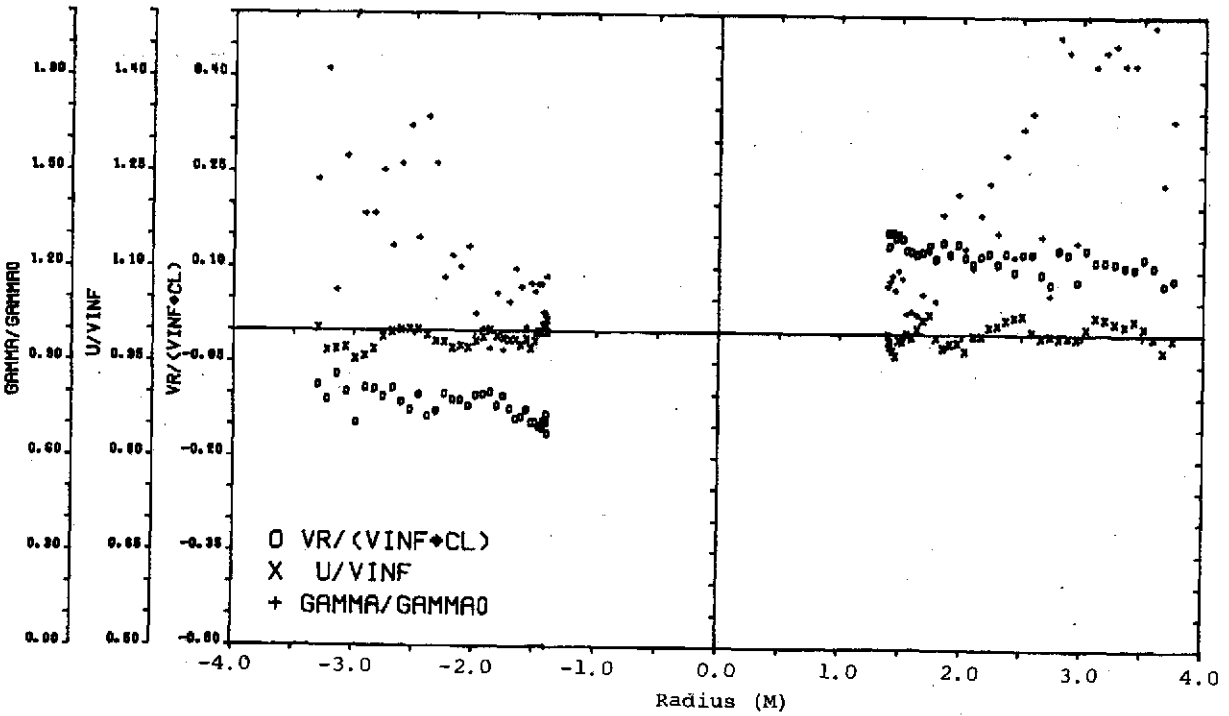

(b) Vortex 2.

Figure 27.- Velocity and circulation distributions for Section 39.

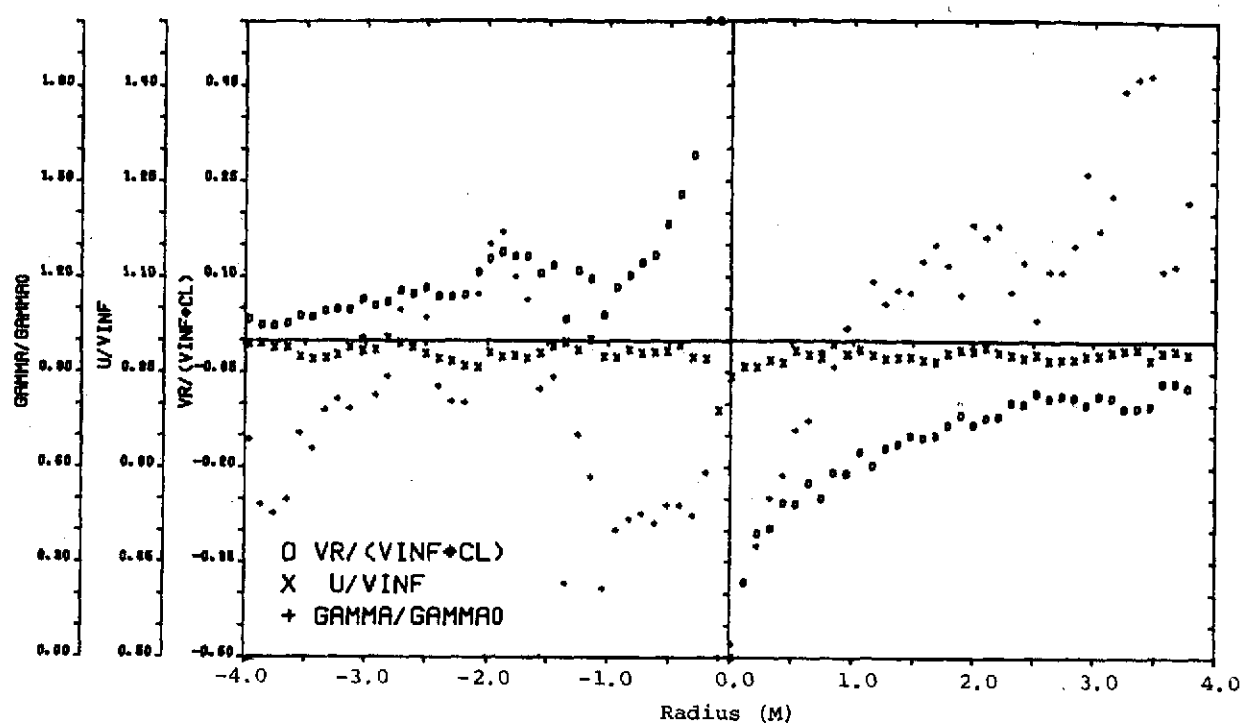

(a) Vortex 1.

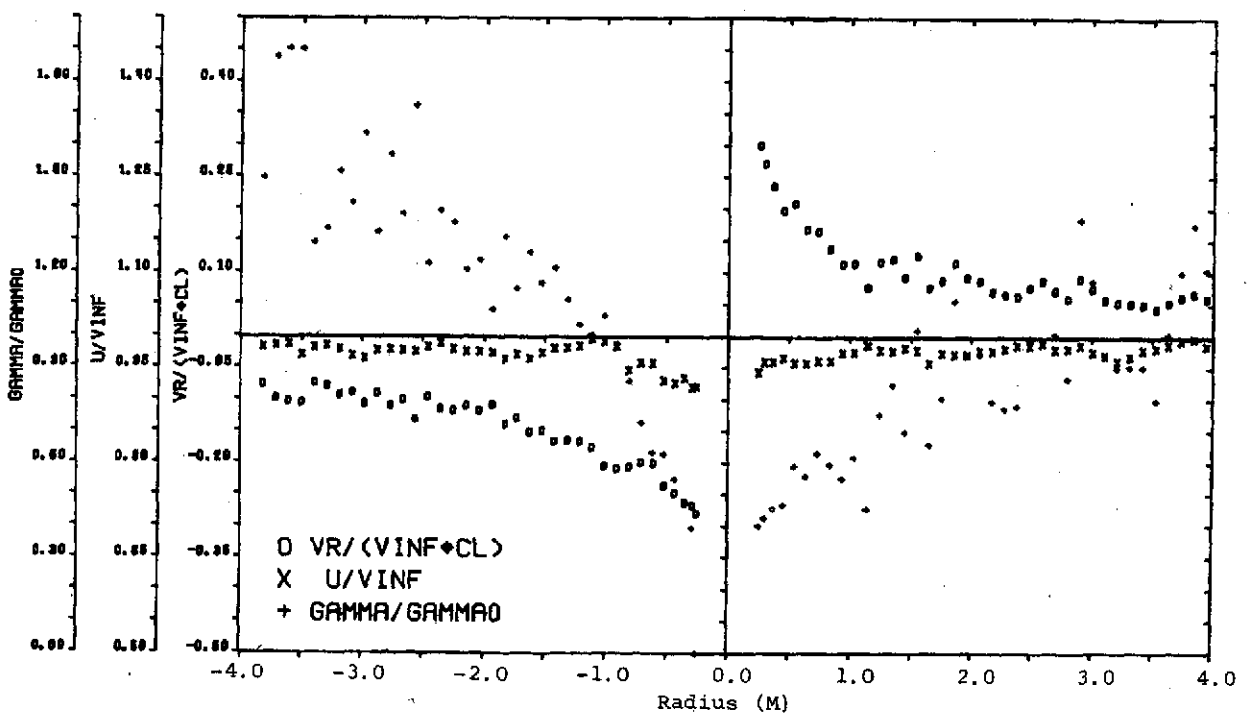

(b) Vortex 2.

Figure 28.- Velocity and circulation distributions for Section 42.

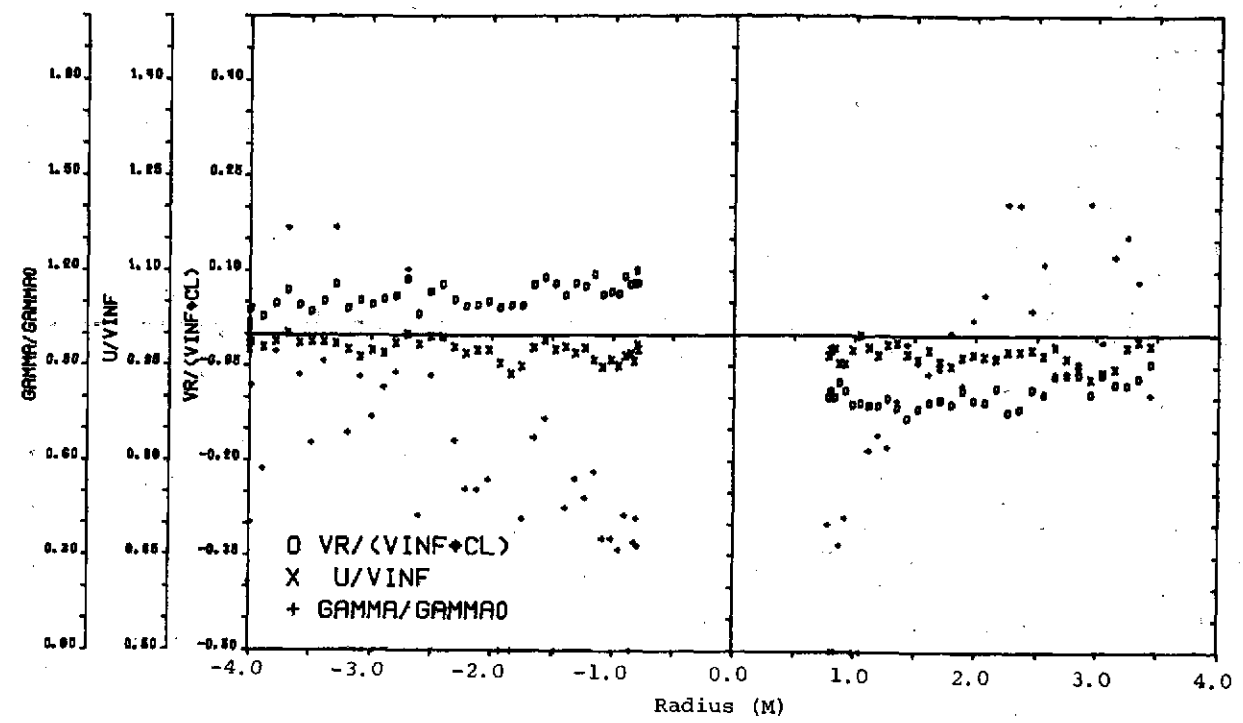

(a) Vortex 1.

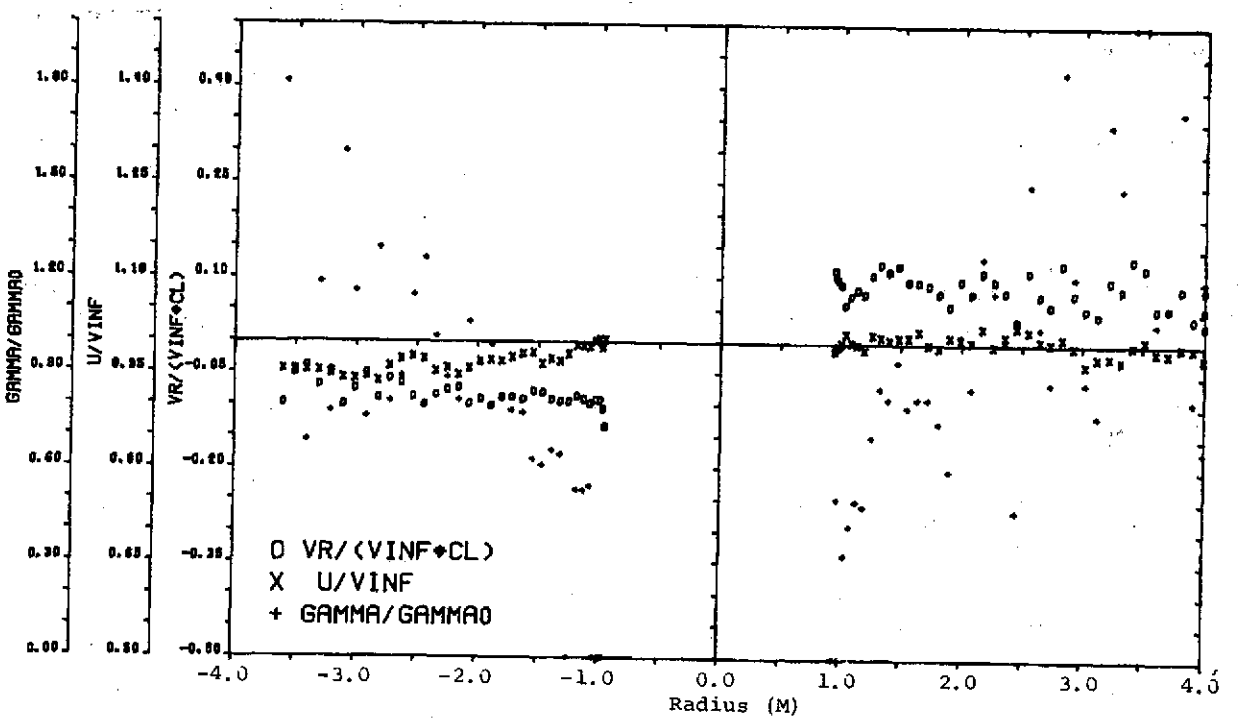

(b) Vortex 2.

Figure 29.- Velocity and circulation distributions for Section 45.

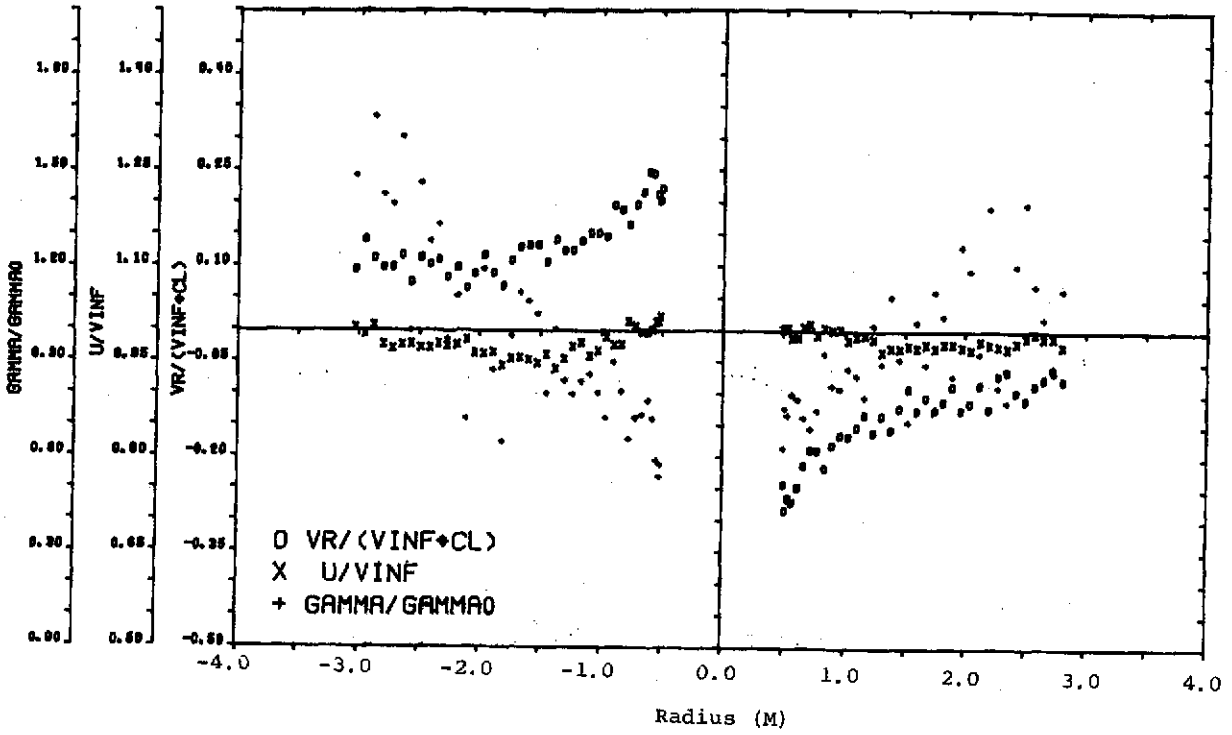

(a) Vortex 1.

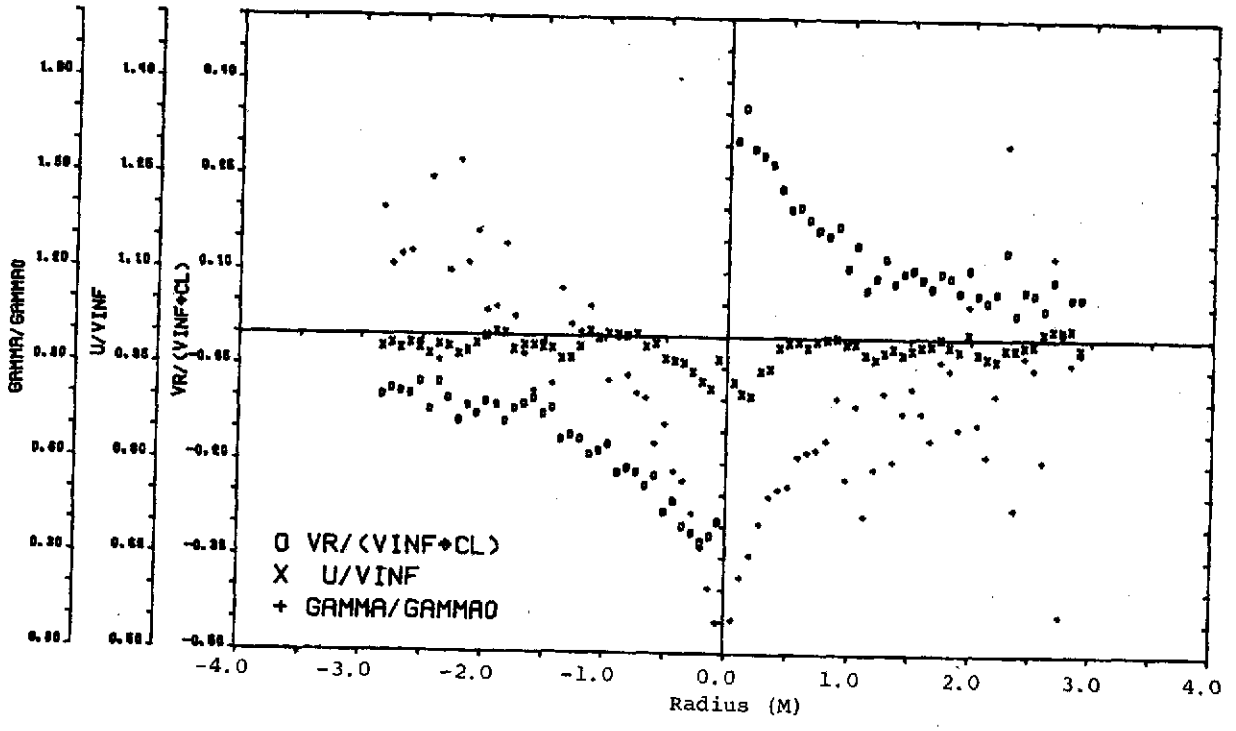

(b) Vortex 2.

Figure 30.- Velocity and circulation distributions for Section 46.

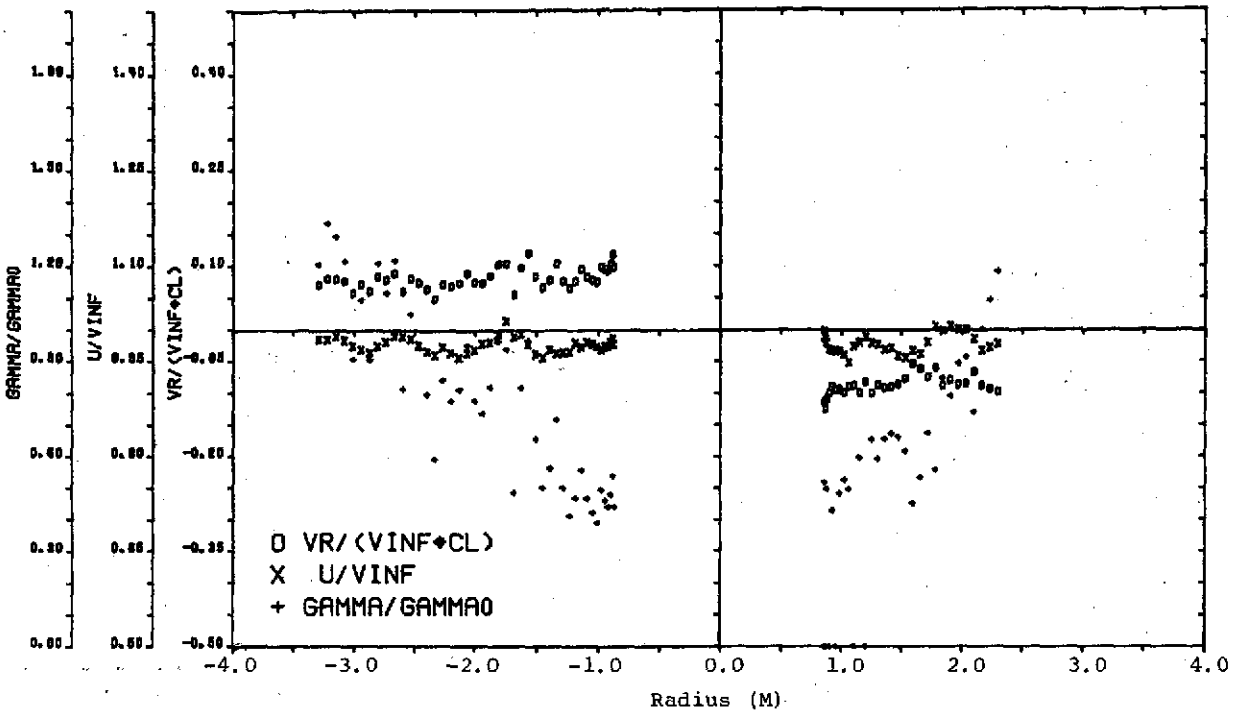

(a) Vortex 1.

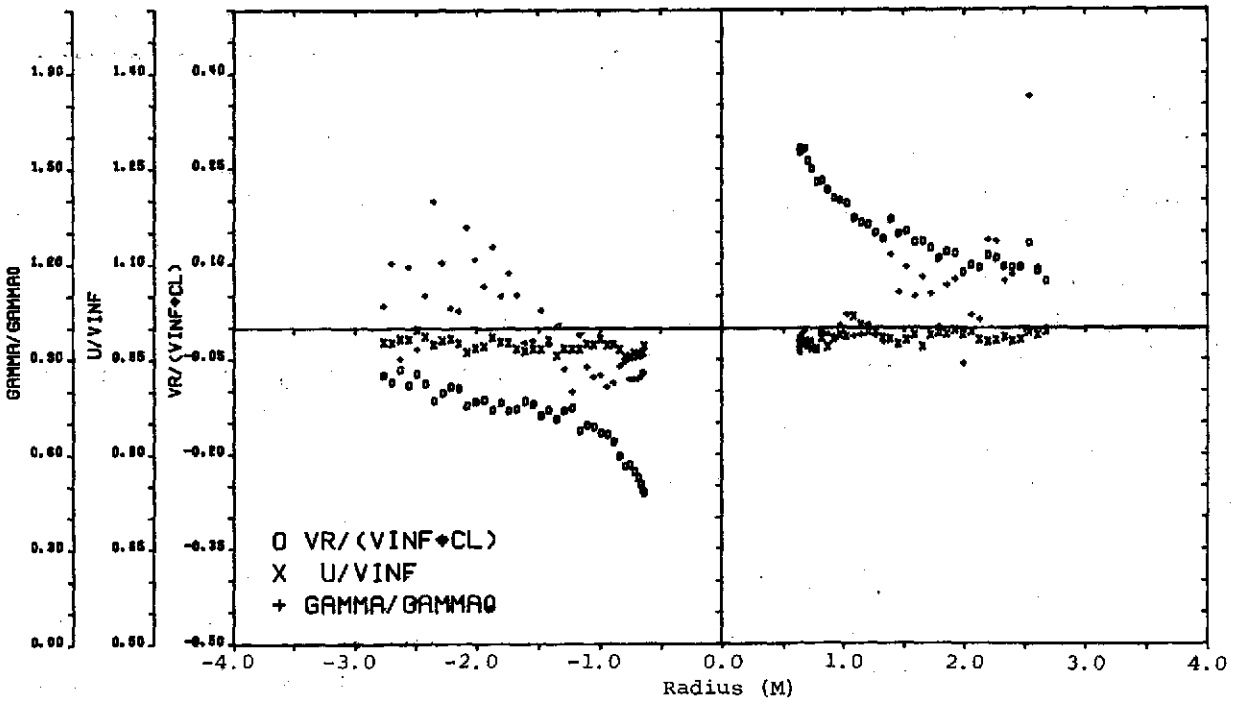

(b) Vortex 2.

Figure 31.- Velocity and circulation distributions for Section 47.

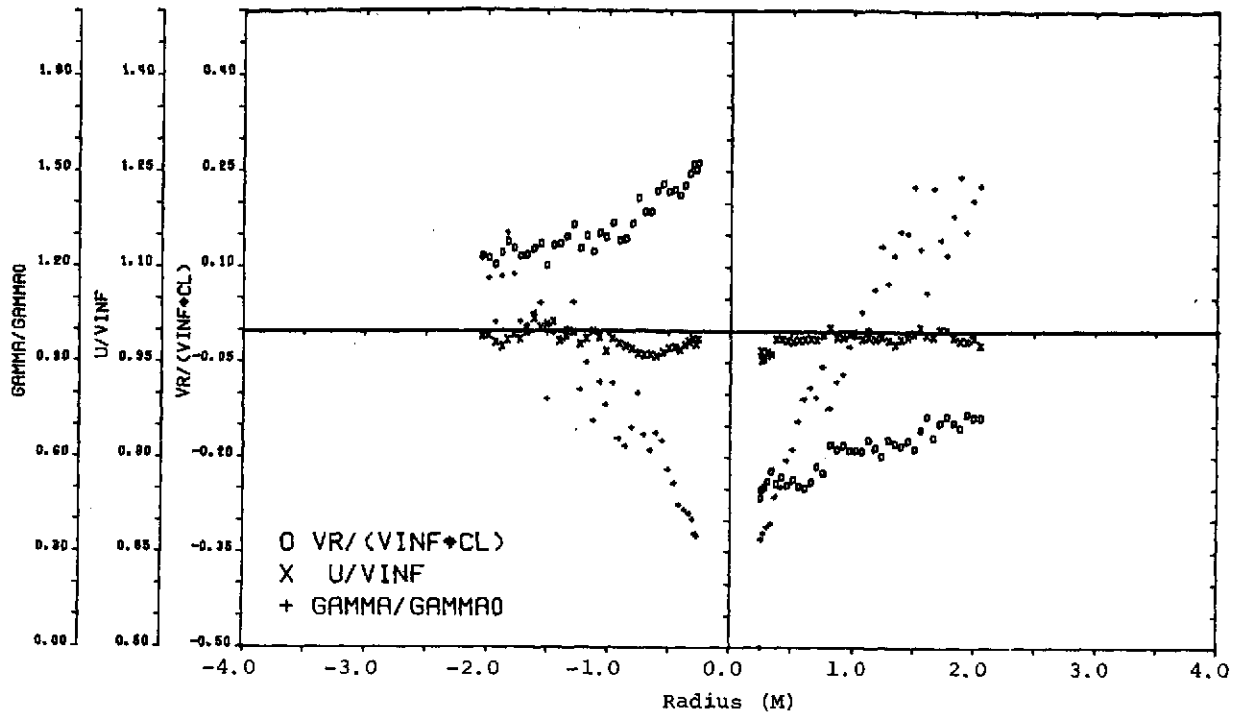

(a) Vortex 1.

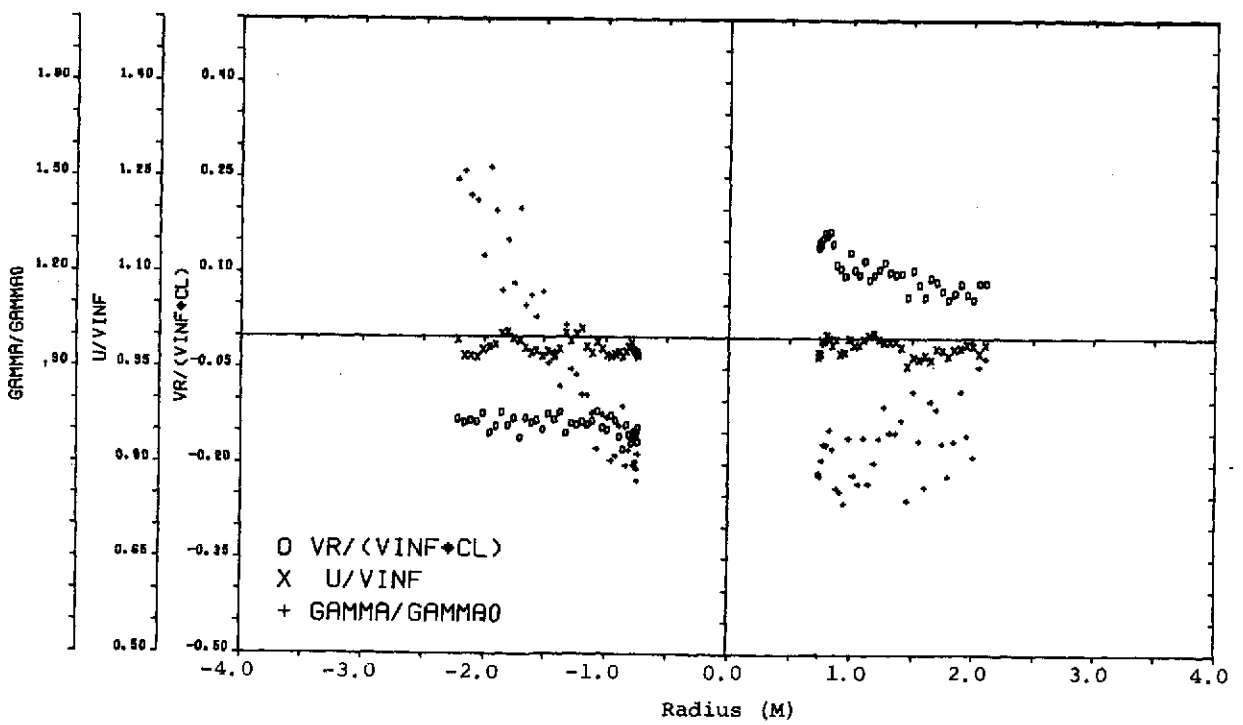

(b) Vortex 2.

Figure 32.- Velocity and circulation distributions for Section 48.

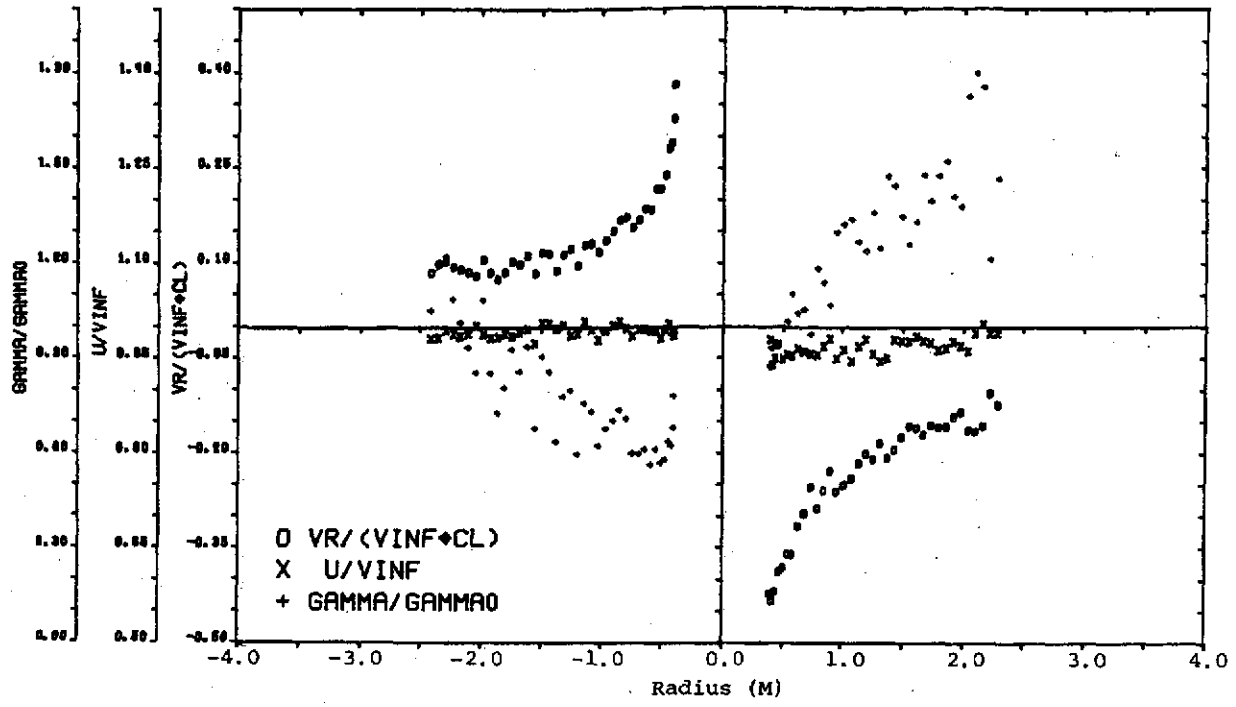

(a) Vortex 1.

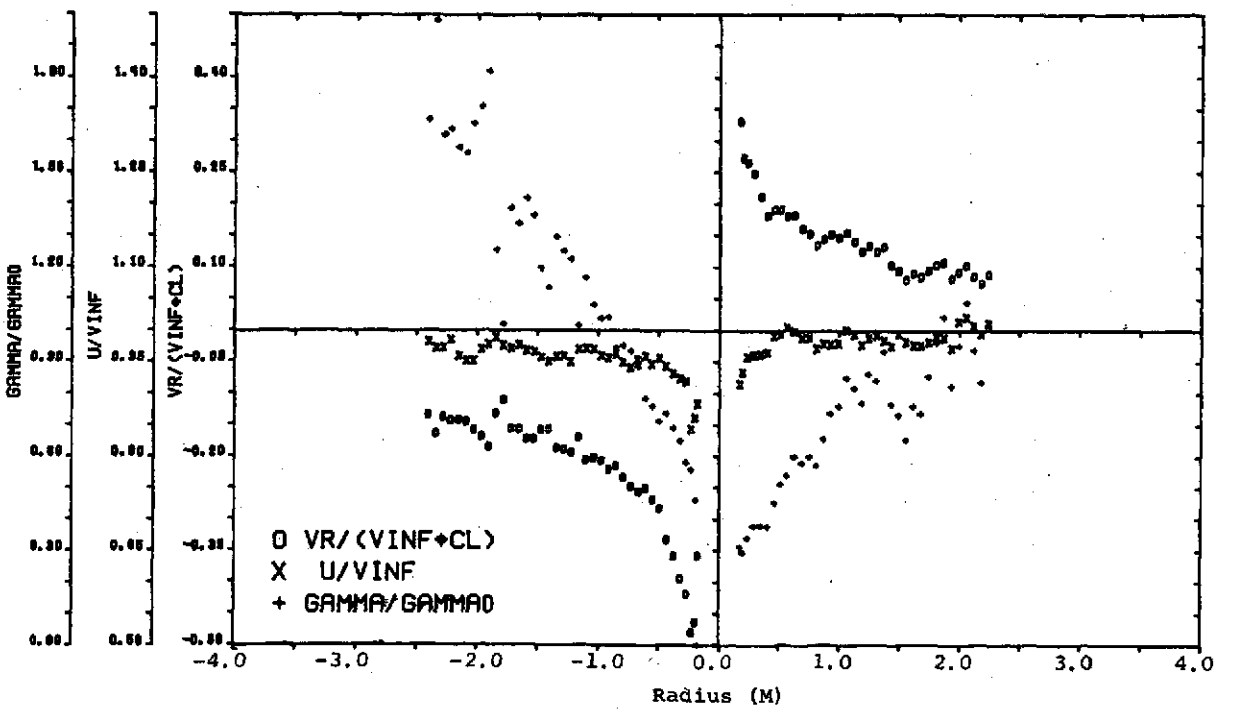

(b) Vortex 2.

Figure 33.- Velocity and circulation distributions for Section 49.

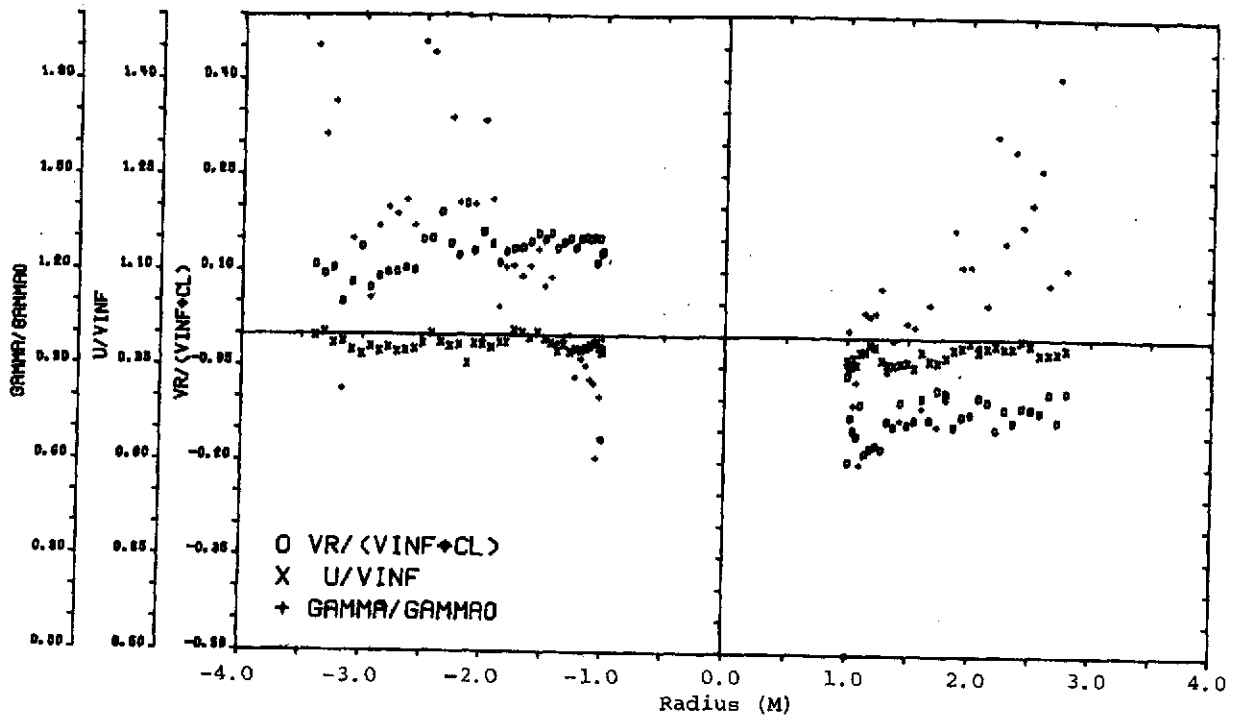

(a) Vortex 1.

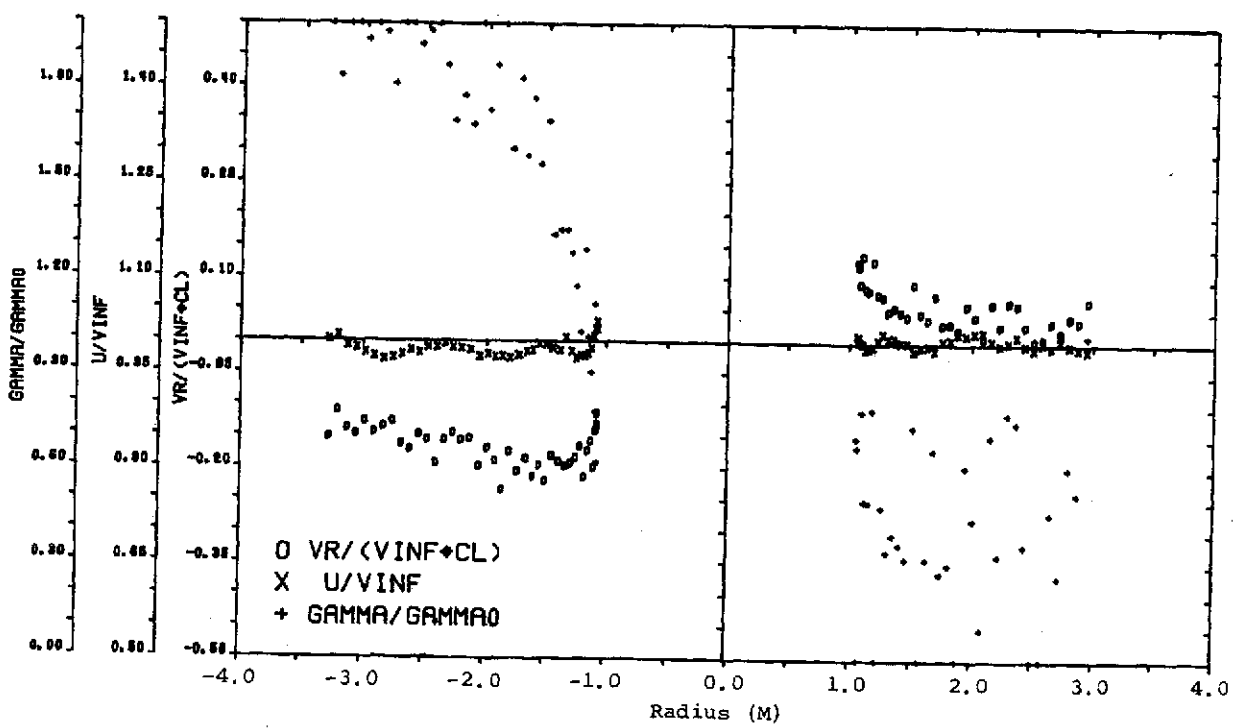

(b) Vortex 2.

Figure 34.- Velocity and circulation distributions for Section 50.

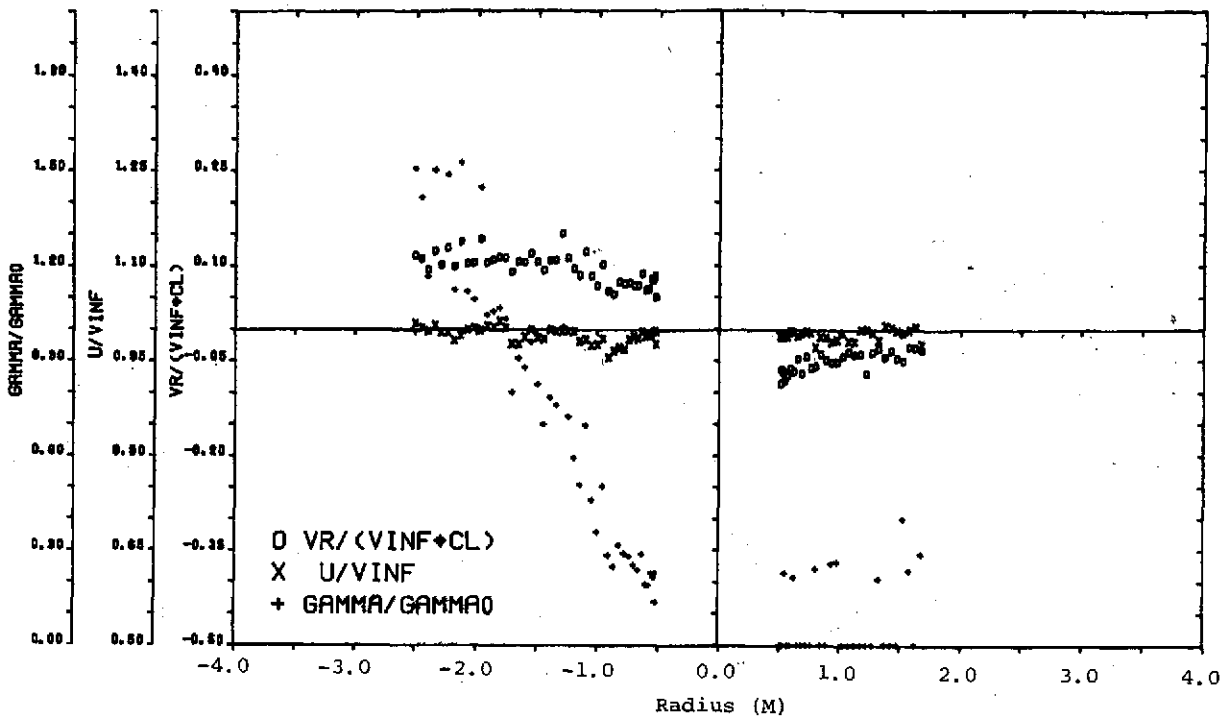

(a) Vortex 1.

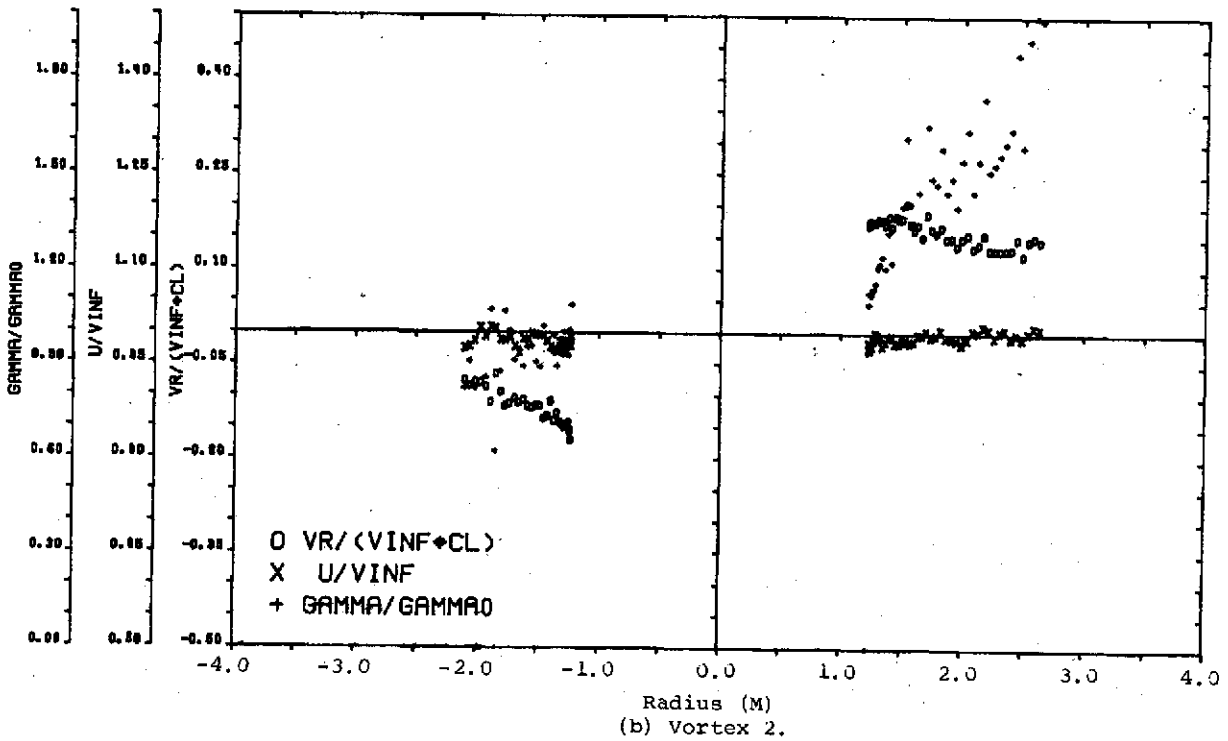

(b) Vortex 2.

Figure 35.- Velocity and circulation distributions for Section 51.

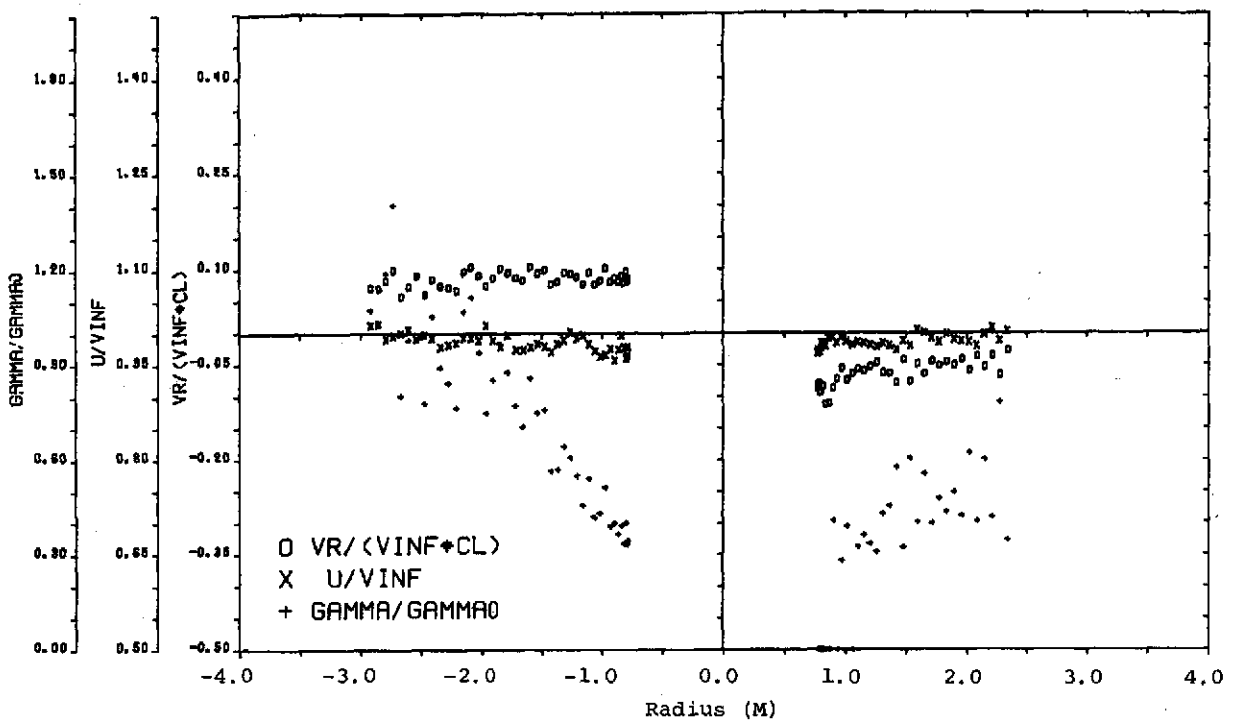

(a) Vortex 1.

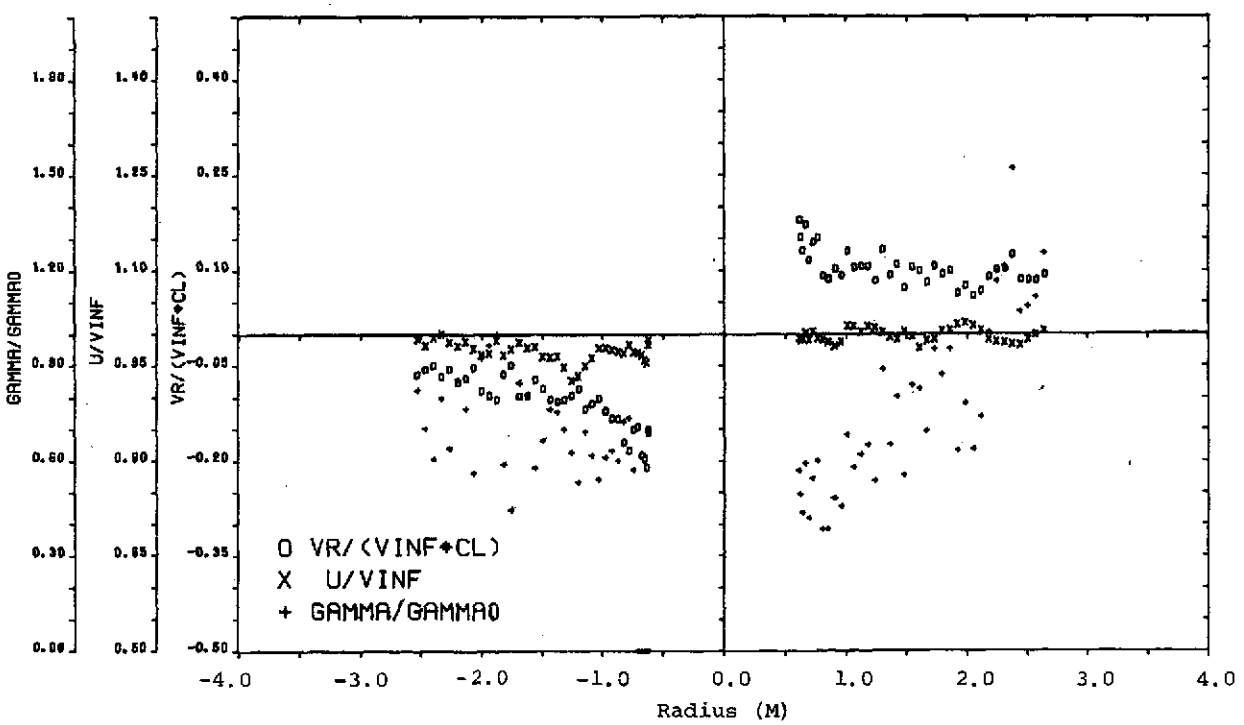

(b) Vortex 2.

Figure 36.- Velocity and circulation distributions for Section 52.

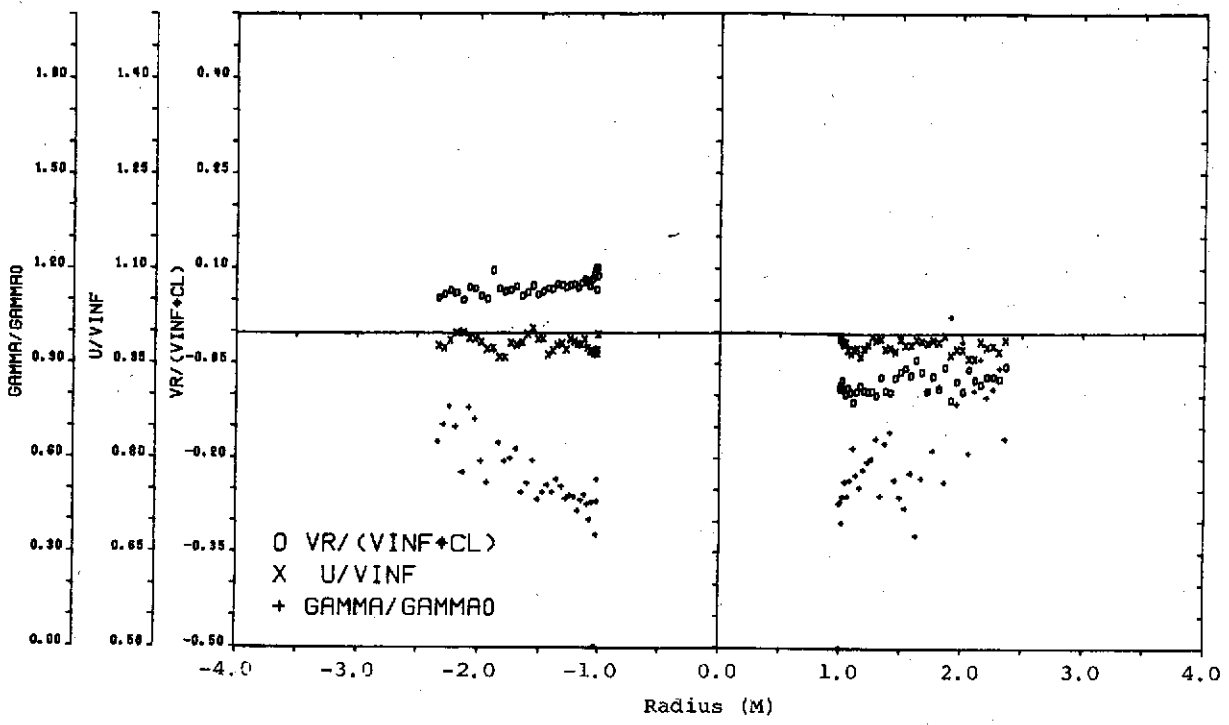

(a) Vortex 1.

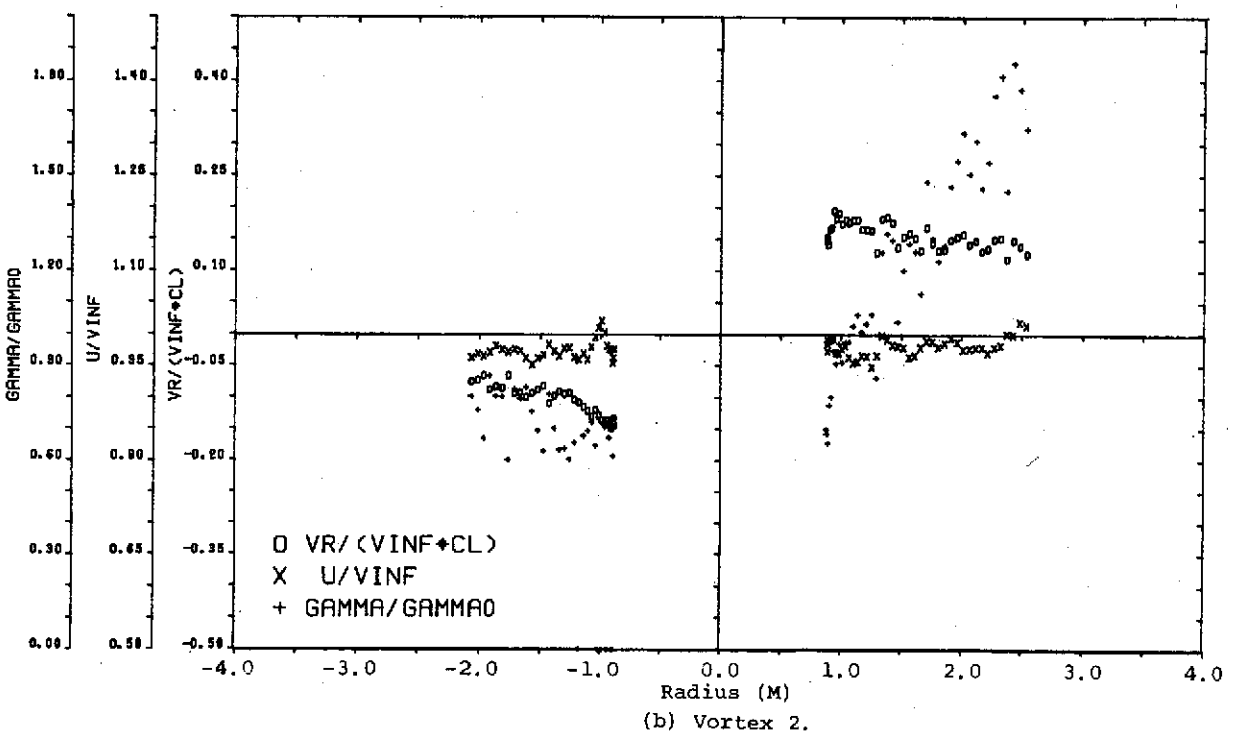

(b) Vortex 2.

Figure 37.- Velocity and circulation distributions for Section 53.

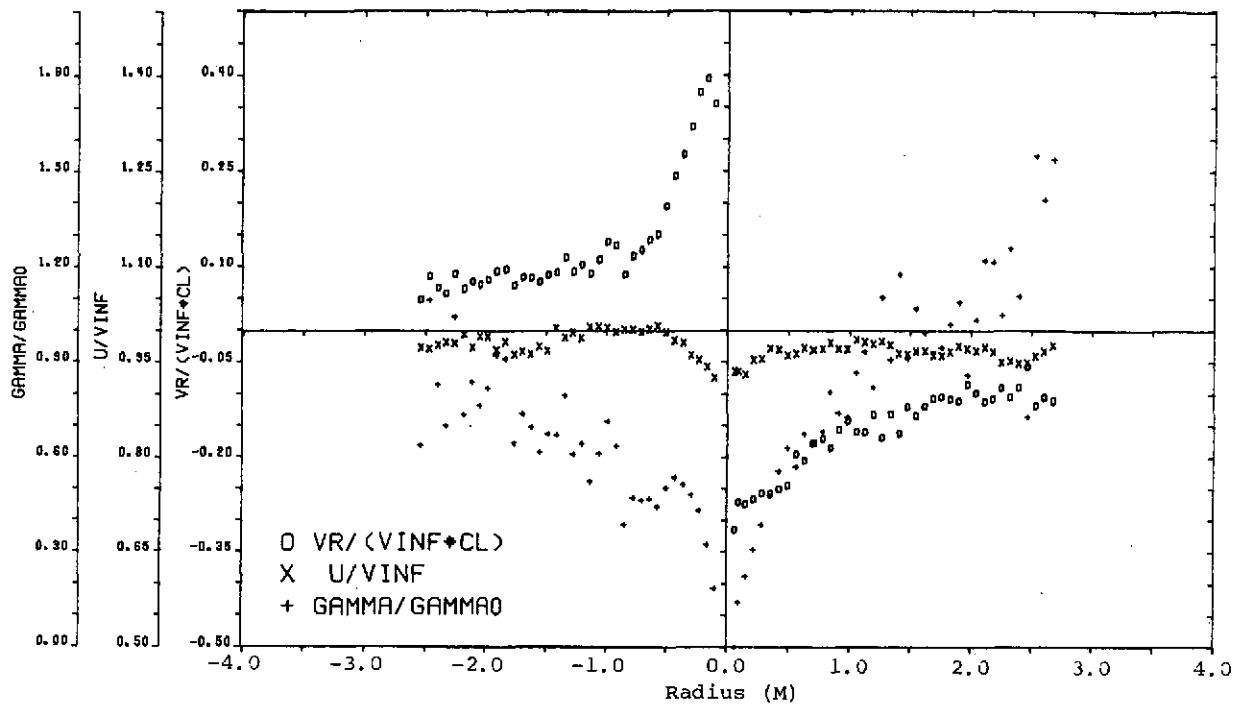

(a) Vortex 1.

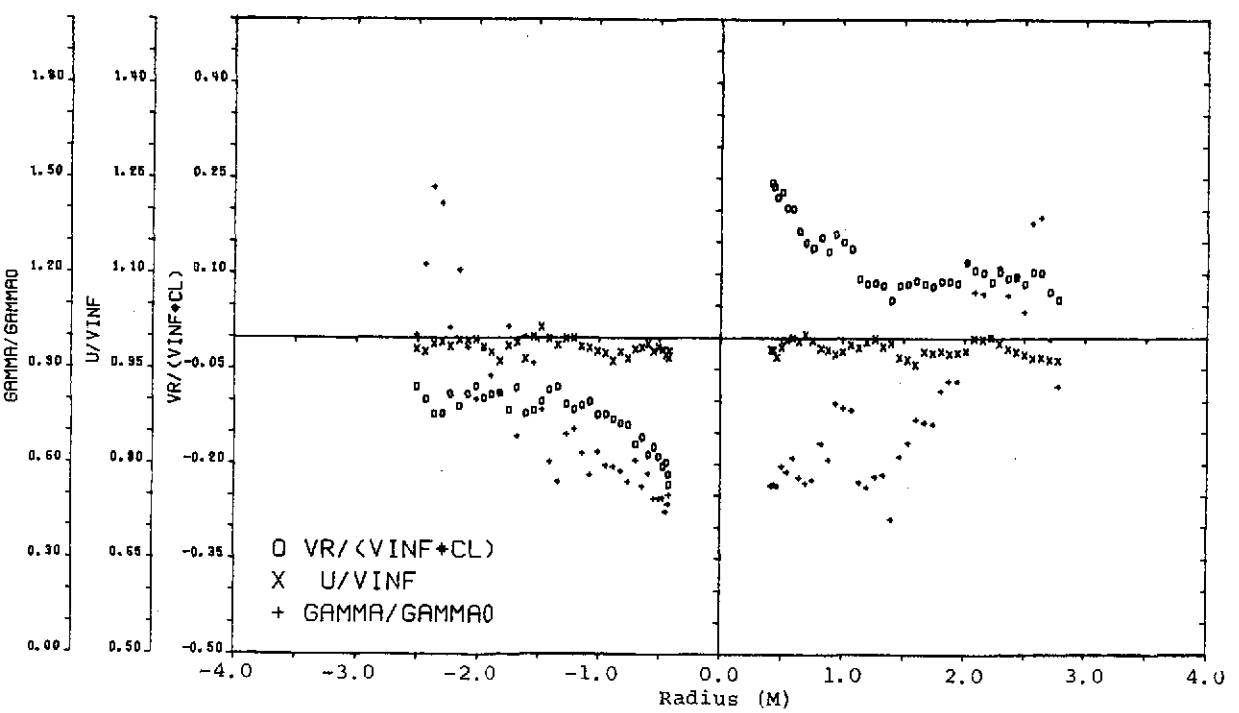

(b) Vortex 2.

Figure 38.- Velocity and circulation distributions for Section 54.

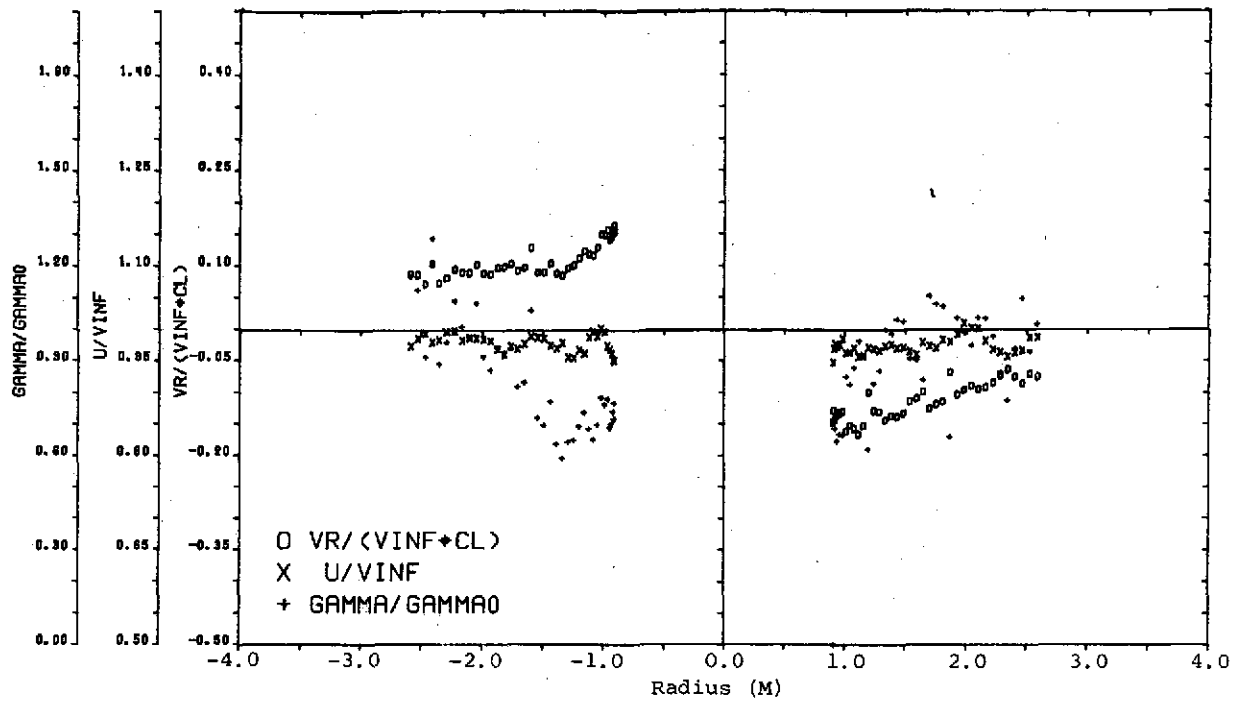

(a) Vortex 1.

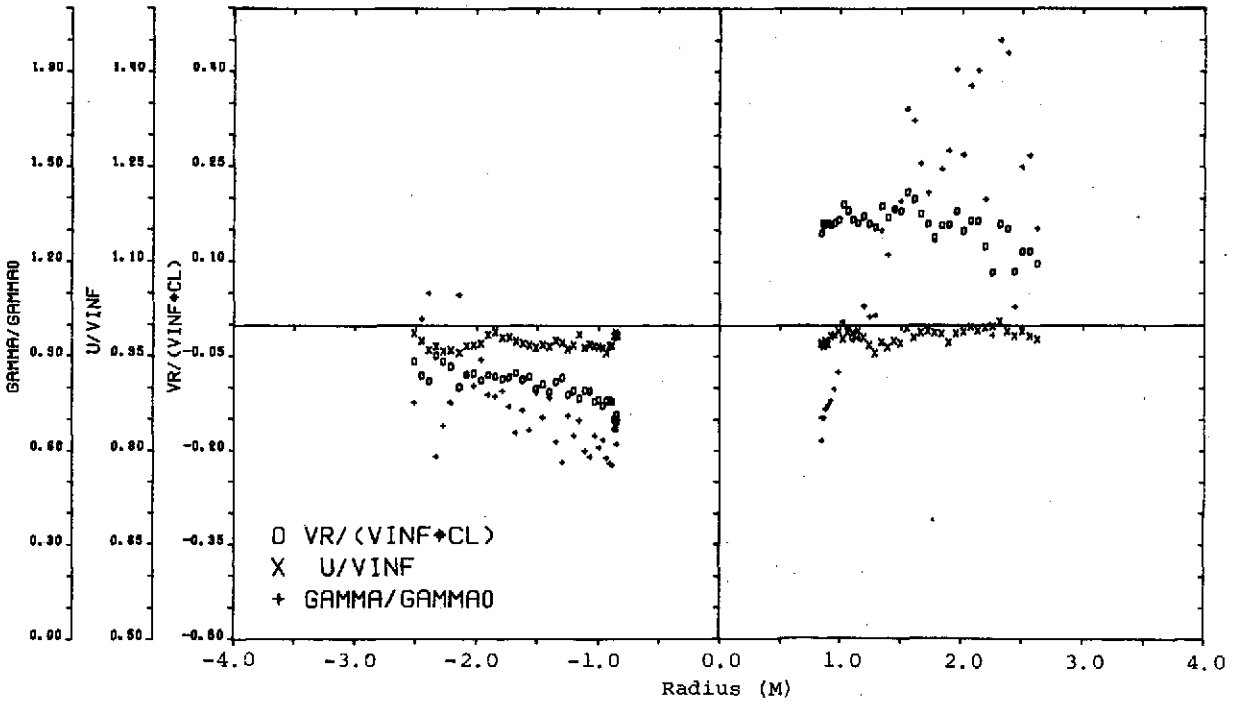

(b) Vortex 2.

Figure 39.- Velocity and circulation distributions for Section 55.

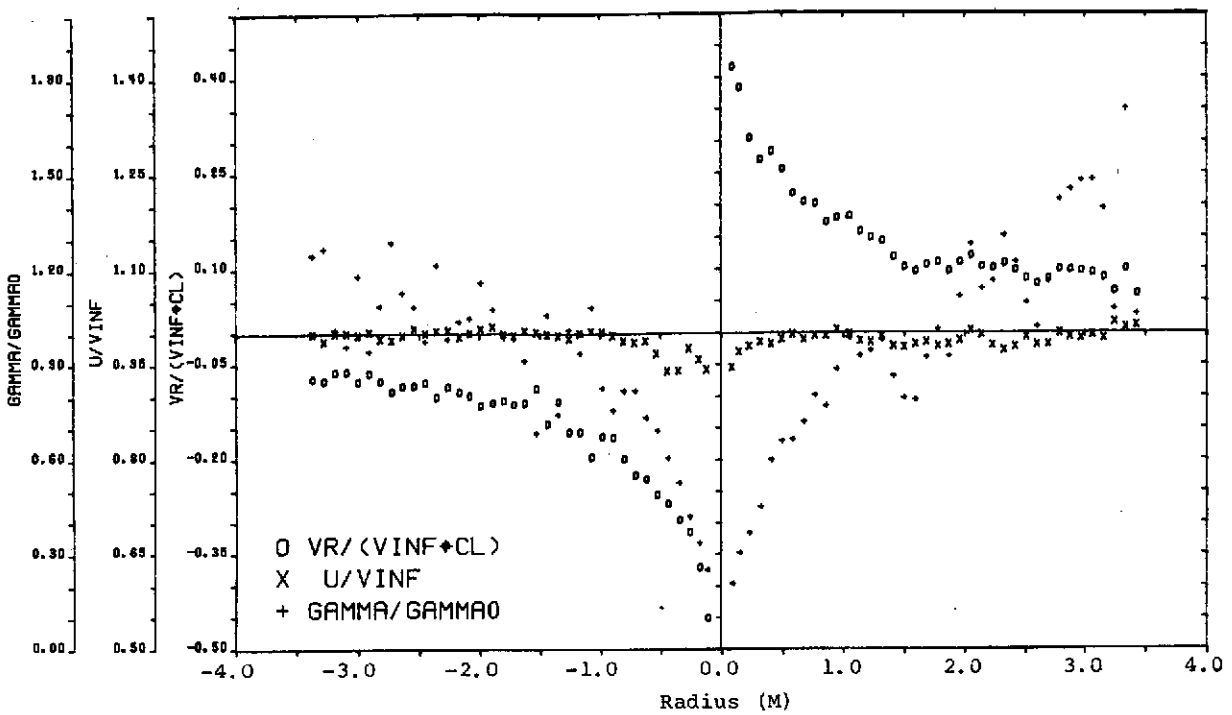

(a) Vortex 1.

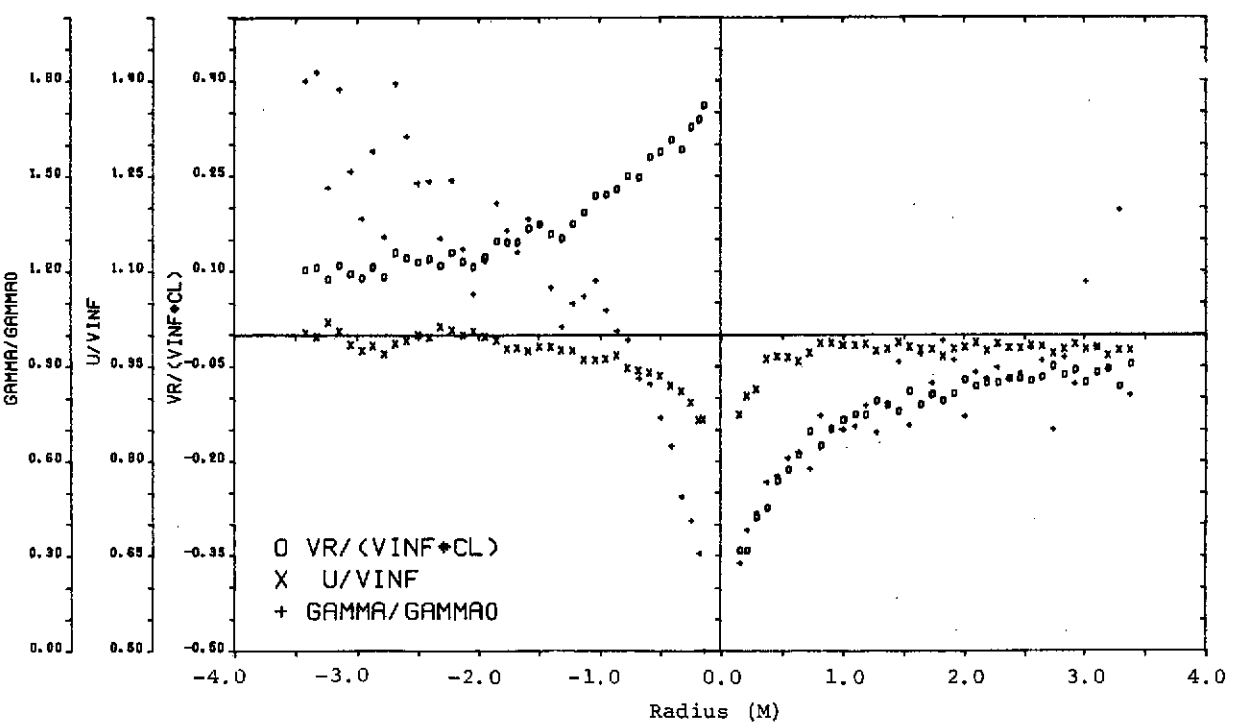

(b) Vortex 2.

Figure 40.- Velocity and circulation distributions for Section 56.

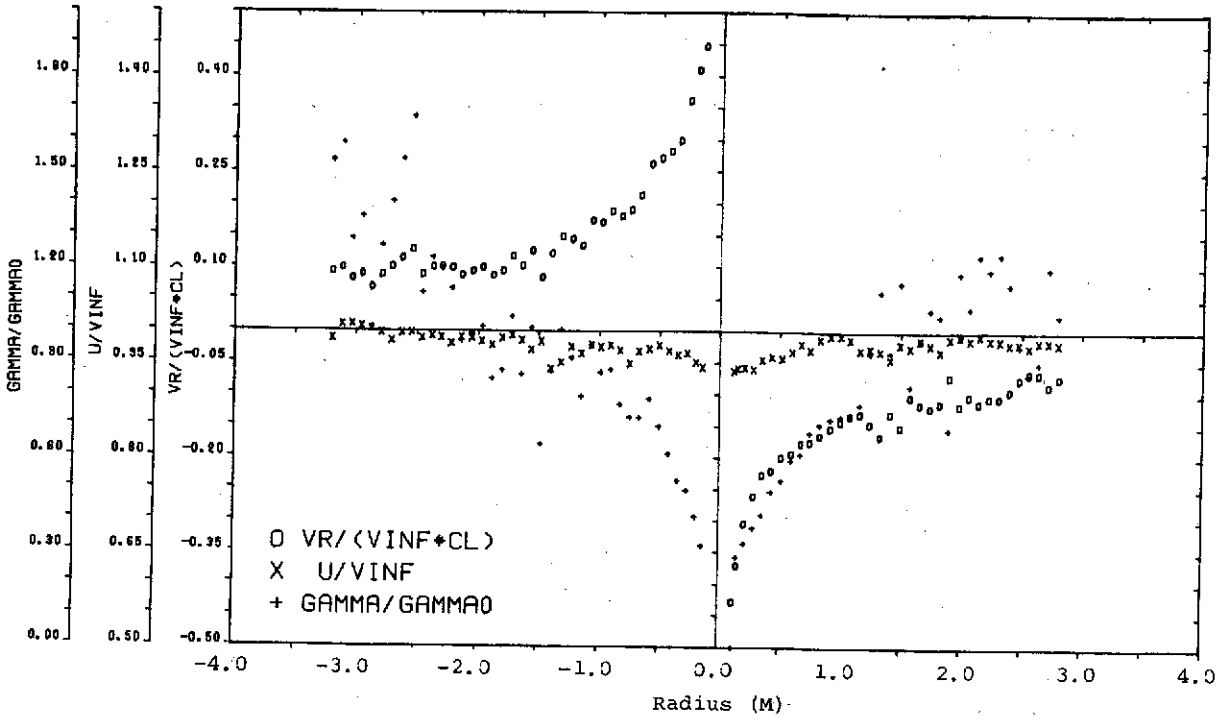

(a) Vortex 1.

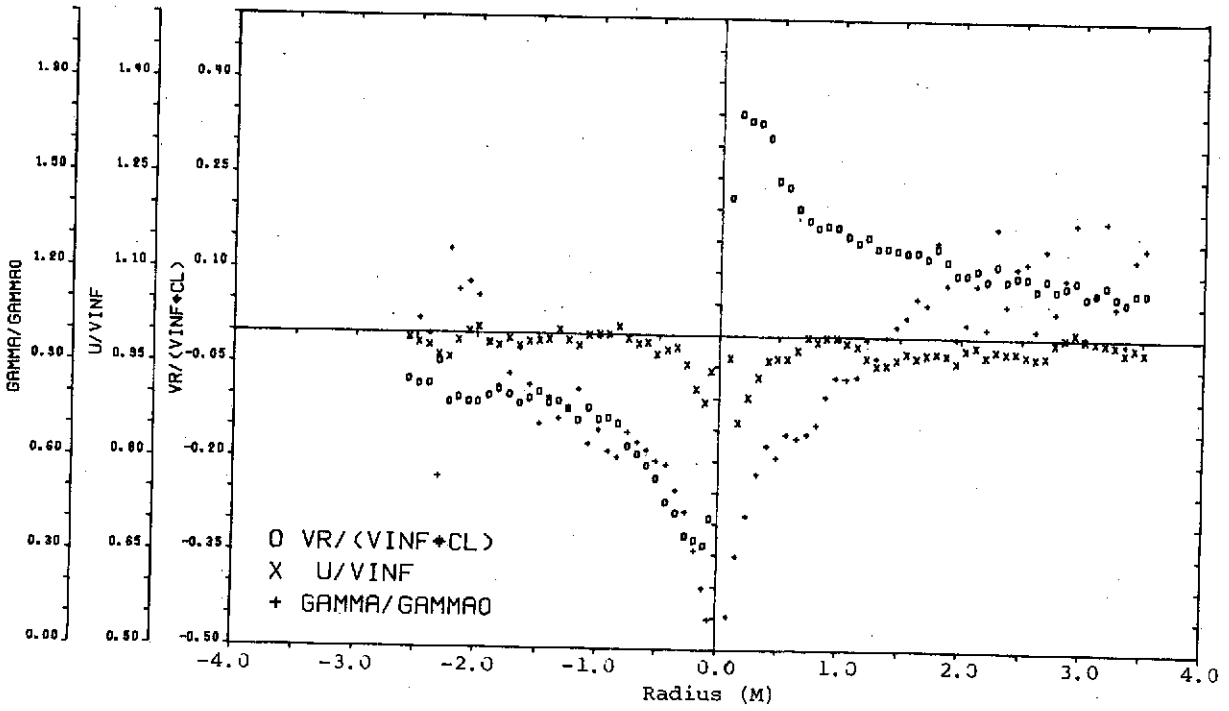

(b) Vortex 2.

Figure 41.- Velocity and circulation distributions for Section 58.

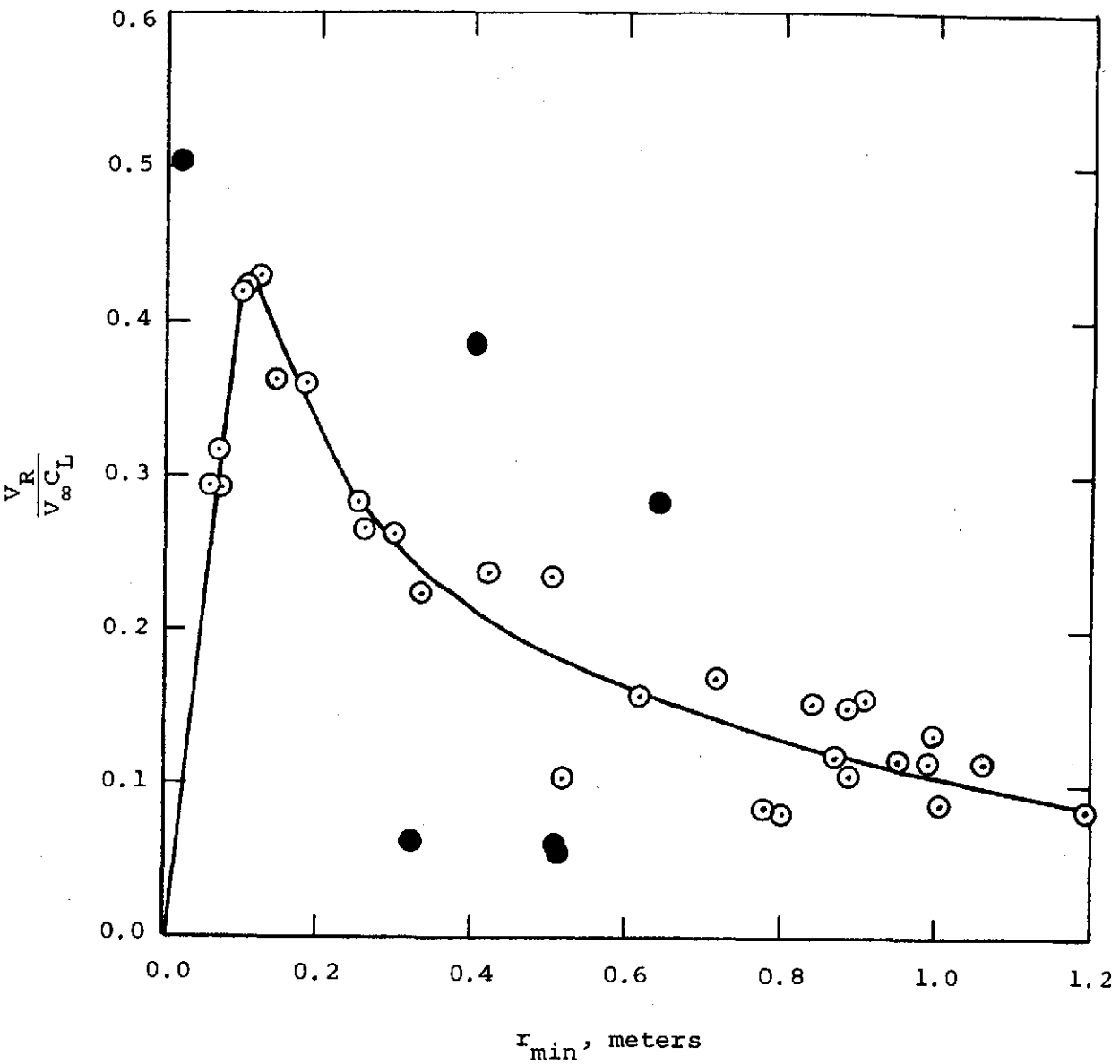

Figure 42.- Distribution of normalized resultant vortex velocities at minimum probe-to-vortex distance (filled symbols refer to sections with bias errors, see text, p. 13).

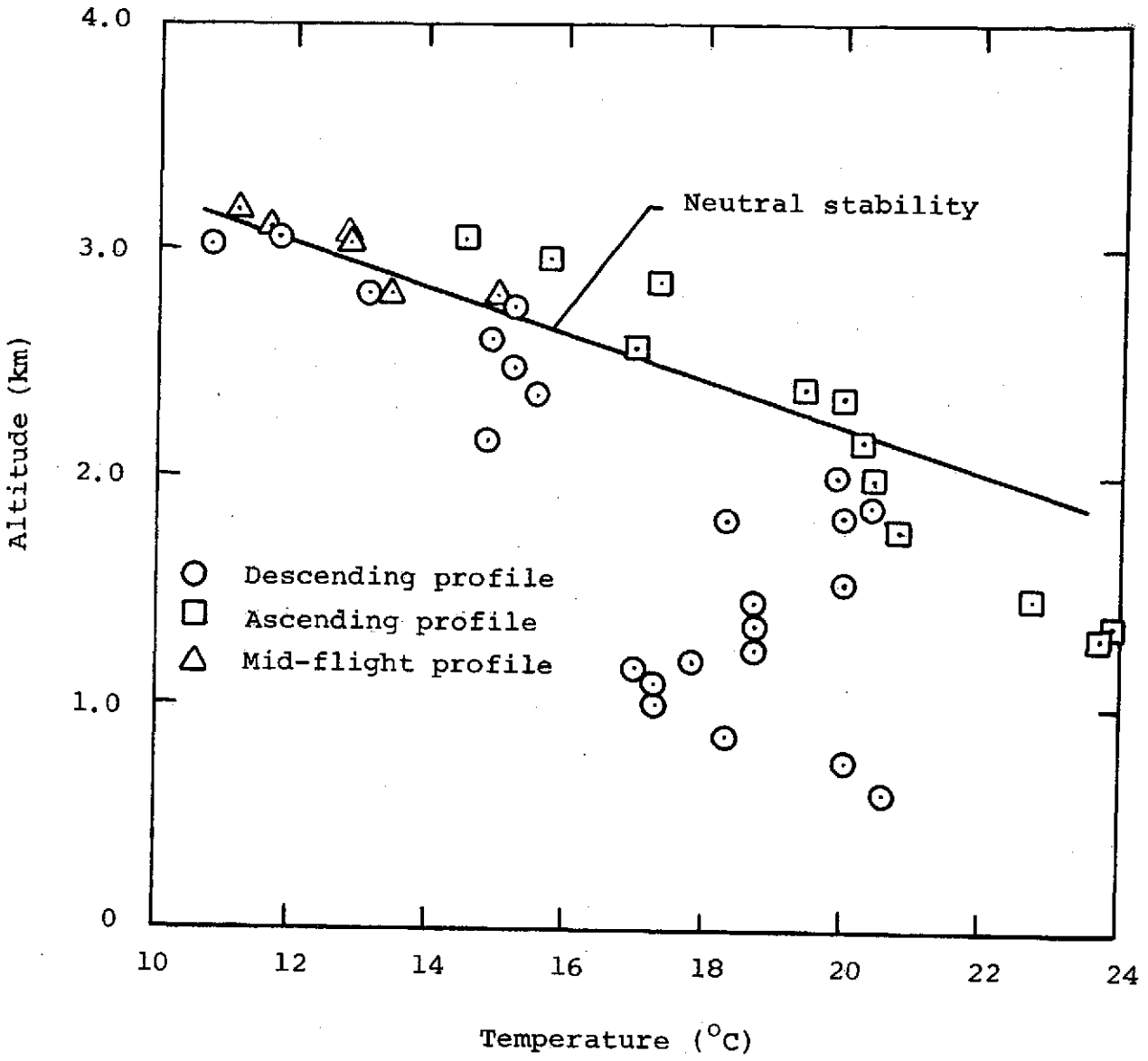

Figure 43.- Atmospheric temperature distribution during flight tests.

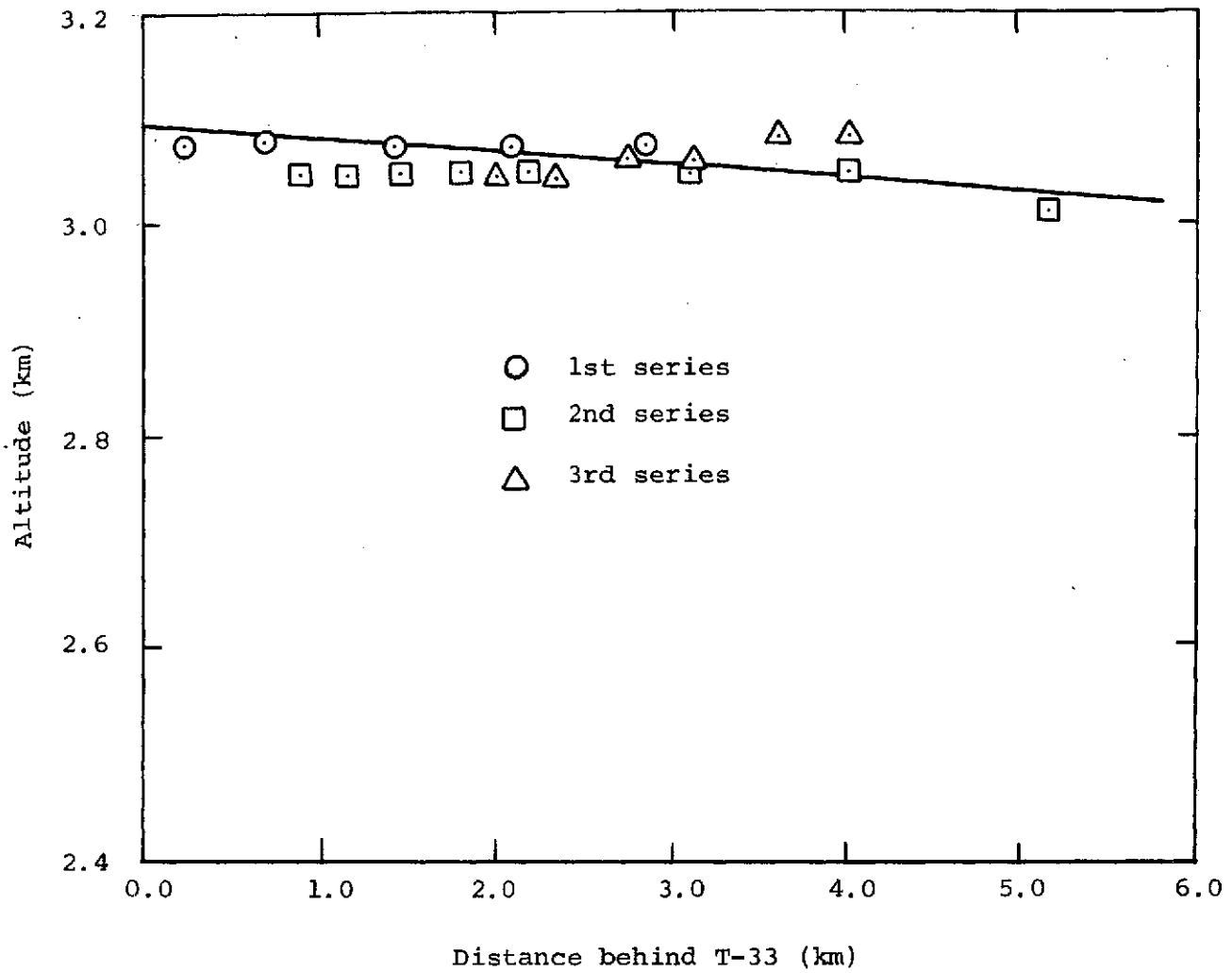

Figure 44.- Variation of vortex wake altitude behind T-33.

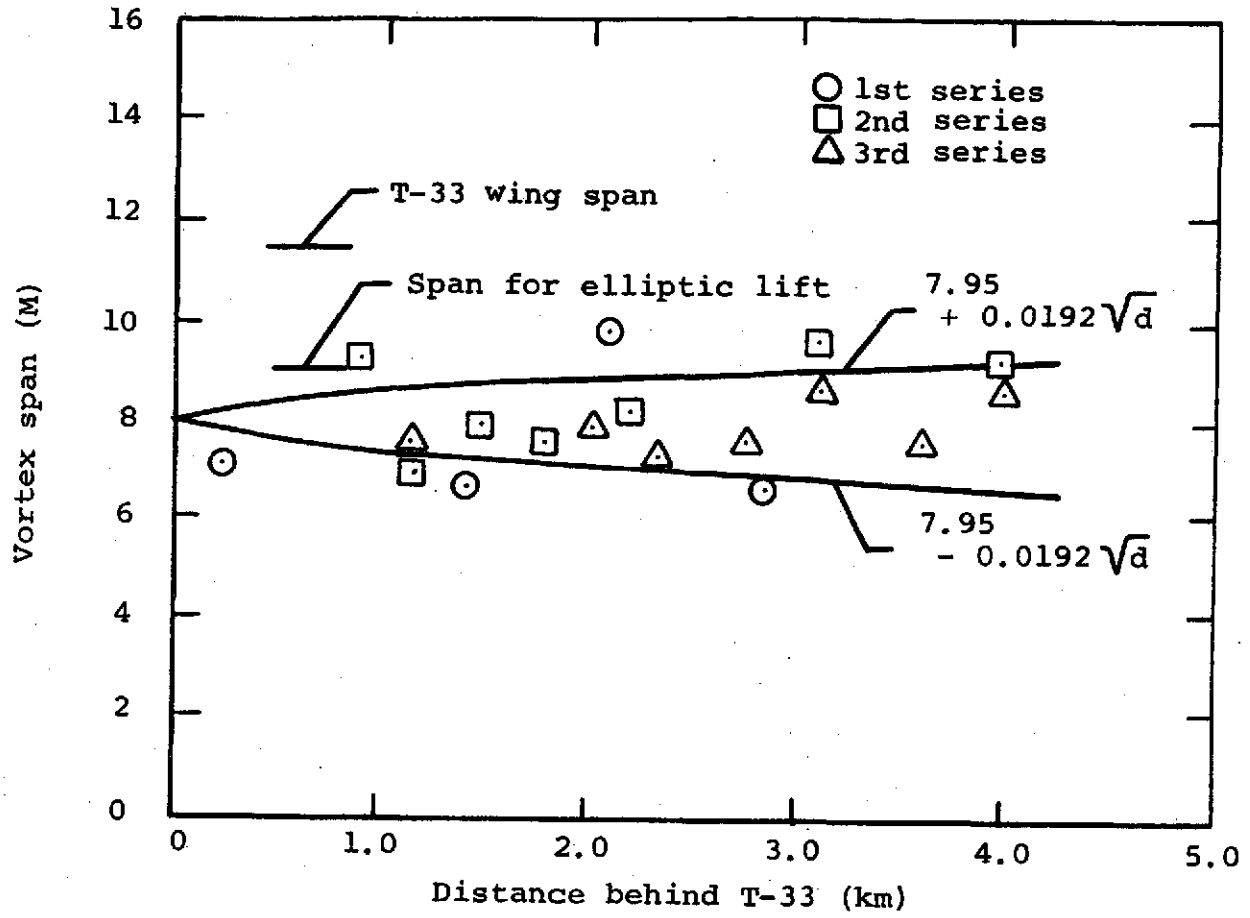

Figure 45.- Variation of vortex span.

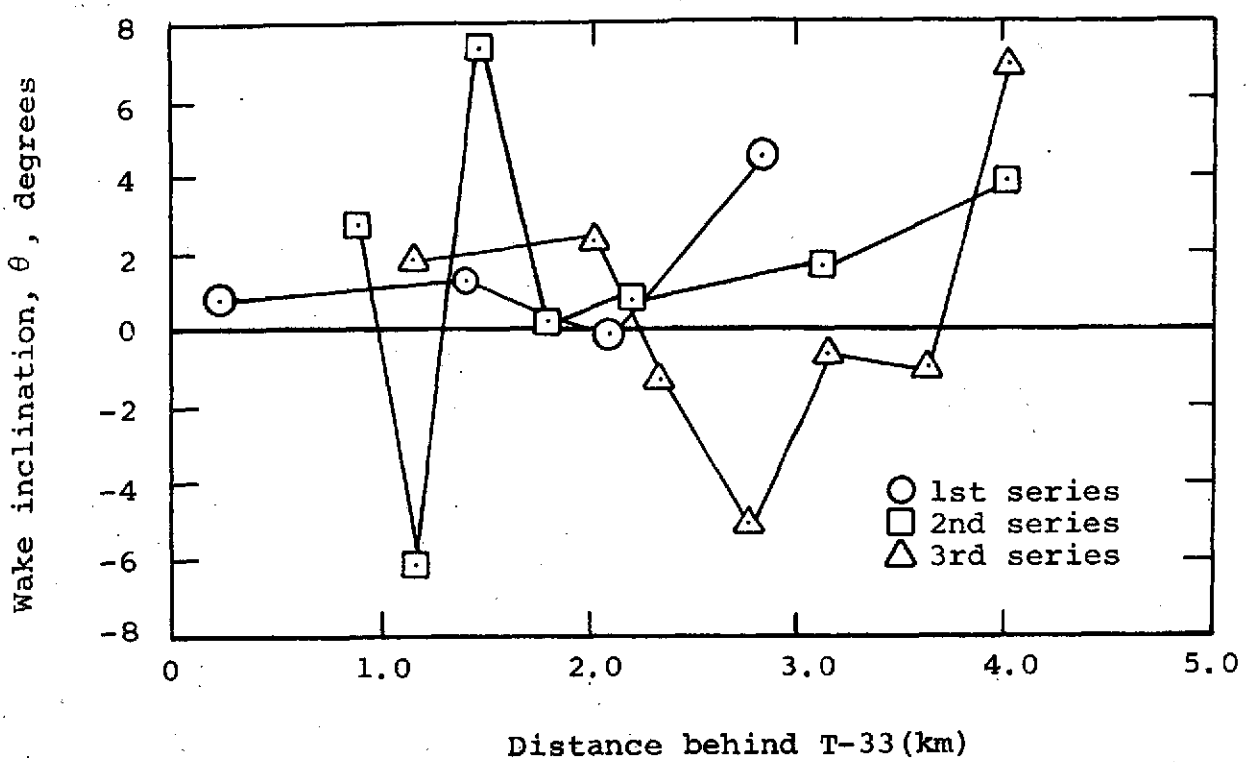

Figure 46.- Inclination of vortex wake cross sections.

APPENDIX A

LEAST-SQUARES METHOD OF ANALYSIS OF AIRCRAFT TRAILING VORTICES

Consider a distribution of N vortices of strengths Γ_i and positions (y_i, z_i), $i = 1,2,\ldots N$. The velocity, V_n, at any point, P, due to the vortices can be expressed in the form

$$V_n = \sum_{i=1}^{N} \frac{\Gamma_i\left[(z_i - z_n)\vec{e}_y - (y_i - y_n)\vec{e}_z\right]}{2\pi\left[(y_i - y_n)^2 + (z_i - z_n)^2\right]} \tag{A-1}$$

where $\vec{e}_y, \vec{e}_z$ are unit vectors in the y and z directions, respectively. Let

$$\Gamma_i = \bar{\Gamma}_i + \gamma_i \tag{A-2}$$

$$y_i = \bar{y}_i + \eta_i \tag{A-3}$$

$$z_i = \bar{z}_i + \zeta_i \tag{A-4}$$

$$r_{in}^2 = (y_i - y_n)^2 + (z_i - z_n)^2 \tag{A-5}$$

It is assumed that

$$\gamma_i \ll \bar{\Gamma}_i$$

$$\eta_i \ll \bar{y}_i$$

$$\zeta_i \ll \bar{z}_i$$

Then, neglecting terms involving products of small quantities, it follows (after substitution of equations (A-2) through (A-5) in (A-1) and expanding) that

$$V_n = \sum_{i=1}^{N} \frac{\bar{\Gamma}_i}{2\pi\bar{r}_{in}^2}\left[(\bar{z}_i - z_n)\vec{e}_y - (\bar{y}_i - y_n)\vec{e}_z\right] + \sum_{i=1}^{3N} c_i\vec{\phi}_{in} \tag{A-6}$$

where

$$C_i = \gamma_i \qquad 1 \le i \le N \tag{A-7}$$

$$C_i = \eta_i \qquad N+1 \le i \le 2N \tag{A-8}$$

$$C_i = \zeta_i \qquad 2N+1 \le i \le 3N \tag{A-9}$$

$$\vec{\phi}_{in} = \frac{(\bar{z}_i - z_n)\vec{e}_y - (\bar{y}_i - y_n)\vec{e}_z}{2\pi\bar{r}_{in}^2} \qquad 1 \le i \le N \tag{A-10}$$

$$\vec{\phi}_{in} = \frac{-\bar{\Gamma}_i}{2\pi\bar{r}_{in}^2}\left\{4\,\frac{(\bar{y}_i - y_n)(\bar{z}_i - z_n)}{\bar{r}_{in}^2}\,\vec{e}_y + \left[1 - 4\,\frac{(\bar{y}_i - y_n)^2}{\bar{r}_{in}^2}\right]\vec{e}_z\right\} \qquad N+1 \le i \le 2N \tag{A-11}$$

$$\vec{\phi}_{in} = \frac{\bar{\Gamma}_i}{2\pi\bar{r}_{in}^2}\left\{\left[1 - 4\,\frac{(\bar{z}_i - z_n)^2}{\bar{r}_{in}^2}\right]\vec{e}_y + 4\,\frac{(\bar{y}_i - y_n)(\bar{z}_i - z_n)}{\bar{r}_{in}^2}\,\vec{e}_z\right\} \qquad 2N+1 \le i \le 3N \tag{A-12}$$

Now, letting

$$\vec{U}_n = \vec{V}_n - \sum_{i=1}^{N} \frac{\Gamma_i}{2\pi\bar{r}_{in}^2}\left[(\bar{z}_i - z_n)\vec{e}_y - (\bar{y}_i - y_n)\vec{e}_z\right] \tag{A-13}$$

the expression (A-6) is reduced to

$$\vec{U}_n = \sum_{i=1}^{3N} C_i\vec{\phi}_{in} \tag{A-14}$$

where C_i are unknown parameters to be determined.

The values of C_i are found by the method of least squares. Let

$$\vec{R}_n = \vec{U}_n - \sum_{i=1}^{3N} C_i \vec{\phi}_{in} \tag{A-15}$$

Then the best set of values of C_i which make the function (A-1) approximate a given set of M values of the velocity $\vec{V}_n$ is that set for which the quantity

$$J = \sum_{n=1}^{M} \vec{R}_n \cdot \vec{R}_n$$

is a minimum. To find that set, require that

$$\frac{\partial}{\partial C_k} \sum_{n=1}^{M} \vec{R}_n \cdot \vec{R}_n = 0 \qquad k = 1,2,\ldots 3N \tag{A-16}$$

or, substituting equation (A-15)

$$\sum_{i=1}^{3N} C_i \sum_{n=1}^{M} \left[\phi_{in_y} \phi_{kn_y} + \phi_{in_z} \phi_{kn_z} \right] = \sum_{n=1}^{M} \left[U_{n_y} \phi_{kn_y} + U_{n_z} \phi_{kn_z} \right] \tag{A-17}$$

This results in $3N$ equations in the $3N$ unknown C_i.

It should be noted that no assumptions are made with regard to symmetry of either strength or position of a group of vortices. It is assumed that all discernible vortices will be included in the calculation as individual vortices.

The final solution fitting the function (A-1) to the measured velocity data is found by iteration. Initially, the values $\overline{\Gamma}_i$, $\overline{y}_i$, and $\overline{z}_i$ are estimated for each vortex. The solution of equation (A-17) yields a set of corrections to those values through equations (A-7), (A-8), and (A-9). The initial values are adjusted according to equations (A-2), (A-3), and (A-4) and the solution is repeated. This procedure is continued until convergence is achieved in terms of the C_i becoming less than a desired tolerance.

It can be shown that the method of least squares produces unbiased estimates of the unknown parameters of a theoretical expression only if the model is correct, and the disturbance or error variables are random. In the present problem, the correctness of the model requires that the correct number of vortices be included in the model, that the assumption of axisymmetry of the vortices be correct, and there be no bias introduced by any recording instrumentation or by any assumptions made in the data reduction procedure.

A typical convergent iteration sequence is shown in figure A-1. It is noted that some of the parameters may converge faster than others. In other cases, the mean-square error may converge even though the solution is diverging. That is due to the fact that the mean-square error is insensitive to changes in the C_i at large distance from the vortex centers. A solution is assured if the mean-square error decreases, the values of C_i stabilize, and the gradient of the mean-square error with respect to the iteration continues to approach zero.

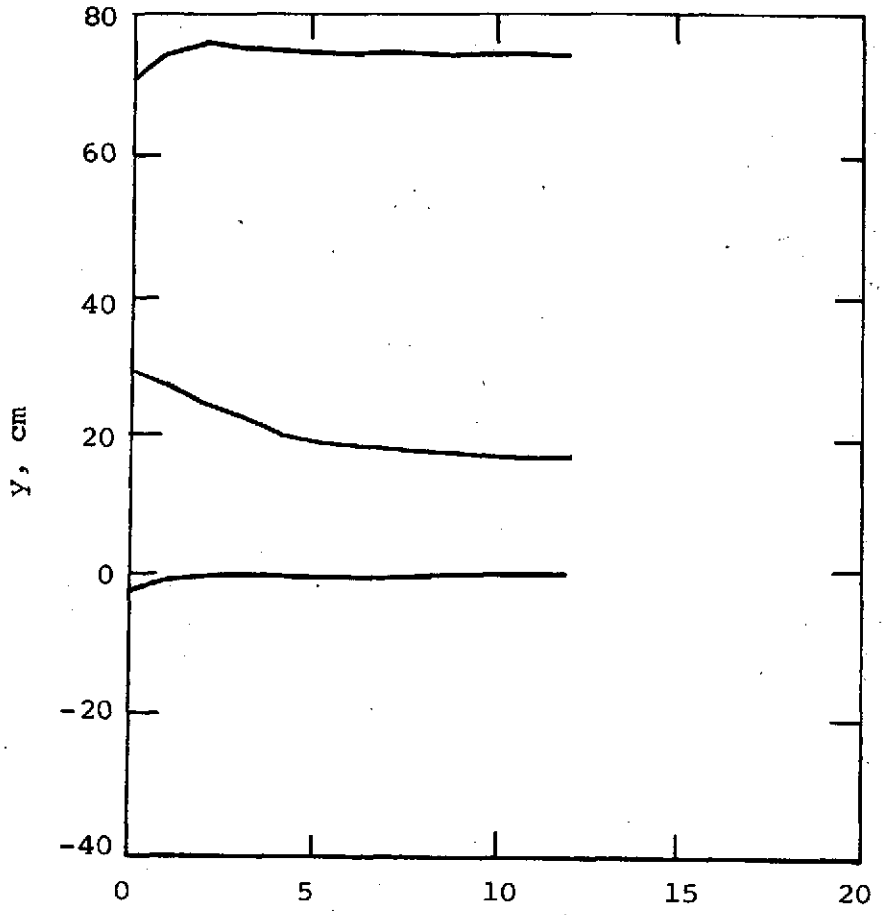

(a) y-coordinates of vortex centers.

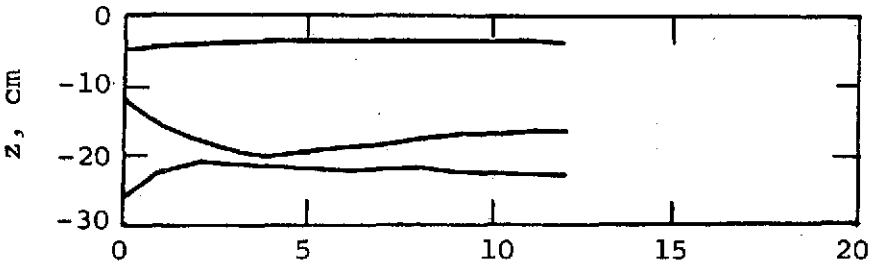

(b) z-coordinates of vortex centers.

Figure A-1.- Typical iteration sequence.

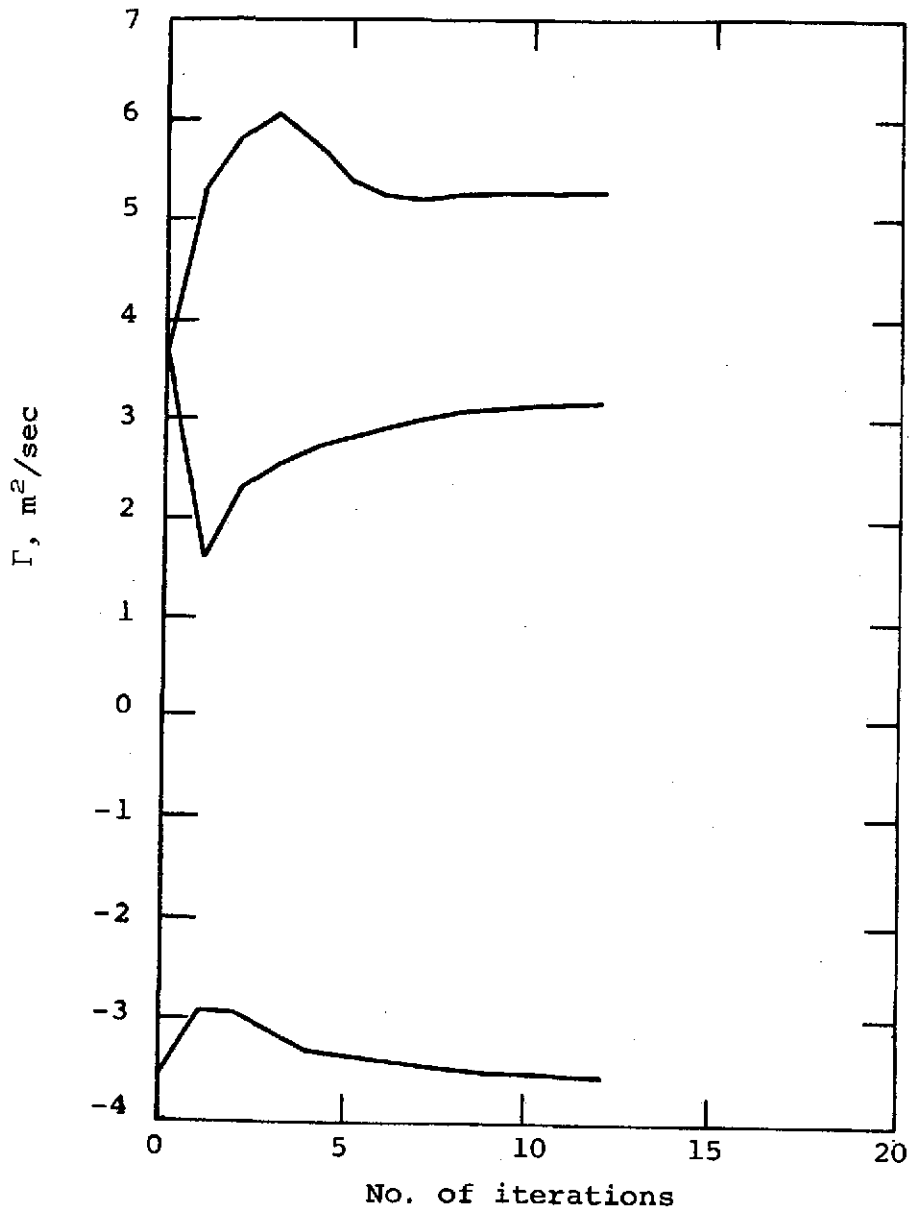

(c) Vortex strength, Γ.

Figure A-1.- Continued.

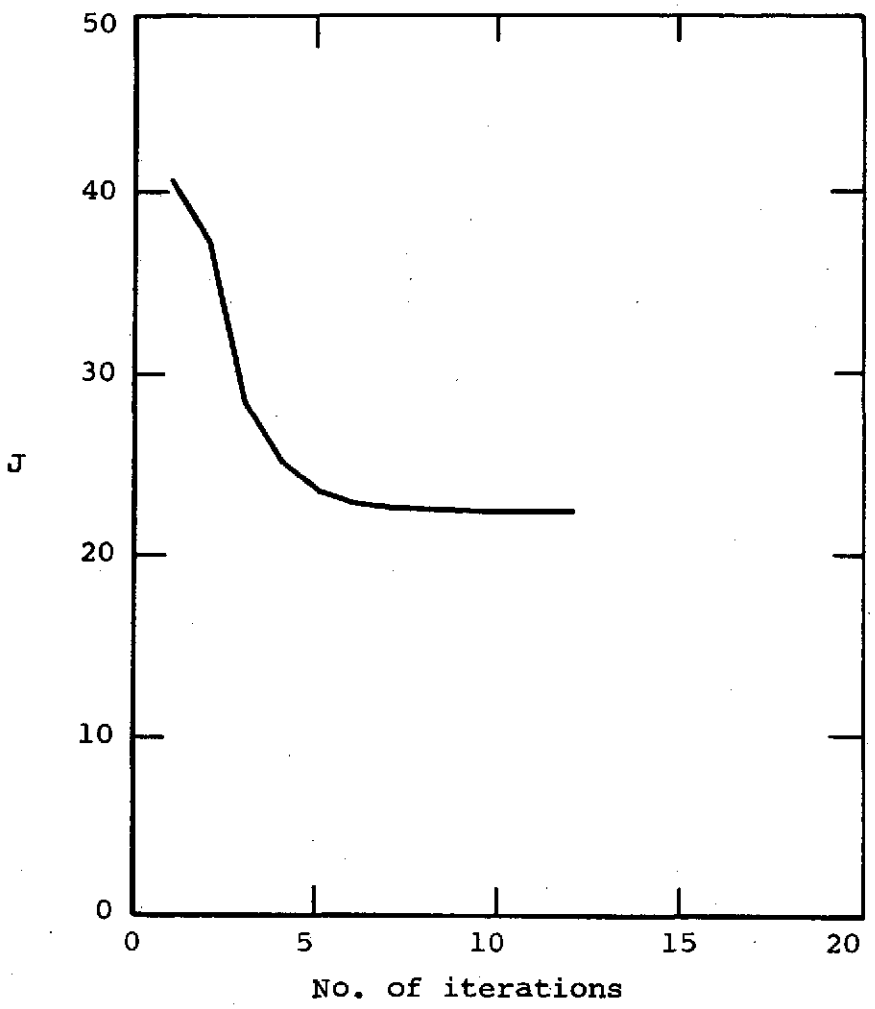

(d) Mean square error, J.

Figure A-1.- Concluded.